Journal of Materials Chemistry A

ROYAL SOCIETY OF CHEMISTRY

REVIEW

View Article Online
View Journal | View Issue



Cite this: J. Mater. Chem. A, 2026, 14, 18450

# Integrated overview of solvents and materials for reactive carbon capture and utilization

Changgwon Choe,[a] Mingi Kim,[b] Cristóbal Quintana *[cd] and Hankwon Lim *[abe]

Received 11th December 2025
Accepted 13th March 2026

DOI: 10.1039/d5ta10129h

rsc.li/materials-a

Carbon dioxide ($CO_2$) capture remains a critical strategy for environmental decarbonization and achieving net-zero emissions in power generation and industrial sectors. Over the last two decades, diverse solvent-based strategies have emerged, involving absorbents such as aqueous amines, deep eutectic solvents (DESs), enzymes, ionic liquids (ILs), porous materials, and electrochemically regenerable solutions. While each class offers distinct advantages in reactivity, stability, and regeneration energy, direct comparisons across solvent types remain limited, hindering rational material selection for specific capture scenarios. Furthermore, emerging applications such as direct air and ocean capture, integrated capture and utilization (ICCU), as well as techno-economic analysis (TEA), introduce new challenges for solvent performance, compatibility, and process integration. This review provides a comprehensive assessment of solvent-based $CO_2$ capture technologies, with an emphasis on performance metrics such as absorption capacity, regeneration energy, cycling efficiency, and economic viability. By integrating insights from molecular design, process engineering, and TEA, this review aims to provide a practical guide for the development and deployment of next-generation $CO_2$ capture sorbents.

[a]School of Energy and Chemical Engineering, Ulsan National Institute of Science and Technology, 50 UNIST-gil, Eonyang-up, Ulju-gun, Ulsan 44919, Republic of Korea. E-mail: hklim@unist.ac.kr

[b]Graduate School of Carbon Neutrality, Ulsan National Institute of Science and Technology, 50 UNIST-gil, Eonyang-up, Ulju-gun, Ulsan 44919, Republic of Korea

[c]Carbon Value, A-401, 15, Ulsan Technopark, Jongga-ro, Jung-gu, Ulsan, Republic of Korea

[d]Czech Advanced Technology and Research Institute (CATRIN), Regional Centre of Advanced Technologies and Materials, Palacký University Olomouc, Šlechtitelů 27, 77900, Olomouc, Czech Republic. E-mail: cristobal.quintana@upol.cz

[e]Carbon Neutrality Demonstration and Research Center, Ulsan National Institute of Science and Technology, 50 UNIST-gil, Eonyang-up, Ulju-gun, Ulsan 44919, Republic of Korea

Changgwon Choe

*Dr Changgwon Choe is a senior researcher at the Korea Institute of Energy Research, South Korea. He received his PhD in Energy and Chemical Engineering in 2025 from the Ulsan National Institute of Science and Technology (UNIST). During his doctoral studies, he focused on low-carbon and carbon-neutral chemical process systems, with particular emphasis on absorption-based carbon capture and integrative process assessment using process design and simulation, techno-economic analysis, and life-cycle assessment. In his current position, his research centers on the development and scale-up of catalytic carbon conversion processes, especially e-fuel production via $CO_2$ hydrogenation and Fischer–Tropsch synthesis.*

Mingi Kim

*Mingi Kim is currently a combined MS-PhD course candidate in the Graduate School of Carbon Neutrality at Ulsan National Institute of Science and Technology (UNIST) in South Korea. He received his BS degree from the School of Chemical Engineering at Yeungnam University in 2024. His research focuses on Carbon Capture and Utilization (CCUS), including Process Intensification (PI) and electrochemical approaches, and aims to develop an integrated framework combining experiments, process simulation, and machine learning.*

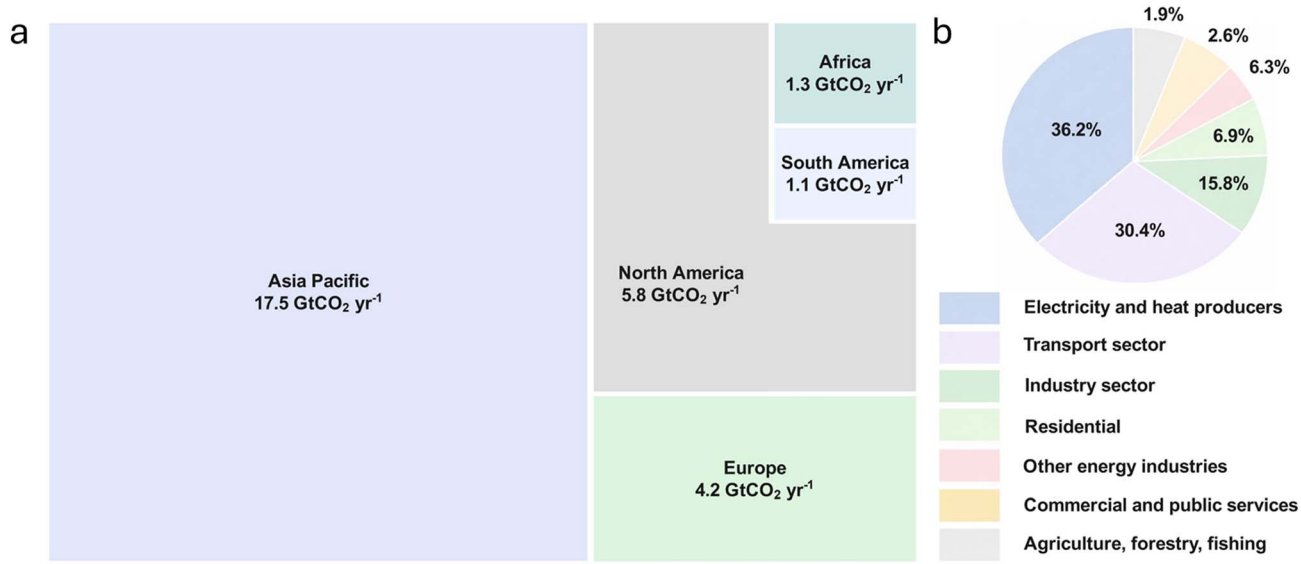


Fig. 1 (a) Proportional area chart of $CO_2$ emissions by global regions including the Americas, Africa, Europe and Asia Pacific, and (b) pie chart of the total emissions of these regions distributed by the activity sector. Data obtained from the International Energy Agency (IEA) Data Services, ref. 3 (CC BY), copyright 2023.

## 1. Introduction

The increasing concentration of atmospheric $CO_2$ has exceeded 400 parts per million,[1] reaching levels that have raised serious global concern.[2] In 2022, the International Energy Agency (IEA) estimated that a total of 29.9 Gt $CO_2$ were emitted from global regions such as Africa, the Americas, Asia Pacific and Europe (Fig. 1a).[3] In this regard, the electricity and heat generators (20.0–54.4%), the industrial (18.0–27.4%) and the transportation (12.3–43.4%) sectors account for over 70% of total $CO_2$ emissions globally. To mitigate the impact of $CO_2$ on the environment, a range of carbon capture storage and utilization (CCUS) technologies have been developed and deployed, aiming to reduce emissions from both distributed and point sources.[4–7] Among the most widely discussed are source point $CO_2$ capture techniques involving pre, post and oxyfuel combustion capture, where $CO_2$ is extracted from flue gases generated by large-scale industrial operations such as coal-fired power plants,[8,9] biogas,[10,11] cement manufacturing,[12,13] and steel production.[14,15] On the other hand, direct $CO_2$ capture techniques such as direct air capture (DAC)[16–19] and direct ocean capture (DOC)[20–22] focus on $CO_2$ sequestration from the atmosphere and the ocean, respectively, and have been also proposed as an efficient alternative for mitigating the negative impacts of increasing environmental $CO_2$ concentrations.

Point source gases contain significantly higher levels, typically between 3–50 vol% $CO_2$,[23] whereas $CO_2$ concentration in the

Cristóbal Quintana

*Cristóbal Quintana earned his PhD in Chemistry in 2020 from the Australian National University under Prof. Mark Humphrey. He subsequently held senior researcher positions at the Institute for Basic Science (2021–2023) with Prof. Bartosz Grzybowski and at Carbon Value (2023–2025). He is currently an MSCA-PF-CZ Fellow at the Czech Advanced Technology and Research Institute (CATRIN) in Prof. Michal Otyepka's group. Dr Quintana's research focuses on hybrid materials for sensing, imaging, and catalysis.*

Hankwon Lim

*Dr Hankwon Lim is a Professor, a Director of SPADE & CNDRC at Ulsan National Institute of Science and Technology (UNIST) in Korea. He received BS summa cum laude from Sogang University, MS from Georgia Tech, and PhD from Virginia Tech all in chemical engineering and also had an industrial experience at Praxair (now Linde) as a development specialist. His research is well-balanced between experimental and theoretical studies with emphasis on energy, environment, sustainability, and AI leading to 235 journal papers published and also aims at an integrative engineering approach for commercialization of technologies from laboratory to industrial scales.*

Table 1 Glossary of KPIs used in benchmarking $CO_2$ capture solvents

| KPI | Symbol | Definition | Units | Notes |
|---|---|---|---|---|
| Rich loading | $\alpha_{rich}$ | Moles of $CO_2$ absorbed per mole active site (amine and alkaline functionality) at the equilibrium rich state | mol $CO_2$ $mol^{-1}$, mol $CO_2$ $g^{-1}$ | Determines maximum loading capacity. High values are preferred |
| Lean loading | $\alpha_{lean}$ | Moles of $CO_2$ per mole active site after regeneration | mol $CO_2$ $mol^{-1}$, mol $CO_2$ $g^{-1}$ | Residual $CO_2$ present in the solvent. Lower values are preferred |
| Cyclic loading | $\alpha_{cyclic}$ | Difference between rich and lean loading ($\alpha_{rich} - \alpha_{lean}$) | mol $CO_2$ $mol^{-1}$, mol $CO_2$ $g^{-1}$ | Usable working capacity per cycle. High values are preferred |
| Cycling lifetime | $q_{cyc}$ | Number of adsorption/desorption cycles | N/A | Enables comparison of solvent lifetime |
| Removal efficiency | $\eta_{CO_2}$ | Fraction of $CO_2$ removed from inlet gas stream | % | Gas-phase metric; depends on reactor design. Typically, >90% removal efficiency is preferred |
| Specific regeneration duty | SRD | Energy required to release one unit mass of $CO_2$ (kg, t) from rich solvent | GJ $tCO_2^{-1}$; MJ $kgCO_2^{-1}$ | Critical cost parameter; used for $CO_2$ processing cost and energy consumption of the process. Allows direct comparison between different processes. Low values are preferred |

atmosphere ranges from 400 to 500 ppm[1] and in seawater the concentration is uniform with *ca.* 100 mg $dm^{-3}$.[24] In this regard point source capture technologies address high-volume emitters and represent a direct mitigation strategy for industrial and energy sector decarbonization, accounting for a significant share of global emissions with 40–50% of total emissions (Fig. 1b). DAC and DOC technologies are also gaining traction for capturing $CO_2$ at lower concentrations; however, their large-scale deployment will depend on improving current pilot plant performance.[25] The economic feasibility of these technologies is subjected to a maximum cost of 100 USD $tCO_2^{-1}$ for point source capture and 200 USD $tCO_2^{-1}$ for direct $CO_2$ capture to deem the process economically feasible.[26] Hence, achieving these $CO_2$ processing costs represents a major challenge for CCUS deployment.

Both point source and direct $CO_2$ capture fundamentally rely on chemical and physical absorbents or sorbents capable of selectively binding $CO_2$ depending on the capture process, ideally under atmospheric conditions.[6,7,27] These materials must allow for efficient regeneration, typically triggered by external stimuli such as pressure,[28] temperature,[29,30] electrochemical,[31,32] or chemical displacement.[27,33] The ability of a sorbent to undergo multiple capture-release cycles with high efficiency and requiring low regeneration energy is central to its practical deployment in capture and storage systems as it defines the operational cost of the process.[6] However, current challenges extend beyond capture and storage alone, as there is increasing governmental pressure to achieve net-zero emissions at a reduced cost of $CO_2$ production. This includes the development of integrated systems that not only remove $CO_2$ from emission streams or the environment but also convert it into products of industrial value such as methanol, ethanol, or syngas.[32–39] In this regard, solvent compatibility with the integrated CCUS process is critical, as the solvent defines $CO_2$ speciation and thus represents the starting point for $CO_2$ derivatization.[40,41] Although significant progress has been achieved using a large variety of materials, including amines,[42] amino acids,[43,44] ILs,[45,46] DESs,[47] polymers,[48] nanoparticles, redox-active molecules,[35,40] porous liquids (PLs),[49,50] and porous frameworks,[48,51–53] a concise comparative assessment that integrates performance metrics with engineering relevance and techno-economic feasibility is still lacking. In this review, we present a concise summary and comparison of current and emerging classes of chemical absorbents for $CO_2$ capture highlighting their key performance indicators (KPIs). Then, recent advancements in the integration of these materials within electrochemical and thermochemical systems for $CO_2$ utilization are discussed, concluding with a critical TEA of most relevant examples and the current challenges of the field.

## 2. Key performance indicators

In the following section we introduce key performance indicators that need to be considered in the selection process of a solvent and why they are relevant for application in CCUS. A summary of each KPI's definition, units, and significance is provided in Table 1.

### 2.1. Loading capacity

One of the most fundamental metrics for evaluating $CO_2$ absorbents is the capture capacity, which refers to the amount of $CO_2$ that a material can absorb per unit mass or mole of sorbent under specific conditions-commonly expressed in mmol $CO_2$ g $sorbent^{-1}$, mol $CO_2$ mol $sorbent^{-1}$, or g $CO_2$ kg $sorbent^{-1}$ depending on the application and material type.[51–53]

 

The capture capacity depends on factors such as the chemical affinity of the solvent/sorbent material toward $CO_2$, the density and accessibility of active binding sites, and operational parameters like temperature, pressure, and $CO_2$ partial pressure. Sorbents possessing high surface areas with accessible porosity such as metal–organic frameworks (MOFs), covalent-organic frameworks (COFs), porous organic polymers (POPs),[54,55] and porous liquids (PLs)[49,50] and those with basic or amine-functional groups,[56] often demonstrate elevated $CO_2$ uptake under synthetic gas mixture testing conditions, which typically omit oxygen, $NO_x$, and $SO_x$ and employ cool gas streams to avoid degradation.[55–60]

The $CO_2$ loading capacity of reactive solvents is primarily determined by their equilibrium binding affinity toward $CO_2$, which can be described by the $CO_2$ binding constant. In molecular systems, this property is closely linked to the p$K_a$ of the reactive functionality, where groups such as amines,[61] alcohols, carbonates, carboxylates, phosphates, and alkoxides provide lone pairs for nucleophilic attack on $CO_2$. Experimental determination of equilibrium constants for carbamate formation, for instance in monoethanolamine (MEA)[62] and diethanolamine (DEA),[63] has established clear correlations between base strength and $CO_2$ loadings. For redox-active molecules, such as quinones and related species, $CO_2$ uptake is often quantified by an analogous parameter referred to as p$K_{CO_2}$, which measures the equilibrium interaction between $CO_2$ and the reduced carrier.[62–65] Recent electrochemical studies have further validated these thermodynamic parameters by demonstrating their role in determining uptake capacity in quinone[66–69]- and amine[70–72]-derived systems, under both point source and dilute $CO_2$ conditions. Taken together, equilibrium constants such as p$K_a$ and p$K_{CO_2}$ serve as molecular-level descriptors that directly link sorbent chemistry to $CO_2$ absorption capacity. Nonetheless, high capture capacity alone does not guarantee effective performance in carbon capture.

There is often a trade-off between $CO_2$ capture strength and regeneration energy: sorbents that bind $CO_2$ strongly, such as primary amines or highly basic functional groups, generally require more energy for desorption, increasing the overall process intensity.[73,74] The rich $CO_2$ loading ($\alpha_{rich}$) of a solvent or sorbent is a critical parameter for evaluating performance. For molecular absorbents such as amines or redox-active molecules, $\alpha\square\square_{ch}$ is expressed as the molar ratio of $CO_2$ to the sorbent (eqn (1)). In contrast, for solid or composite sorbents including polymers, nanoparticles, MOFs, and COFs, $\alpha_{rich}$ is more appropriately normalized to sorbent mass (eqn (2)), reflecting their heterogeneous structures and diverse binding sites.[75,76]

$$\alpha_{rich} = \frac{n_{CO_2}}{n_{sorbent}} \quad (1)$$

$$\alpha_{rich} = \frac{n_{CO_2}}{m_{sorbent}} \quad (2)$$

where $n_{CO_2}$ are the moles of $CO_2$ and $n_{sorbent}$ and $m_{sorbent}$ are the moles and the mass of the carbon capture sorbent, respectively. The amount of $CO_2$ in the sorbent after saturation can be determined gravimetrically, volumetrically, with a $CO_2$ analyzer or using spectroscopic techniques, for example.

### 2.2. Regeneration energy

Regeneration energy refers to the amount of energy required to release absorbed $CO_2$ from a sorbent and restore its capacity for reuse. It is a critical parameter for evaluating the practical viability of capture technologies, as it directly impacts both energy efficiency and economic feasibility.[6] In thermal swing absorption, regeneration energy is commonly expressed as the specific regeneration duty (SRD), reported in GJ $tCO_2^{-1}$ (or MJ $kgCO_2^{-1}$), whereas in electrochemical systems it is expressed as the electrochemical work in GJe $tCO_2^{-1}$. Both metrics quantify the energy input required per unit mass of regenerated $CO_2$. The SRD can be estimated under steady-state conditions using eqn (3)

$$\mathrm{SRD}\left(\frac{\mathrm{GJ}}{\mathrm{tCO_2}}\right) = \frac{P_{heater}(W) \times t(\mathrm{h})}{n_{CO_2} \times \mathrm{MWCO_2}} \quad (3)$$

where $P_{heater}$ is the reboiler power (W), $t$ is the time in hours (h), $n_{CO_2}$ is the moles of $CO_2$ released, and MW $CO_2$ is the molar mass of $CO_2$.[61] Strong chemisorption, as observed in aqueous amines, typically results in higher regeneration energies, with reported values of 2.7–4.3 GJ $tCO_2^{-1}$ under heat-integrated operation.[74,76,77] In contrast, weaker physisorption interactions in materials such as MOFs, COFs, and POPs often allow regeneration at <2 GJ $tCO_2^{-1}$.[51–53] In electrochemical systems, regeneration energy is defined as the electrical work ($W_{echem}$) required to release a unit mass of $CO_2$. This can be estimated from cyclic voltammetry or galvanostatic cycling, where the charge applied is correlated with the moles of $CO_2$ released.[64,68,78] The energy per unit mass can be expressed by using eqn (4):

$$W_{echem}\left(\frac{\mathrm{GJ}}{\mathrm{tCO_2}}\right) = \frac{F}{\varepsilon_{CO_2}} E_{cell} \quad (4)$$

where $E_{cell}$ is the peak potential difference of the cell, $F$ is the Faraday constant (96 485 C $mol^{-1}$), and $\varepsilon_{CO_2}$ is the electron utilization.[64,79]

Electrochemical regeneration avoids thermal input and offers precise control *via* applied potential, which can improve solvent stability and cycling durability compared to conventional high-temperature operation. However, parasitic reactions such as hydrogen evolution or oxidative degradation at the electrode–electrolyte interface may reduce efficiency.[34,71] Thus, designing efficient sorbents requires balancing regeneration energy with $CO_2$ capacity and selectivity. While excessively weak interactions lower regeneration energy but compromise uptake, excessively strong binding increases energy penalties. Thermal stability and durability therefore remain key challenges for amine-based solvents,[61] while electrochemical systems present a promising route to minimize thermal stress and extend cycle lifetimes.[64] Comparing SRD across sorbents is complex, and reported values are typically disparate. The extent of heat integration in the process largely sets the SRD, so fair comparisons require consistent integration assumptions.

### 2.3. Lean loading

Sorbents often retain some $CO_2$ after regeneration, since complete removal may require longer residence time or higher energy input. This residual $CO_2$ loading after regeneration is defined as the lean loading. Lean loading directly affects the absorption performance as excessive $CO_2$ concentration in the solvent after regeneration will lead to a reduction in $CO_2$ capture performance compared to the fresh sorbent. Increasing lean loading is also an indicator of inefficient solvent regeneration.

The lean loading capacity ($\alpha_{lean}$) of the solvent reported as mol $CO_2$ mol sorbent$^{-1}$ or mol $CO_2$ g sorbent$^{-1}$ can be determined using eqn (5)

$$\alpha_{lean} = \frac{n_{CO_2,rich} - n_{CO_2,des}}{n_{active\ material}} \quad (5)$$

where $n_{CO_2,des}$ refers to the moles of $CO_2$ in the solvent before regeneration, and $n_{CO_2,des}$ refers to the moles of $CO_2$ released during the stripping step. A higher $\alpha_{lean}$ indicates that more $CO_2$ remains in the solvent after regeneration, thereby reducing the cycling capacity and overall efficiency of the capture process. Minimizing lean loading is thus a key design consideration in both conventional amine scrubbing and emerging solvent systems, as it maximizes absorption capacity and improves process efficiency.[61,74]

### 2.4. Cycling capacity

Cyclic loading refers to the net amount of $CO_2$ absorbed and subsequently released by a sorbent in a single capture-regeneration cycle. It is defined as the difference between the $CO_2$ loading in the rich state ($\alpha_{rich}$) and the lean state after regeneration ($\alpha_{lean}$), typically reported in units of mol $CO_2$ mol sorbent$^{-1}$, mol $CO_2$ g sorbent$^{-1}$ or g $CO_2$ kg$^{-1}$ sorbent. The cyclic loading capacity ($\alpha_{cyclic}$) can be expressed using eqn (6).

$$\alpha_{cyclic} = \alpha_{rich} - \alpha_{lean} \quad (6)$$

This parameter is critical for solvent-based thermal swing systems, where solvents are not fully regenerated after each cycle.[80] Higher cyclic loading reduces solvent circulation rates and associated energy demands, thereby improving process efficiency and lowering operating costs. For example, aqueous MEA typically exhibits a cyclic loading of 0.2–0.3 mol $CO_2$ mol$^{-1}$ amine under standard flue gas conditions, though values depend on temperature, $CO_2$ partial pressure, and the absorber-stripper configuration.[74,81] In solid sorbents, cyclic loading is strongly influenced by pore accessibility, diffusion limitations, and the structural stability of the framework during repeated cycling. In electrochemical systems, cyclic loading corresponds to the number of $CO_2$ molecules captured and released per redox cycle of the active mediator and is governed by electron transfer stoichiometry, mediator solubility, and mass transport to the electrode surface. Ultimately, maximizing cyclic loading while maintaining low regeneration energy and long-term durability is a key design criterion for advanced carbon capture materials. This balance is especially important in CCUS applications, where solvent circulation rates and sorbent inventory directly constrain overall process viability.

### 2.5. Cycling lifetime

Cycling lifetime refers to the number of absorption–desorption cycles a sorbent can undergo with minimal performance loss in capturing and releasing $CO_2$. It reflects the durability and lifetime of the sorbent and is a key factor in assessing long-term

Table 2 Comparison of material classes for reactive $CO_2$ capture

| Material/solvent class | Representative examples | Capture mechanism | Application | Advantages | Limitations/research gaps |
|---|---|---|---|---|---|
| Alkylamine small molecules | MEA | Carbamate and/or bicarbonate | PCC and DAC | Fast kinetics | Oxidative/thermal degradation<br>Corrosive |
| Redox-active systems | Quinones, phenazines, and bipyridines | Organic carbonate (quinones and quinoidal systems)<br>Bicarbonate (azo compounds) | PCC, DAC and DOC | Modular and decoupled from thermal regeneration | Oxygen and moisture stability<br>Complex scaling up technology |
| Porous materials | MOF, COF, POPs, and ILs | Carbamate, bicarbonate and $CO_2$ adsorption | PCC and DAC | Low volatility<br>High surface area | Moisture/impurity sensitive |
| Inorganic bases | KOH/NaOH and $Ca(OH)_2$/CaO | Bicarbonate and carbonate | PCC and DAC | Highly reactive<br>Robust | High SRD (*e.g.*, calcination)<br>Caustic corrosion |
| Amine-functionalized nanoparticles | Polyamine coated silica particles | Carbamate and bicarbonate | PCC and DAC | High surface area | Aggregation/dispersion control<br>Heat management<br>Regeneration kinetics and durability |
| Enzymes | CA | Catalytic $CO_2$ hydration to form bicarbonate/carbonate | PCC and DAC | Faster apparent absorption rates | Degradation under harsh conditions<br>Requires immobilization for retention under industrial conditions |

 

Table 3 KPIs of amine-based solvents

| Solvent | Rich loading (mol $CO_2$ $mol^{-1}$) | Regeneration energy (GJ $tCO_2^{-1}$) | Regeneration temperature (K) | Gas composition[a] | Ref. |
|---|---|---|---|---|---|
| MEA 30 wt% | 0.46 | 2.9–4.1 | 388 | 3.5 vol% $CO_2$ | 77 and 93 |
| PZ 40 wt% | 0.88 | 2.6 | 423 | 12 vol% $CO_2$ | 88 |
| MDEA 20–30 wt%/PZ 10–20 wt% | 0.61–0.75 | 2.24 | 398 | 12 vol% $CO_2$, 10 vol% $H_2O$ | 94 and 95 |
| CESAR1 (3 mol $dm^{-3}$ AMP/1.5 mol $dm^{-3}$ PZ) | 0.50 | 2.97 | 393 | 15.2 vol% $CO_2$, 5 vol% $O_2$, $NO_2$ 2–6 ppm, $SO_2$ < 1 ppm | 96 and 97 |
| HS-3 (15 wt% 3AP/30 wt% HEP) | 0.506 | 2.98 | 393 | 5.5–12 vol% $CO_2$ | 98 |
| ENEA/NMP 5 mol $dm^{-3}$ | 0.28 | 3.6 | 353 | 16.5–17.5 vol% $CO_2$, air | 99 |
| EEMPA | 0.0933 | 2.27 | 392 | $CO_2$ 14.4 vol%, $O_2$ 3.7 vol% $SO_2$ 5 ppm, NO 50 ppm | 100 |
| KTau 4 mol $dm^{-3}$ | 0.48 | 2.4 | 393 | 20% $CO_2$ | 101 |
| [Ch]Cl MEA (1 : 5) | 0.50 | — | 298–313 | 100 vol% $CO_2$ | 102 |
| [Ch]Cl·DEA (1 : 6) | 0.45 | — | 298–313 | 100 vol% $CO_2$ | 102 |
| [Ch]Cl MDEA (1 : 7) | 0.20 | — | 298–313 | 100 vol% $CO_2$ | 102 |
| [TEPA]Cl : thymol (1 : 3) | 1.282 | — | 298 | 100 vol% $CO_2$ | 103 |
| [MEA]Cl : ethylenediamine (1 : 3) | 31.5 wt% | — | 373 | 100 vol% $CO_2$ | 104 |
| (Pro/Gly) + [MEA][EG] | 0.10–0.35 | — | 383 | 100 vol% $CO_2$ | 105 |
| $[N_{1111}]$[Gly]/MDEA (30–40 wt%) | 0.64 | — | | 100 vol% $CO_2$ | 106 |
| [MTBDH][Im] | 1.03 | — | 353 | 100 vol% $CO_2$ | 107 |
| $[P_{66614}]$[3-HMPz] | 0.96 | — | 333 | 100 vol% $CO_2$ | 108 |
| $[P_{66614}]$[1-HMPz] | 0.83 | — | 333 | 100 vol% $CO_2$ | 108 |

[a] Balance with $N_2$.

process performance, maintenance requirements, and economic feasibility. A high initial $CO_2$ loading capacity is not sufficient if the sorbent degrades rapidly, accumulates irreversible byproducts, or suffers structural changes during repeated cycling.[41] Factors influencing cycling capacity include the chemical stability of the sorbent, resistance to oxidative or thermal degradation, mechanical robustness in the case of solid frameworks, and the severity of regeneration conditions. In liquid systems such as aqueous amines, exposure to hot flue gas and contaminants (*e.g.* $SO_x$, $NO_x$ and particulates) can accelerate solvent degradation, leading to a gradual decline in cycling capacity over time.[55–58] The cycling capacity of a sorbent can be calculated using the total number of absorption/desorption cycles. In liquid systems the figure of merit can be calculated using eqn (7).

$$q_{cyc} = \frac{Q_{solvent} \times V_{solvent}}{t_{operation}} \quad (7)$$

where $Q_{solvent}$ is the solvent flow rate in the absorber in L $min^{-1}$, $V_{solvent}$ is the total solvent inventory in L and $t_{operation}$ is the total operation time in hours. Similarly, in solid sorbents such as MOFs, COFs, POPs, or amine-functionalized porous solids and PLs, cycling capacity is instead quantified by the retention of $CO_2$ uptake after a specified number of adsorption–desorption cycles.[50,82,83] Loss in capacity often arises from pore collapse, amine leaching, or oxidative degradation under repeated cycling conditions. In electrochemical systems, cycling capacity corresponds to the number of charge–discharge cycles that can be performed while maintaining a stable $CO_2$ capture/release capacity, typically limited by stability of redox active species and electrode degradation.[64,71] Overall, cycling capacity is a critical durability metric: achieving thousands of stable cycles is necessary to meet industrial deployment targets, since solvent makeup, sorbent replacement, or electrode regeneration significantly increases operating costs and reduces system viability.

### 2.6. Removal efficiency

Removal efficiency refers to the percentage of $CO_2$ captured from a gas stream as it passes through a sorbent or capture system. It is typically calculated under steady-state conditions by comparing the $CO_2$ concentration at the absorber inlet and outlet. This parameter is central to assessing real-world performance, since regulatory standards and climate mitigation goals often require removal efficiencies above 90% in post-combustion capture (PCC) systems. The removal efficiency ($\eta_{CO_2}$) can be expressed using eqn (8).

$$\eta_{CO_2}(\%) = \left(\frac{C_{in} - C_{out}}{C_{in}}\right) \times 100 \quad (8)$$

where $C_{in}$ and $C_{out}$ are the inlet and outlet $CO_2$ concentrations, respectively. The removal efficiency of the process can always be adjusted by tuning the gas-to-liquid (G/L) ratio. For example, decreasing the G/L ratio usually leads to an increase in removal efficiency.

## 3. Solvents and materials

In this section we review the major categories of $CO_2$ capture solvents, emphasizing their composition and performance

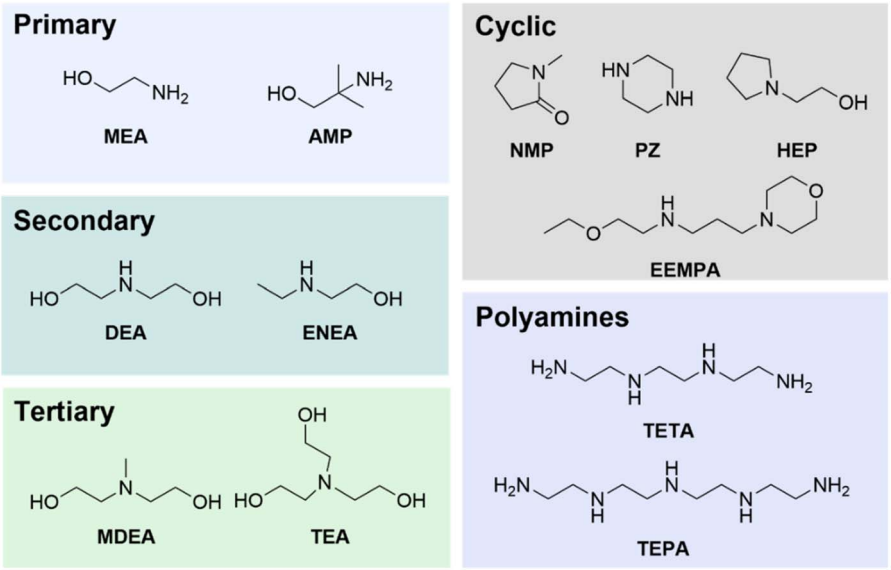


Fig. 2 Chemical structures of selected alkylamine small molecules used in carbon capture.

against the KPIs addressed in Section 2. The discussion begins with amine-based solvents (Section 3.1), and then moves to redox-active liquids (Section 3.2), inorganic bases (Section 3.3), porous solid sorbents (Section 3.4), amine-functionalized nanoparticles (Section 3.5), and finally enzyme-based systems (Section 3.6). In Table 2 a general comparison of the classes discussed in this review is provided.

### 3.1. Amine-based solvents

Amine-based solvents are the most established and commercially deployed technology for PCC. Their effectiveness arises from the strong nucleophilicity of amine groups, which react readily with $CO_2$ to form carbamate or bicarbonate ($HCO_3^-$).[84] This reactivity, combined with fast absorption kinetics, relatively low cost, and favorable physicochemical properties such as moderate viscosity and thermal stability, makes them the benchmark against which newer solvents are evaluated. Aqueous 30 wt% MEA has long served as the industrial reference,[74,85] while piperazine (PZ)-based mixtures are increasingly regarded as improved benchmarks due to higher stability[86,87] and lower regeneration energy.[88,89] Despite challenges including oxidative and thermal degradation,[90,91] corrosion, and high regeneration energy requirements,[92] amines remain dominant in large-scale capture owing to their maturity and well-understood process integration. The following subsections review different families of amine-based solvents, including small molecules, amino acids, DESs and ILs. The KPIs of selected solvents discussed in this section are presented in Table 3.

**3.1.1. Alkylamine small molecules.** Alkylamine small molecules such as cyclic and linear alkyl amines have long been studied due to their high reactivity toward $CO_2$ under atmospheric conditions.[85] The technological maturity of amine-based solvents is unparalleled, especially for applications in PCC and DAC using scrubbers[74] and rotating packed beds (RPBs).[109,110] These molecules are typically soluble in water and capture $CO_2$ *via* carbamate or $HCO_3^-$/carbonate formation,[84] and their regeneration energy is strongly influenced by $CO_2$ speciation during capture, linking equilibrium chemistry to energy demand.[111] In general amine small molecules for $CO_2$ capture have the following features: (1) primary, secondary, or tertiary amine groups that react with $CO_2$; (2) alcohol or ethylene glycol functionalities to improve water solubility and reduce volatility; and (3) short alkyl chains (2–4 carbons) to prevent phase separation.[42] The structures of selected examples of alkylamine small molecules discussed in this section are presented in Fig. 2. Early work focused on single-component aqueous amines, such as 30 wt% MEA, diethanolamine (DEA), triethanolamine (TEA) and 2-amino-2-methyl-aminopropanol (AMP) with the aim of understanding how the substitution degree of the amine influences its $CO_2$ loading.[73] It was found that at 313-K hindered primary amine (AMP) displayed the highest $CO_2$ uptake of 0.626 mol $CO_2$ $mol^{-1}$, followed by secondary amine (DEA) with 0.502 mol $CO_2$ $mol^{-1}$ and benchmark primary amine (MEA) with 0.469 mol $CO_2$ $mol^{-1}$ and with the lowest performance tertiary amine (TEA) with 0.266 mol $CO_2$ $mol^{-1}$. A list of commonly reported amines including their lean, rich and cycling capacity can be found elsewhere.[80] It is worth noting that depending on the system configuration (*e.g.* if it has heat integration) the SRD of MEA can vary from 2.9 to 4.1 GJ $tCO_2^{-1}$.[77,93] Furthermore, it has been found that the SRD can be further decreased by 12–14% using 40 wt% instead of 30 wt% MEA.[112] In this regard, primary and secondary amines react rapidly with $CO_2$ *via* carbamate formation, but this typically entails higher regeneration energy. In contrast, tertiary amines lack an N–H bond and therefore do not form carbamates; instead, they act as bases that catalyze $CO_2$ hydration to $HCO_3^-$. Tertiary amines generally provide high $CO_2$ equilibrium solubility and lower regeneration energy, but their intrinsically slow absorption rates limit standalone use in capture processes. To

 

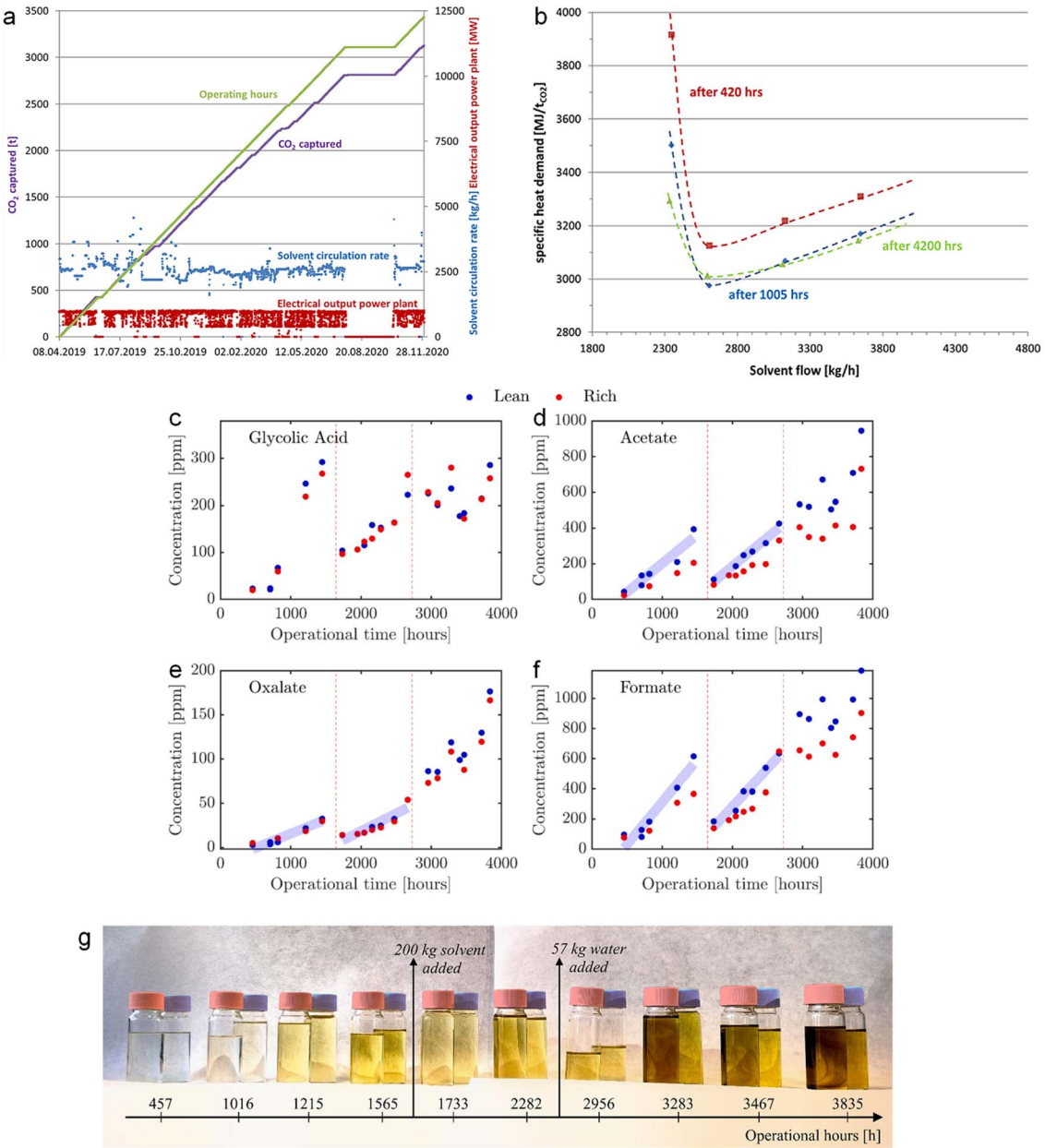


Fig. 3 (a) Cumulative $CO_2$ captured in the ALIGN-CCUS project using CESAR1. The capture plant operated for 12 275 h captured a total of 3127 $tCO_2$. (b) Specific heat demand and solvent circulation (flow) rate used to establish baseline conditions for a 90% $CO_2$ capture rate. Reproduced from ref. 96 with permission from Elsevier, copyright 2021. Concentrations of major degradation products in CESAR1 over time during 3900 h of operation on cement flue gas: (c) glycolic acid, (d) acetate, (e) oxalate, and (f) formate, shown for lean (blue) and rich (red) solvent streams. Blue shaded regions indicate the data ranges used for linear regression. (g) Photographs illustrating progressive solvent darkening over time; rich samples are capped in red and lean samples in blue. Reproduced from ref. 114 with permission from Elsevier (CC BY), copyright 2025.

mitigate these trade-offs, dual-amine aqueous blends combining a primary or secondary amine with a tertiary amine have been widely explored to couple fast uptake with reduced energy demand for regeneration. For example, a mixture of PZ/MDEA exhibits outstanding $CO_2$ loading and SRD compared to MEA 30 wt%.[94,95] Simulations for on board carbon capture in marine ships suggest that the MDEA/PZ mixture would represent a 10% SRD reduction and 32% increase in $CO_2$ absorption compared to MEA 30 wt%.[94]

A remarkable example of a PZ-based solvent that has reached industrial maturity is CESAR1 which is composed of AMP (3 mol $dm^{-3}$) and PZ (1.5 mol $dm^{-3}$); the solvent was tested at the Niederaussem carbon capture plant (ACT ALIGN CCUS project) for over 18 months with an SRD of 2.97 GJ $tCO_2^{-1}$ compared to MEA 30 wt% with 3.45 GJ $tCO_2^{-1}$.[96,113] The scrubber-type plant was able to process 3127 $tCO_2$ during an operation time of 12 275 h (*ca.* 6 $tCO_2$ $d^{-1}$), keeping the solvent circulation in the range of 2500 ± 200 kg $h^{-1}$ (Fig. 3a). Furthermore, the solvent

flow rate was adjusted so the SRD can be minimized. Thus, the specific heat demand for solvent regeneration reached an optimal SRD of 2.95 GJ $tCO_2^{-1}$ after 1005 h of operation at a solvent flow rate of *ca.* 2750 kg $h^{-1}$ (Fig. 3b). Campaigns focused on the determination of solvent degradation in cement plant operation have observed the formation of glycolic acid (Fig. 3c), mostly from degradation of PZ and acetates (Fig. 3d), oxalates (Fig. 3e) and formates (Fig. 3f) derived from the degradation of AMP. From the plots it is clear that AMP exhibits the highest degradation rate after 3900 h operational time with a total of *ca.* 800 ppm of acetates and *ca.* 180 ppm of formates as these species stem exclusively from AMP, whereas an increasing concentration of glycolic acid (*ca.* 280 ppm) and oxalate (*ca.* 180 ppm) is observed due to the contribution of the degradation of PZ and AMP. It is worth noting that the acetate and formate species tend to accumulate in the lean solvent due to process layout. The degradation products are formed as a consequence of the high reboiler temperature (383–393 K) and the oxidization conditions sustained by flue gas impurities such as $O_2$, $NO_x$, and $SO_x$. While fresh CESAR1 is colorless, solvent degradation becomes evident with increasing operating time, resulting in a gradual color change from yellow to orange (Fig. 3f).

Studies of HS-3 solvent which combines 15 wt% 3-amino-1-propanol (AP) with 30 wt% 1-2-hydroxyethylpyrrolydine (HEP) show an SRD reduction of 21% compared to MEA.[98] Concentrated aqueous solution of PZ can also be used as a solvent, though its limited solubility requires storage and operation at elevated temperature.[87] Oligo(ethylenediamines) such as triethylenetetramine (TETA)[115–117] and tetraethylenepentamine (TEPA)[118] offer a high number of amine sites and therefore high $CO_2$ uptake. However, their chain length and viscosity promote biphasic behavior upon $CO_2$ loading in aqueous media.[117,118] Hence, these amines are often used as coatings on nanomaterial supports to mitigate phase separation and amine loss and improve mass transfer (see Section 3.5). Water-lean amine solvents have been also proposed as alternatives to aqueous amine solvents as they can overcome the decomposition reactions of amines in aqueous environments.[119,120] These solvents offer extended operation lifetime, reduced corrosion, lower regeneration energy and higher $CO_2$ capacity; however, when rich, these solvents exhibit increased viscosity and density leading to higher OPEX.[100,121,122] Other bottlenecks are associated with the need of using dry flue gas to maintain the performance of water-lean solvent due to dilution. For example, 2-(ethylamine)ethanol (ENEA)/1-methyl-2-pyrrolidinone (NMP) solvent with a total amine concentration of 5 mol $dm^{-3}$ displays a lean loading of 0.038–0.138 mol $CO_2$ $mol^{-1}$ with viscosity in the range of 3.36–5.12 mPa s and a rich loading in the range of 0.24–0.28 mol $CO_2$ $mol^{-1}$ with viscosity in the range of 6.92–8.75 mPa s compared to a lean loading of 0.332 mol $CO_2$ $mol^{-1}$ with a viscosity of 2.27 mPa s, and a rich loading of 0.49 mol $CO_2$ $mol^{-1}$ with a viscosity of 2.50 mPa s.[99] There is a clear difference between the viscosity of MEA 5 mol $dm^{-3}$ and ENEA/NMP which is expected to lead to higher power consumption associated with the work needed to be done by the solvent pumps of the system. However, in this case the energy consumption from the pumps can be compensated for with the low SRD that ENEA/NMP displays equivalent to 3.6–5.4 GJ $tCO_2^{-1}$ compared to 11.7 GJ $tCO_2^{-1}$ for MEA 5 mol $dm^{-3}$ under the same experimental conditions without heat integration. One remarkable exception is *N*-(2-ethoxyethyl)-3-morpholinopropan-1-amine (EEMPA) which displays a loading capacity of 0.0933 mol $CO_2$ $mol^{-1}$ and outstanding SRD of 2.0 GJ $tCO_2^{-1}$ using a synthetic flue gas composition of 14.4 vol% $CO_2$, 3.7 vol% $O_2$, 4.5 ppm $SO_2$ and 51.9 ppm NO.[100] Interestingly, EEMPA can increase its loading capacity to up to 1 mol $CO_2$ $mol^{-1}$ *via* the formation of tetramers.[123] One of the main drawbacks of this solvent is that rich EEMPA exhibits increased viscosity in the range of *ca.* 2–100 mPa s depending on the $CO_2$ loading displaying up to 4 times higher viscosity than the example of ENEA/NMP discussed above.

Although numerous alkylamine solvents have been reported, the efficiency of the thermal-swing industrial process depends on the energy consumption associated with the solvent pumps and the reboiler.[124] In this regard, small alkylamine-based solvents increase their viscosity when the $CO_2$ loading increases; this is of particular importance for solvents with high $CO_2$ loading, highly concentrated aqueous solvents and water-lean solvents. As mentioned above, primary and secondary amines such as MEA exhibit fast kinetics due to carbamate formation, but require relatively high regeneration energy,[84,125] whereas tertiary amines suppress carbamate formation and can lower regeneration energy at the expense of slower absorption rates and larger absorber requirements.[126] Sterically hindered amines (*e.g.*, AMP) partially mitigate this trade-off by increasing $CO_2$ loading through carbamate destabilization but typically exhibit reduced intrinsic kinetics and therefore require higher circulation rates or activators to achieve comparable mass transfer performance. In parallel, viscosity, particularly at high $CO_2$ loadings or in water-lean formulations, emerges as a key limiting factor, as increased viscosity reduces gas–liquid mass transfer and increases pumping and heat-transfer penalties.[124,127] For example, fresh MEA 30 wt% (5 mol $dm^{-3}$) at 298 K exhibits a viscosity of 1.67 mPa s and its viscosity increases to 2.9 mPa s and 3.9 mPa s with $CO_2$ loadings of 0.2 and 0.5 mol $CO_2$ $mol^{-1}$.[128] Fresh MDEA (1.7 mol $dm^{-3}$)/PZ (0.6 mol $dm^{-3}$) solvent at 303 K has a viscosity of 2.30 mPa s and an increase in viscosity of 2.39 mPa s is observed when the solvent has a $CO_2$ loading of 0.32 mol $CO_2$ mol $amine^{-1}$ and a viscosity of 2.49

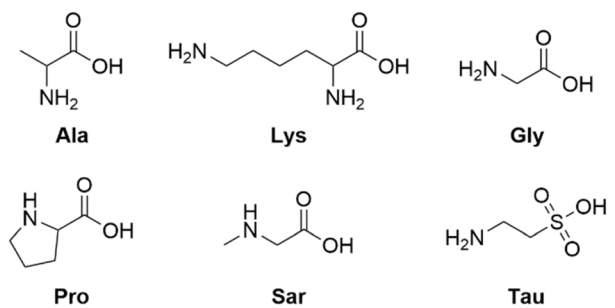


Fig. 4 Chemical structures of selected amino acids used in carbon capture.

 

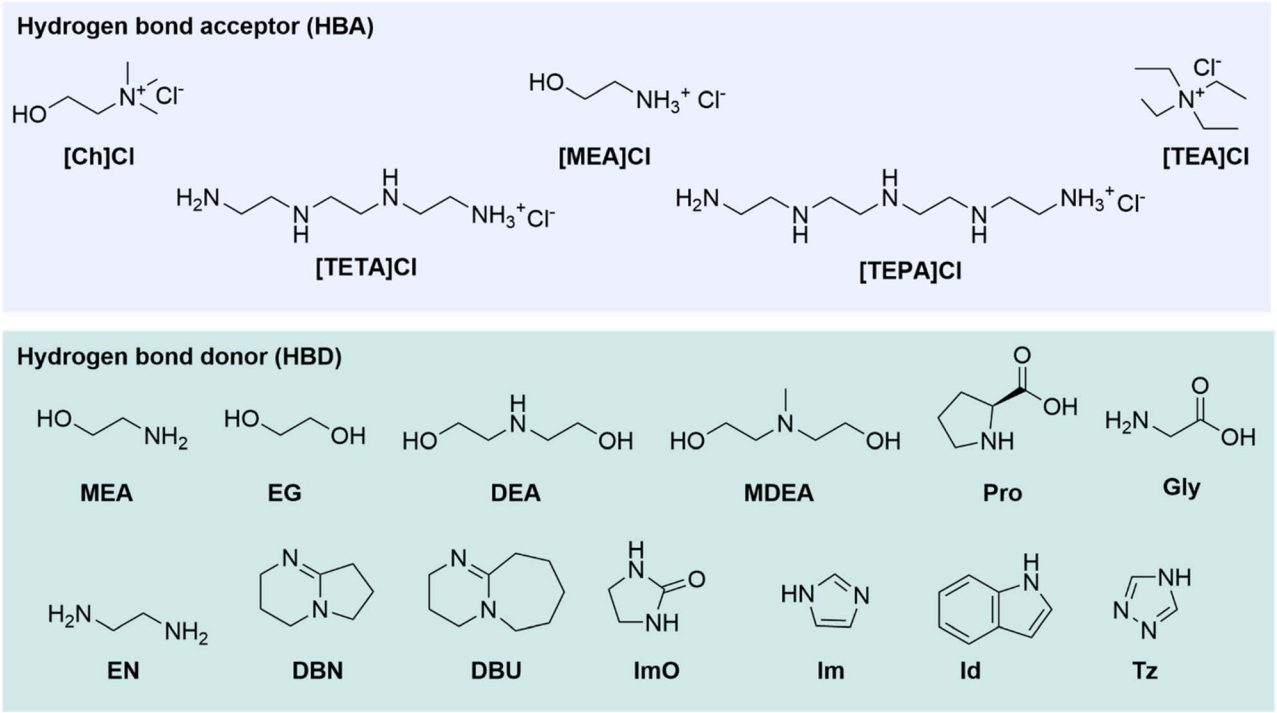


Fig. 5 Chemical structures of selected HBA and HBD components used in DESs for carbon capture.

mPa s when the $CO_2$ loading is 0.74 mol $CO_2$ mol$^{-1}$.[129] Fresh CESAR1 solvent at 303 K shows a viscosity of 6.11 mPa s which increases to 10.82 and 13.96 mPa s with increasing $CO_2$ loading of 0.20 and 0.59 mol $CO_2$ mol$^{-1}$, respectively.[130] These interdependencies explain why blended systems dominate practical deployment: no single alkylamine simultaneously optimizes capacity, kinetics, viscosity, and stability, and solvent design remains a balance of competing process-level constraints rather than maximization of any single metric. Amine-based solvents remain the industrial benchmark for PCC due to their high reactivity and maturity, though their long-term viability requires reducing energy penalties and improving oxidative and thermal stability under real flue gas conditions.

**3.1.2. Amino acids.** Amino acids are bifunctional molecules containing both amine and carboxylic acid groups, enabling two primary modes of $CO_2$ capture: the nucleophilic amine-to-$CO_2$ reaction forming carbamates, and carboxylate-assisted $HCO_3^-$ formation *via* acid–base chemistry, both conditioned on pH, amino acid structure, and $CO_2$ loading.[43,44] The structures of selected examples of amino acids discussed in this section are presented in Fig. 4. This dual reactivity distinguishes them from monofunctional amines and enables tunable capture behaviour. Commonly studied amino acids such as glycine (Gly), alanine (Ala), proline (Pro), leucine (Leu) and taurine (Tau) show $CO_2$ loadings between 0.3–0.7 mol $CO_2$ mol$^{-1}$, comparable to 30 wt% MEA solutions.[43,44,131] Structurally, effective amino acid solvents share two motifs: (1) a primary/secondary amine for $CO_2$ reaction; (2) a carboxylate that provides buffering and promotes $HCO_3^-$ formation, thereby improving kinetics and capacity.[131]

To increase the effectivity of amino acids in the capture process they are usually reacted with KOH to form its conjugate potassium salt. This improves the $CO_2$ solubility by stabilizing excess $CO_2$ in the form of potassium bicarbonates.[132] When rich, amino acids tend to form insoluble carbamates and carbonates which can lead to complications in carbon capture system design. However, the formation of two phases has been perceived by some as beneficial, as the phases can be separated and the precipitate or carbamate-containing slurry can be thermally regenerated at considerably lower energy expenditure.[133] Literature reporting experimental regeneration energy for amino acid solvents is scarce and most of the data reported is based on simulations in Aspen Plus, mostly for KTau.[133–136] Notably, the DECAB process proposes the utilization of 4 mol dm$^{-3}$ KTau as the precipitating solvent because of its low solubility in water of 94.9 g L$^{-1}$ and a loading capacity similar to that of MEA of 0.48 mol $CO_2$ mol$^{-1}$.[101,133] The DECAB process suggests a substantial energy reduction of 35% with 2.4 GJ $tCO_2^{-1}$ for KTau 4 mol dm$^{-3}$ compared to 3.7 GJ $tCO_2^{-1}$ for MEA 5 mol dm$^{-3}$.[101]

Viscosity is usually associated with high energy consumption by pumping systems, and recent studies comparing the influence of counter cations such as Li, Na, and K on the viscosity of Pro, Gly and Ala and Sar at 4 mol dm$^{-3}$ concentration and Lys at 2 mol dm$^{-3}$ concentration have shown viscosities in the range of 3–8 kPa s for K, 4–17 kPa s for Na and 6–19 kPa s for Li.[137] Furthermore, it was noted that all Li-containing solvents formed precipitates when loaded with $CO_2$. The $CO_2$ loadings of the solvents range between 0.58 and 0.70 mol $CO_2$ mol$^{-1}$ with the highest $CO_2$ capacity observed for KLys. However, oxidative

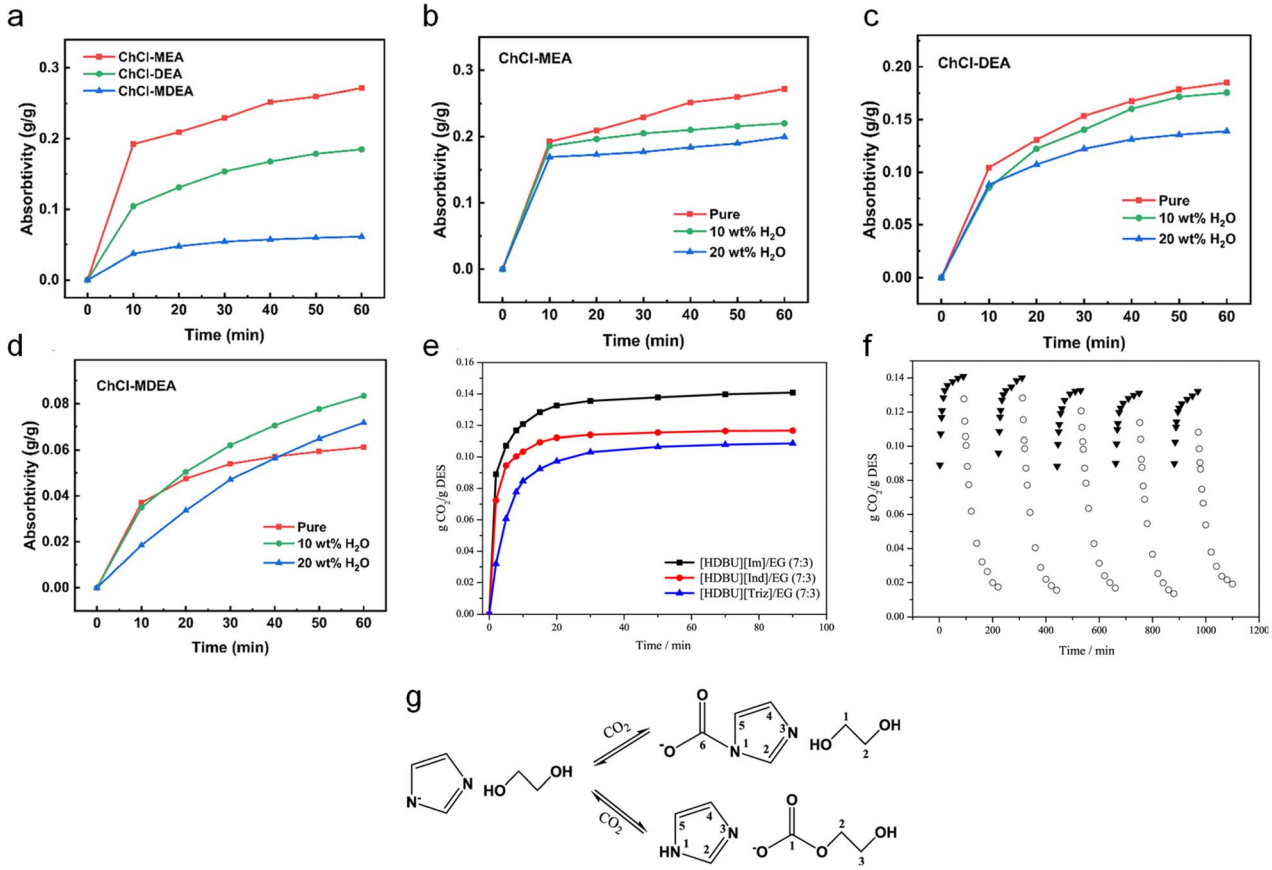


Fig. 6 (a) $CO_2$ absorption profiles of [Ch]Cl : MEA, [Ch]Cl : DEA, and [Ch]Cl : MDEA. Effect of water content on $CO_2$ uptake for (b) [Ch]Cl : MEA, (c) [Ch]Cl : DEA, and (d) [Ch]Cl : MDEA. Reproduced from ref. 102 with permission from IOP publishing (CC BY), copyright 2024. (e) $CO_2$ loading capacities of IL/EG DES measured at 313 K and 101 kPa. (f) Five consecutive absorption/desorption cycles for [HBDU][Im]/EG (7 : 3): absorption ($CO_2$, 100 kPa, 313 K) and desorption ($N_2$, 100 kPa, 343 K). (g) Proposed $CO_2$ capture reaction mechanism. Reproduced from ref. 147 with permission from the American Chemical Society, copyright 2020.

degradation studies on $CO_2$ rich solvents have shown that KLys degrades completely after 168 h, about three times faster than MEA, while KPro, KSar and KAla only degrade about 15–21% at the time MEA degrades completely after 504 h.[138] On the other hand, these amino acid potassium salts thermally degrade at a much faster rate than MEA. For example, MEA does not degrade after 500 h at 393 K-whereas KAla and KLys degrade 100% and KGly, KPro and KSar, degrade by 13%, 15% and 21%, respectively, under the same conditions.

Recent laboratory scale experiments for KGly reported a regeneration energy of 2.92 GJ $tCO_2^{-1}$ an about 24% reduction compared to that of MEA of 3 mol $dm^{-3}$ and $CO_2$ loading of 0.646 mol $CO_2$ $mol^{-1}$.[139] More advanced applications of amino acids involve the incorporation of KGly in DAC systems integrated to electrochemical systems for production of CO.[43] In this regard KGly displays a high loading capacity of 0.7 mol $CO_2$ $mol^{-1}$, faster reaction kinetics and low cost posing significant advantages to amino acids such as Lys, Pro, Ser, Arg, Tyr, Cys and Tau. Others have proposed binary mixtures of KGly with glyoxal-bis-iminoguanidine (GBIC) as a co-precipitating agent of $HCO_3^-$ for improving the $CO_2$ loading capacity of the precipitating layer.[140] The incorporation of GBIC leads to simultaneous KGly regeneration, increasing the loading capacity of the solvent to 1.36 mol $CO_2$ $mol^{-1}$ Furthermore, ternary solvent composed of KSar/KGly/GBIC exhibits a regeneration energy of 3.44 GJ $tCO_2^{-1}$ which is 24% less than that of MEA 30 wt% with 4.50 GJ $tCO^{-1}$.[141]

The main foreseen drawback of amino acids in industrial scale systems is the formation of insoluble carbamates/carbonates which can lead to a series of issues such as pipe and pump clogging. Furthermore, recent studies have shown that amino acids accelerate the oxidation rate of PZ during the capture process due to the formation of stable complexes with $Fe^{2+/3+}$.[142] It is therefore suspected that carboxylic acid/carboxylate containing compounds, especially amino acids, may degrade at a faster rate compared to other amine derivatives. In summary, amino acids offer green, tunable, and high-performing $CO_2$ capture mechanisms. Although issues like precipitation, viscosity in concentrated solutions, and scale-up must be addressed, their environmental compatibility and competitive SRD and loading capacity make them suitable candidates for sustainable capture technologies.

**3.1.3. Deep eutectic solvents (DESs).** DESs are a class of designer solvents formed by mixing a hydrogen bond donor

 

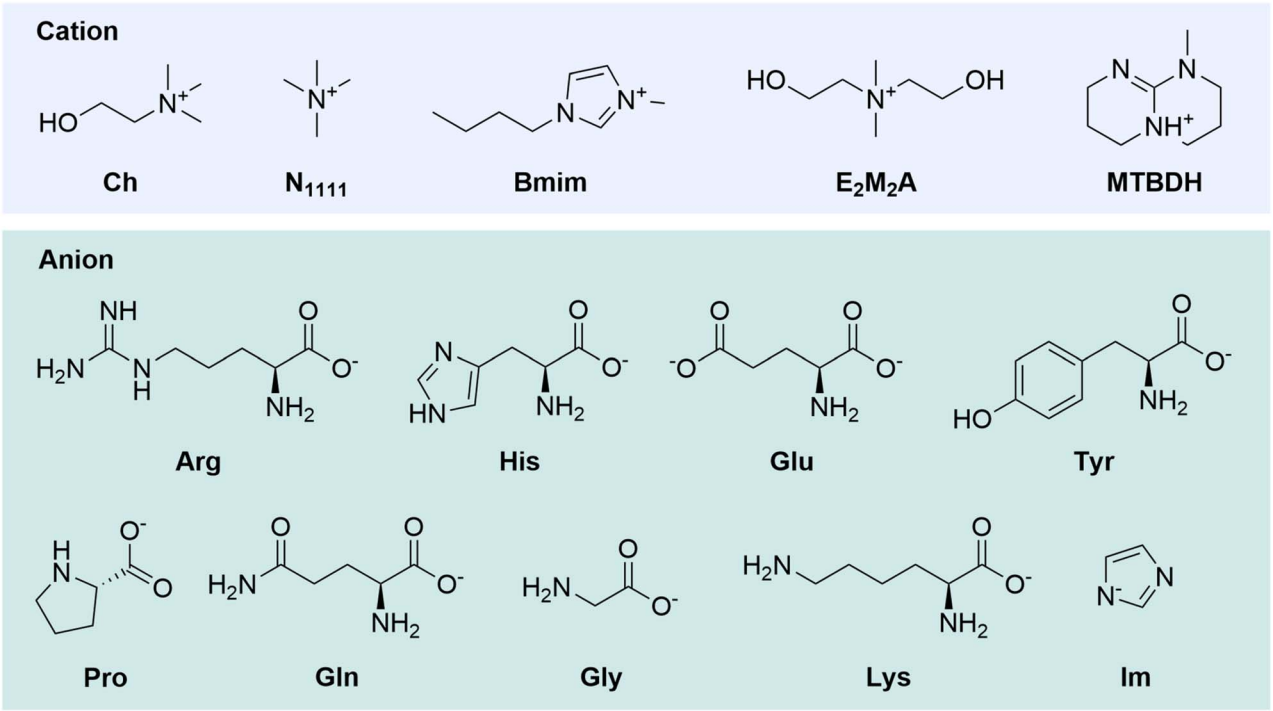


Fig. 7 Chemical structures of selected anions and cations used in ILs for carbon capture.

(HBD) and a hydrogen bond acceptor (HBA), which interact to produce a eutectic mixture with a melting point significantly lower than that of either component.[143,144] DESs often use inexpensive, biodegradable constituents such as ammonium chlorides as the HBA and urea, glycerol, or organic acids as the HBD, making them attractive alternatives to conventional ILs and alkanolamines for $CO_2$ capture.[47,104] In addition to their economic viability, their low volatility, low toxicity, high thermal stability, and synthetic tunability position DESs as promising materials in green solvent design. The nature and strength of $CO_2$ interaction in DESs strongly depend on the HBD-HBA pair, their molar ratio, and the presence of functional groups capable of hydrogen bonding or acid–base interactions.[47] The structures of selected examples of DESs discussed in this section are presented in Fig. 5.

Early work in this field demonstrated that choline chloride ([Ch]Cl)/urea DES can be utilized in carbon capture; however, the solvent requires high pressure to efficiently absorb $CO_2$ reaching a maximum $CO_2$ loading of 0.309 mol $CO_2$ $mol^{-1}$ at 12.5 MPa and 313 K.[145] Although this value is well below the *ca.* 0.5 mol $CO_2$ $mol^{-1}$ of MEA 30 wt%, these initial findings laid the foundation for the development of task-specific DES (TS-DES). To overcome the limitations of physical absorption at high pressure, more reactive functional groups such as alkylamines have been incorporated into the chemical structure of DESs to enable effective operation under atmospheric conditions. Subsequent studies have focused on understanding the role of water in $CO_2$ capture behavior in DESs.[102,146] Fundamental studies assessing $CO_2$ absorption using [Ch]Cl : MEA 1 : 5, [Ch]Cl : DEA 1 : 6 and [Ch]Cl : MDEA 1 : 7 (Fig. 6a) determined that incorporation of 10 to 20 wt% water leads to a decrease in absorption performance of *ca.* 25% for [Ch]Cl : MEA (Fig. 6b) and ca. 30% for [Ch]Cl : DEA (Fig. 6c), whereas [Ch]Cl : MDEA exhibits an increase in the $CO_2$ loading capacity of *ca.* 30% when the water content is 10 wt% (Fig. 6d).[102] The authors concluded that the presence of water disrupts the HBA-HBD interaction between the active species and protonates the primary and secondary amines, reducing their activity. The main mechanism of $CO_2$ capture in both MEA and DEA based DESs is *via* carbamate, whereas for tertiary amines it is *via* the formation of $HCO_3^-$, therefore supporting the fact that the presence of water leads to an increase in $CO_2$ uptake in MDEA based DES. These observations emphasize that water acts as both a facilitator and inhibitor depending on the amine class and capture mechanism.

Combination of MEA with [Ch]Cl, $NH_4Cl$ or tetraethylammnonium chloride ([TEA]Cl) shows a similar absorption capacity of *ca* 25 wt% $CO_2$ in the range of 303–333 K; however, at 293 ,K MEA/[Ch]Cl and MEA/[TEA]Cl outperforms the other two combinations.[148] These DESs displayed poor cycling lifetime as the $CO_2$ loading capacity decreased from *ca.* 27 wt% $CO_2$ in the first absorption/desorption cycle to *ca.* 15 wt% $CO_2$ after 7 cycles. Others have suggested that DES based on monoethanolammnium chloride ([MEA]Cl) and ethylenediamine (EN)[104] exhibits an outstanding loading capacity of 31.5 wt% $CO_2$ when the ratio of [MEA]Cl/[EN] is 1 : 3; interestingly this DES exhibits a corrosion rate of 0.124 mm per year which is 3-fold less corrosive than its individual components with 0.385 mm per year and 0.448 mm per year for MEA and EN, respectively. Furthermore, the solvent displays

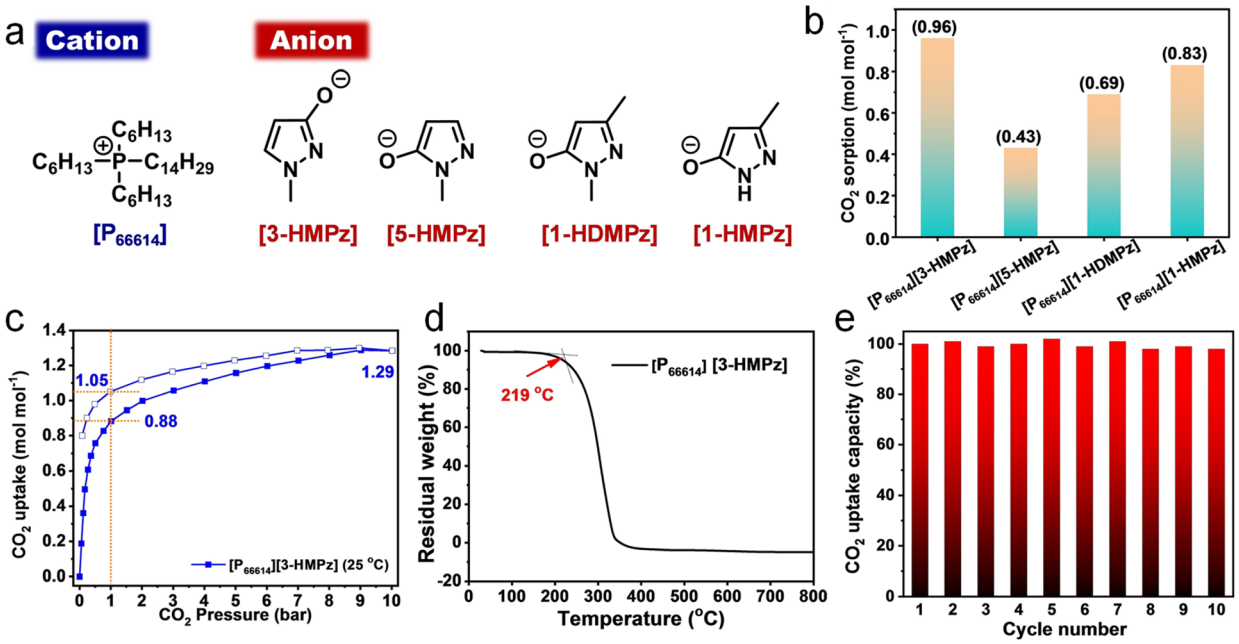


Fig. 8 (a) Chemical structures of the phosphonium and pyrazolonate TS-ILs. (b) $CO_2$ uptake capacities measured by bubbling pure $CO_2$ through the ILs at 298 K and ambient pressure. (c) Pressure-swing $CO_2$ absorption/desorption isotherms of $[P_{66614}][3\text{-HMPz}]$ at 298 K. (d) Thermogravimetric analysis (TGA) trace of $[P_{66614}][3\text{-HMPz}]$ under a nitrogen atmosphere. (e) Cycling stability of $[P_{66614}][3\text{-HMPz}]$ over ten consecutive $CO_2$ absorption/desorption cycles. Reproduced from ref. 108 with permission from Wiley VCH, copyright 2023.

constant performance over five thermal swing cycles involving absorption at 303 K and desorption at 373 K.

DESs involving ammonium salts of oligoethylamines have also been proposed,[103,149,150] for example, TEPA hydrochloride ([TEPA]Cl) or TETA hydrochloride ([TETA]Cl) as HBAs with thymol as the HBD with a HBA/HBD ratio of 1 : 3.[103] The absorption capacity of [TEPA]Cl/thymol DES is considerably larger than that of [TEPA]Cl alone with 1.282 mol $CO_2$ $mol^{-1}$ compared to 0.584 mol $CO_2$ $mol^{-1}$, respectively. As expected, the proposed mechanism of $CO_2$ capture is through the formation of carbamates *via* interaction with secondary amines. Remarkably, the density and viscosity of [TEPA]Cl/thymol and [TETA]Cl/thymol DESs are significantly lower than that of the free oligo amines in their fresh and rich states, where rich [TETA]Cl and [TEPA]Cl solidify, demonstrating a practical advantage over their pure amine counterparts. Additionally, ternary DES comprising a mixture of amino acids such as Pro or Gly with [MEA][EG] showed a $CO_2$ loading capacity of 0.1–0.35 mol $CO_2$ $mol^{-1}$. However, the solvent required a temperature of 383 K in the regeneration process, contrary to DES containing secondary alkyl amines or amine heterocycles.[105] It is worth noting that regeneration data with metrics such as GJ $tCO_2^{-1}$ on DES with chemical absorption are largely omitted in reviews and papers suggesting that there is a large gap in knowledge and technology maturity.[104–107,151,152]

**3.1.4. Ionic liquids (ILs).** ILs are liquid salt solutions, typically consisting of bulky, asymmetric organic cations and weakly coordinating anions.[153] Their low vapor pressure, wide electrochemical windows, and high thermal stability have positioned them as attractive candidates for solvent-based $CO_2$ capture and utilization. Common IL structures include imidazolium, pyrrolidinium, or quaternary ammonium cations paired with anions such as tetrafluoroborate, hexafluorophosphate, bis(trifluoromethanesulfonyl)imide, or carboxylates.[154] One of the characteristic properties of ILs is their high viscosity, which stems from strong coulombic interactions. The viscosity, while contributing to high thermal and chemical stability, imposes a practical barrier for large-scale implementation by impeding mass transfer, slowing $CO_2$ diffusion rates and increasing energy expenditure in pumping systems.[155,156] ILs typically absorb $CO_2$ *via* physical dissolution, with reported capacities up to ~0.8 mol $CO_2$ $mol^{-1}$. However, such values are often obtained under elevated $CO_2$ pressures (1000–3000 kPa) limiting their applicability for low pressure applications such as DAC and PCC. Nevertheless, physical absorption enables low regeneration energies, typically in the range of 1–3 GJ $tCO_2^{-1}$, allowing for desorption through temperature or pressure swing processes.[156] To overcome the limitations of purely physisorptive ILs, task-specific ILs (TSILs) have been developed by incorporating chemically reactive groups such as primary or secondary amines, thus providing physical and chemical means for carbon capture.[157] The structures of selected examples of TS-ILs discussed in this section are presented in Fig. 7. These modified ILs form carbamate or $HCO_3^-$ species upon $CO_2$ binding, enabling higher uptake capacities (up to 1 mol $CO_2$ $mol^{-1}$) under atmospheric pressure conditions and aqueous conditions.[158] For example, ILs composed of choline (Ch) and amino acids were synthesized and tested for $CO_2$ absorption with compositions involving ion pairs of choline arginate ([Ch][Arg]), choline histidinate ([Ch]

 

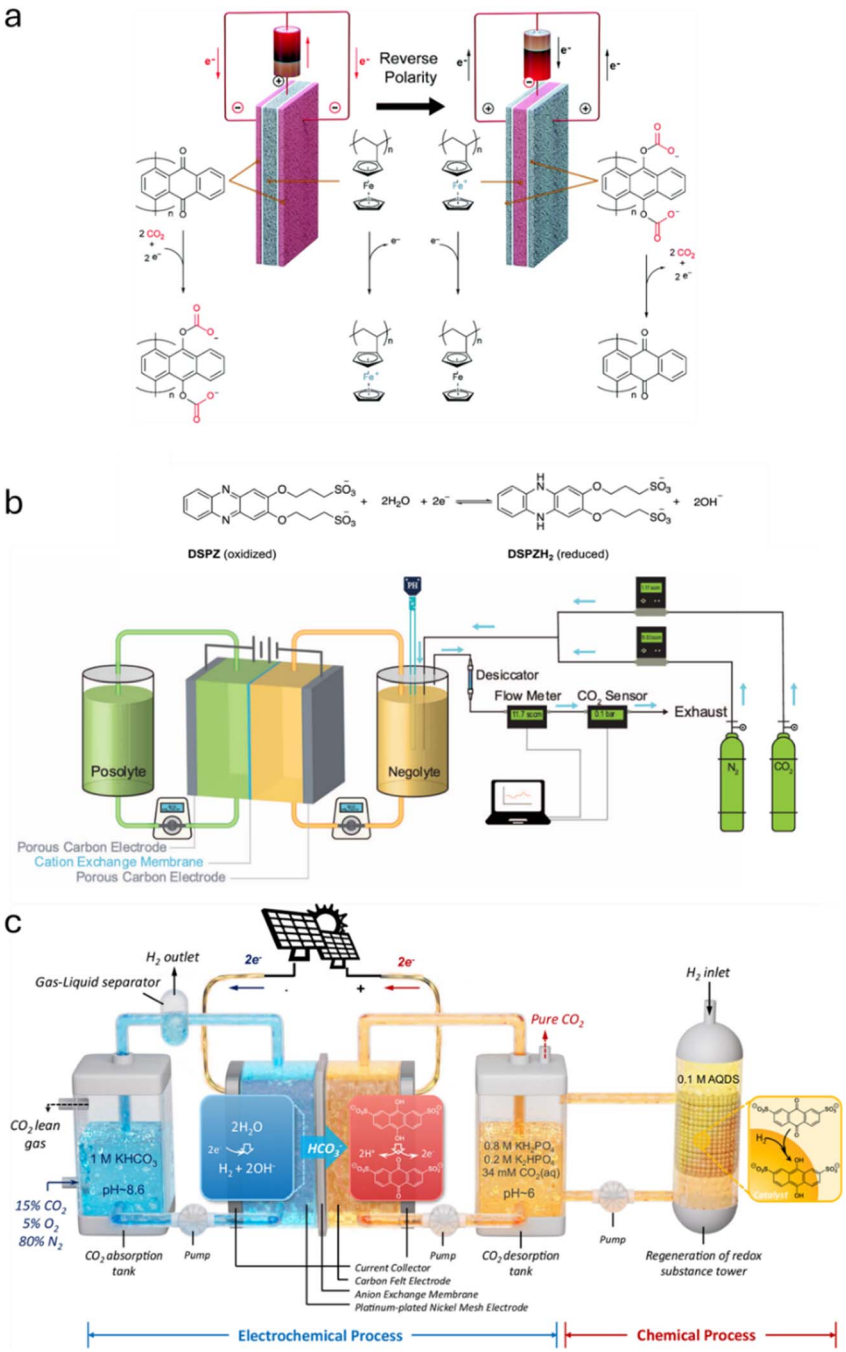


Fig. 9 Schematic illustrations of EMCC configurations. (a) Direct EMCC system using compounds **10** and **19**. Reproduced from ref. 78 with permission from the Royal Society of Chemistry, copyright 2019. (b) Indirect EMCC system using compound 14 as the negolyte and compound 20 as the posolyte. Reproduced from ref. 168 with permission from the Royal Society of Chemistry, copyright 2022. (c) Decoupled EMCC system using compound **9**. Reproduced from ref. 173 with permission from Springer Nature, copyright 2024.

[His]), choline tyrosinate ([Ch][Tyr]), choline glutamate ([Ch][Glu]), choline glutaminate ([Ch][Gln]), and choline prolinate ([Ch][Pro]). At 318.15 K and atmospheric pressure, their sorption capacities for [Ch][His], [Ch][Arg], [Ch][Gln], [Ch][Glu], [Ch][Pro], and [Ch][Tyr] were 1.00 > 0.95 > 0.83 > 0.72 > 0.58 > 0.56 mol $CO_2$ mol $^{-1}$, respectively. This order highlights the influence of amino acid side-chain chemistry: imidazole- and guanidinium-based ILs ([Ch][His], [Ch][Arg]) exhibit the highest affinities, while aromatic residues such as Tyr provide the lowest $CO_2$ loading, likely due to steric hindrance and reduced basicity of the functional group.[159] More complex TS-IL formulations have been proposed with the aim of further improving the $CO_2$ capture and reduction of viscosity. MDEA has been studied in combination with [$N_{1111}$][Gly], [Bmim][Gly] and [Bmim][Lys] in aqueous solution.[106] It was found that a MDEA concentration of 30–40 wt% in MDEA-[Bmim][Gly] leads to

a loading capacity of in the range of 0.64 mol $CO_2$ mol $IL^{-1}$ largely outperforming MDEA/MEA and MDEA-DMA2P solvents with 0.55 mol $CO_2$ $mol^{-1}$ and 0.49 mol $CO_2$ $mol^{-1}$, respectively. Designer TS-ILs involving diethanol dimethyl ammonium ($E_2M_2A$) with glycinate (Gly) and MDEA showed outstanding $CO_2$ loading capacity at 303 K with compositions for MDEA/$H_2O$/[$E_2M_2E$][Gly] varying from 50–70 wt% of water and 0–20 wt% of [$E_2M_2E$][Gly] while keeping the concentration of MDEA constant at 30 wt%.[160] The highest capacity observed for the aqueous ternary mixture was 2.98 mol $CO_2$ kg $solvent^{-1}$ with superior performance to [Ch]Cl/amino acid IL with $CO_2$ loading capacity in the range of 0.26–1.07 mol $CO_2$ kg $solvent^{-1}$.

Superbases have also been proposed as counter anions in ILs; they offer high $CO_2$ uptake, but their performance is undermined by the presence of water or moisture. For example, [MTBDH][Im] displays a $CO_2$ loading capacity of 1.03 mol $CO_2$ mol $IL^{-1}$, remains in the liquid phase after saturation and can be regenerated at 353 K while flushing $N_2$ gas.[107] ILs composed of phenoxide or pyrazolonate ions with a phosphonium cation ($P_{66614}$) (Fig. 8a) show a loading capacity of 0.96, 0.43, 0.69 and 0.83 mol $CO_2$ mol $IL^{-1}$ for anions [3-HMPz], [5-HMPz], [1-HDMPz] and [1-HMPz], respectively (Fig. 8b). The best candidate [$P_{66614}$][3-HMPz] displays a maximum of a 30% increase in $CO_2$ loading upon increasing the pressure from 100 to 900 kPa (Fig. 8c) and high thermal stability as observed from TGA (Fig. 8d). The solvent can be regenerated over 10 cycles while losing *ca.* 5% performance (absorption at 298 K under ambient $CO_2$ pressure and desorption at 333 K under ambient $N_2$ pressure) (Fig. 8e). This performance is higher than that observed for early reported analogues including analogues which displayed $CO_2$ loading capacity in the range of 0.673–0.842 mol $CO_2$ $mol^{-1}$.[161] Superbase TS-IL comprising

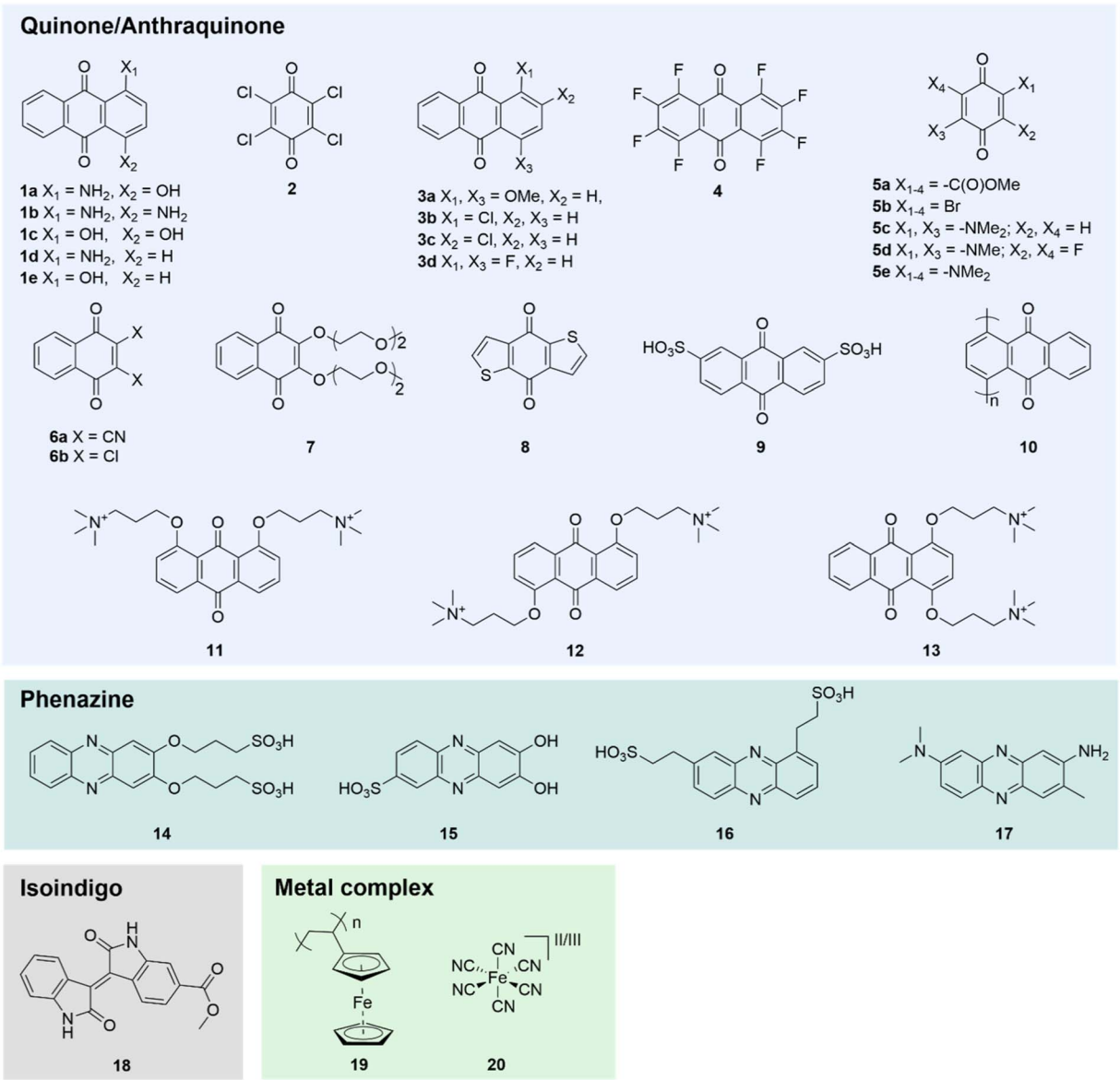


Fig. 10 Chemical structures of selected redox active compounds used in carbon capture organized by functional group.

 

Table 4 KPIs for selected redox active molecules

| Solvent | Rich loading (mol $CO_2$ $mol^{-1}$) | Regeneration energy (GJ $tCO_2^{-1}$)[a] | Regeneration temperature (K) | Gas composition[b] | Ref. |
|---|---|---|---|---|---|
| 7 | 1.1 | 1.14–4.55 | 295 | 15 vol% $CO_2$, 5 vol% $O_2$ | 180 |
| 8 | 1.6 | 2.45 | 295 | 13 vol% $CO_2$, 3.5 vol% $O_2$ | 79 |
| 9 | 0.5 | 1.12 | 303 | 15 vol% $CO_2$ gas | 173 |
| 10/19 | 1.9 | 0.91–2.05 | 298 | 0.6–10 vol% $CO_2$ | 78 |
| 14 | 2 | 1.39 | 298 | 10 vol% $CO_2$ | 168 |
| 15 | 2 | 0.49 | 298 | 15 vol% $CO_2$ | 72 |
| 16 | 1.76 | 1.25 | 298 | 10 vol% $CO_2$ | 169 |
| 17 | 0.71 | 0.80–1.25 | 298 | 15% $CO_2$ | 178 |
| 18 | 2 | 3.24 | 298 | 10 vol% $CO_2$ | 183 |

[a] Values originally reported in kJ $mol^{-1}$. [b] Balance with $N_2$.

benzimidazolide (Benzim) and trihexyltetradecylphosphonium ($P_{66614}$) shows a $CO_2$ loading of 0.78 mol $CO_2$ $mol^{-1}$ in the presence of $NO_2$ gas.[162] The loading capacity decreased 60% from the initial value after ten absorption/desorption cycles, evidencing the susceptibility of superbases to the presence of acidic impurities.

Recent research has extended IL applications beyond capture to electrochemical conversion[163] and chemical synthesis.[164,165] In these systems, ILs function not only as $CO_2$ absorbents but also as electrolytes or co-solvents in electrochemical cells for $CO_2$ reduction, enabling integrated capture-conversion cycles. Despite their promising physicochemical properties and potential industrial implementation, key challenges remain. Many ILs are poorly biodegradable and may pose toxicity risks due to their persistence and interaction with biological systems.[166,167] Similar to DESs, the energy requirements for regenerating these solvents are not broadly studied or reported in the literature, leading to limited understanding of the technology and their applicability in real-life scenarios.[45]

### 3.2. Redox active molecules

Redox-active molecules can capture $CO_2$ upon electrochemical reduction, a process known as electrochemically mediated carbon capture (EMCC).[68,78,168,169] After $CO_2$ is captured it is released after subsequent oxidation of the reduced redox-active species, following either a direct or indirect mechanism.[170,171] In the direct pathway or electro-swing, the reduced molecule reacts with $CO_2$, typically forming a covalent bond (Fig. 9a). In the indirect mechanism or pH swing, electrochemical reduction of water generates hydroxide ions, which subsequently react with $CO_2$ to form $HCO_3^-$ (Fig. 9b). EMCC is implemented in electrochemical flow cells, similar in design to redox flow batteries.[172] The specific system configuration varies depending on the capture mechanism.[170] In direct EMCC, $CO_2$ is introduced into the half-cell containing the redox-active molecule. While this allows direct interaction, it introduces challenges such as oxygen sensitivity: reduced organic species may be rapidly oxidized by dissolved oxygen, leading to efficiency losses. In the decoupled configuration, $CO_2$ is introduced into the opposite half-cell, avoiding direct contact with the redox-active molecule and improving tolerance to oxygen. In the latter case the organic electrolyte participates in an oxidation reaction leading to the reduction of water on the cathode to generate hydroxyl as the active carbon capture species (Fig. 9c).[173]

Electrochemical carbon capture offers a non-thermal regeneration route, relying only on electricity. This provides a path toward potentially lower regeneration energy and compatibility with intermittent renewable sources such as solar and wind. As a result, redox-active capture systems are being explored as scalable and energy-efficient alternatives to thermally driven absorption processes.[78] Several classes of molecules have been proposed for EMCC, including quinones and quinoidal systems,[63,68,69,132–137,174] phenazines,[168,169,175] pyridines,[69,175] disulfides,[176] and transition metal complexes.[177] The structures of selected examples of molecules studied in EMCC discussed in this section are presented in Fig. 10 and their KPIs are presented in Table 4. These systems are attractive due to their reversible redox behavior, synthetic accessibility, and potential for post-synthetic modification. However, many of these organic molecules exhibit low solubility in aqueous media and often require functionalization with solubilizing side chains, hydrotropes, or buffering agents to enable practical use.[170,178] Redox molecules for carbon capture are engineered to display the following features: (1) reversible redox species such as quinones, aromatic heterocycles, and transition metal complexes, (2) solubilizing groups such as alkylammonium, sulfonic acids and polyethylene glycol chains, and (3) redox potential outside the window of the oxygen evolution reaction (OER) and hydrogen evolution reaction (HER). Quinones[64,179] and quinoidal systems such as naphthoquinones[180] and anthraquinones[63,134–136,181] are amongst the most studied species in redox mediated carbon capture, as they are inexpensive and electrochemically reversible and their chemical structure can be easily modified. One of the former bottle necks of this family of molecules is that they are required to operate under anaerobic conditions, otherwise the hydroquinone intermediate is readily oxidized to its quinone analog, resulting in loss of efficiency in the carbon capture process limiting their application in DAC or PCC. The effect of the substituents on anthraquinone was systematically studied in compounds **1a–e** using cyclic voltammetry, spectro-electrochemistry and self-consistent charge density functional tight binding (SCC DFTB).[182] The results

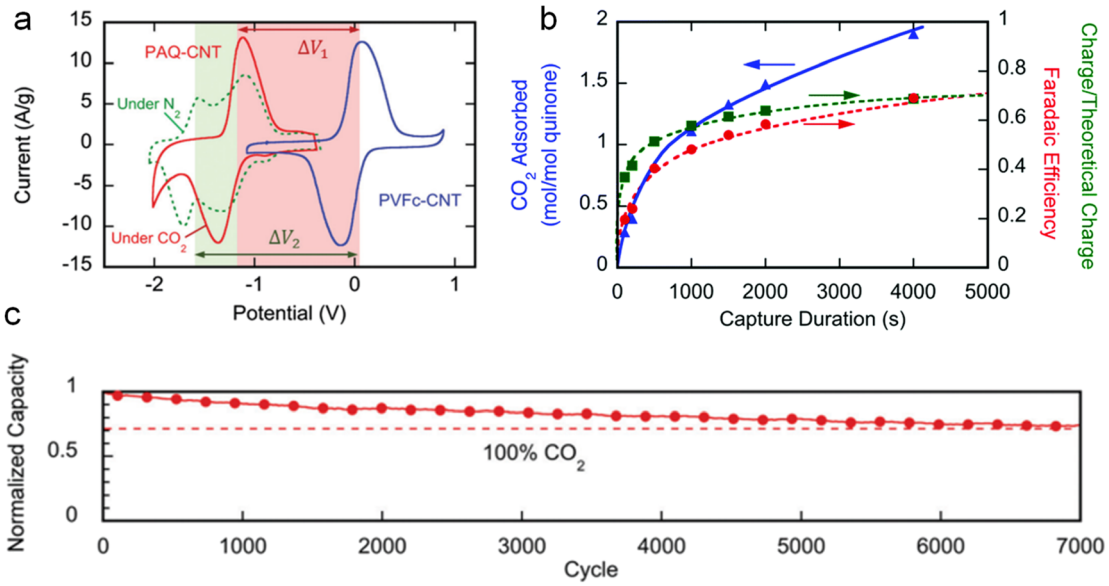


Fig. 11 (a) Superimposed cyclic voltammograms of **10** and **19** supported on carbon nanotubes recorded under $N_2$ and $CO_2$, highlighting the effect of $CO_2$ on the redox response. (b) $CO_2$ loading of 10 as a function of time at an applied potential of 1.8 V, approaching the theoretical maximum capacity of 2 mol $CO_2$ per mol of active species. (c) Cell capacity retention over 7000 charge–discharge cycles. Reproduced from ref. 78 with permission from the Royal Society of Chemistry, copyright 2019.

suggest that introduction of amine or hydroxyl groups in anthraquinone can lead to the stabilization of redox active radical species *via* hydrogen bonding which is crucial for capturing $CO_2$. Consistently, it was found that the oxygen stability of 2,3,5,6-tetrachloro-*p*-benzoquinone (**2**) can be further improved by addition of 2 mol $dm^{-3}$ EtOH to DMF.[70] Furthermore, the influence of substituents on the anthraquinone backbone was examined across a series of –F–, –Cl, –OMe and –OH functionalized AQs (**3a–d**), showing that shifting the two-electron reduction potential to more positive values lowers the energetic cost of activation but simultaneously weakens $CO_2$ binding. In other words, there is a clear, approximately linear trade-off between redox potential and capture strength ($\Delta G$ for the chemical step becomes less negative as potential becomes more positive).[65] To obtain a favorable outcome, for example, reduced reduction overpotential without sacrificing $CO_2$ affinity in the capture step free energy must remain sufficiently exergonic, a balance that is illustrated for perfluorinated AQs (**4**). Similar studies were performed for a set of quinones using functionalities such as –CN, –Cl, –Br, –F, –$NMe_2$, and–COOMe (**5a–e** and **6a–b**).[179] Glyme-functionalized naphthoquinone (**7**) was tested using an electrochemical flow cell using diglyme as the solvent and a ferrocene derivate as the counter electrolyte.[180] The system displayed an energetic cost of $CO_2$ capture in range of 1.14–4.55 GJ $tCO_2^{-1}$ at the early stage of the EMCC process, although a reduction in overall capture-release efficiency from 100% to about 80% was observed when a synthetic flue gas mimicking that of a PCC (15 vol% $CO_2$. 5 vol% $O_2$, and 80 vol% $N_2$) was used. Benzodithiophene quinone (**8**) showed excellent $CO_2$ stability under simulated flue gas conditions of 3.5 vol% $O_2$ and 13 vol% $CO_2$ and the flow system was stable over the testing period of 20 cycles with an electrochemical work of 2.45 GJ $CO_2^{-1}$.[79] More advanced setups involving decoupling of electrolyte anthraquinone-2,7-disulfonate (**9**) from interacting with the flue gas but rather serve as an electron reservoir to induce reduction of water in the counter electrode permit avoidance of oxidation of the organic electrolyte (Fig. 9c). The active capture agent is a hydroxyl ion which reacts with $CO_2$ with the inlet gas to form $HCO_3^-$. Then $HCO_3^-$ is transferred to the organic electrolyte reservoir *via* an anionic exchange membrane when the $HCO_3^-$ rich solution reaches a reservoir at pH = 6 inducing release of $CO_2$ gas. The anthraquinone then reduces in an adjacent flow reactor with $H_2$ gas and Pt. The system showed good tolerance to oxygen when using a flue gas composition of 15 vol% $CO_2$, 5 vol% $O_2$ and 80 vol% $N_2$ with an energetic efficiency of 1.12 GJ $tCO_2^{-1}$, a high $CO_2$ removal efficiency of 99.6% and a desorption of 99.5%, and therefore a very low lean loading during each cycle. Poly(anthraquinone) (**10**)/polyvinylferrocene (**19**) electrolytes are one of the most prominent technologies in EMCC.[78] Both electrolytes are supported on carbon nanotubes which are stacked inside the electrochemical cells and thus no liquid solvent is required (Fig. 9a). The cyclic voltammogram of the electrolytes under $N_2$ shows two reduction potentials, $E_1 = -1.21$ V and $E_2 = -1.63$ V *vs.* Fc. In the presence of $CO_2$, these collapse into a single quasi-reversible redox couple at $E_{01}$ (Fig. 11a). The double carboxylation of anthraquinone to form the bis(carbonate) dianion proceeds *via* a two stepwise one-electro transfer chemical reaction process (ECEC) mechanism. Extending the capture time to 4000 s at a fixed potential of −1.8 V yields a maximum $CO_2$ capture ratio of 1.9 mol $CO_2$ per mol anthraquinone, approaching the theoretical limit of 2.0 (two $CO_2$ per quinone unit) (Fig. 11b). Remarkably, the electrochemical cell displays a removal efficiency of 100% $CO_2$ over 7000 absorption/desorption cycles

 

(Fig. 11c). An energy equivalent to 0.91 GJ $tCO_2^{-1}$ is required to regenerate the solvent when a feed gas containing 10 vol% $CO_2$ is used. Currently, this technology is being developed by MIT spin-off Verdox. Phenazines have emerged as a promising alternative to quinones because of their higher tolerance to oxidation in the reduced form.[168,169,175] Although they do not form a covalent adduct with $CO_2$, they serve as efficient mediators for indirect capture *via* the reduction of water to hydroxide ions ($OH^-$). A pH-swing process employs sodium 3,3'-(phenazine-2,3-diylbis(oxy)bis(propane-1-sulfonate)) (**14**), where reduction generates $OH^-$ *in situ* to capture $CO_2$ as $HCO_3^-$; the cycle is reversed by acidifying the medium and applying an oxidation potential to release $CO_2$, giving an electrochemical work of 1.39 GJ $tCO_2^{-1}$ depending on operating conditions.[168] To further counter $O_2$-induced drift and capacity loss as a result of loss in coulombic efficiency, chemical rebalancing can be invoked at intervals where the posolyte is deliberately reduced while the negolyte is driven to oxidize accumulated $OH^-$ to $O_2$, thereby removing excess base, restoring the original state-of-charge/pH balance, and recovering the full working capacity of the cell. Similarly, 7,8-dihydroxyphenazine-2-sulfonic acid (**15**) delivers ~96% current efficiency at 10 mA $cm^{-2}$ with 0.49 GJ $tCO_2^{-1}$ electrical work, and the chemistry is compatible with periodic electrochemical rebalancing to correct $O_2$-driven drift.[72] 2,2′-(phenazine-1,8-diyl) bis(ethane-1-sulfonate) (**16**) is highly soluble across acidic and alkaline media and shows strong $O_2$ tolerance, maintaining coulombic efficiencies of 89% and 82% with 10 and 20 vol% $O_2$ in the inlet gas, respectively.[169] Under optimized conditions it achieves a loading capacity of 1.75 mol $CO_2$ $mol^{-1}$, competitive with leading amine and amino-acid solvent systems, and exhibits only ~9% capacity fade over 1200 cycles with an energetic cost of 1.25 GJ $tCO_2^{-1}$ at 10 mA $cm^{-2}$. Another representative example of phenazine for EMCC is neutral red (**17**), which operates effectively for both PCC and DAC and remains stable in air; the electrochemical work scales with inlet $CO_2$ concentration, requiring 0.80 GJ $tCO_2^{-1}$ at 15 vol% $CO_2$ and 1.25 GJ $tCO_2^{-1}$ at 410 ppm CO, highlighting its versatility in concentrated and dilute feed gas.[178] Isoindigo-based systems have been evaluated for their $CO_2$ capture performance and electrochemical tunability.[183] In a systematic study involving 21 isoindigo derivatives, compound **18** was identified as the most

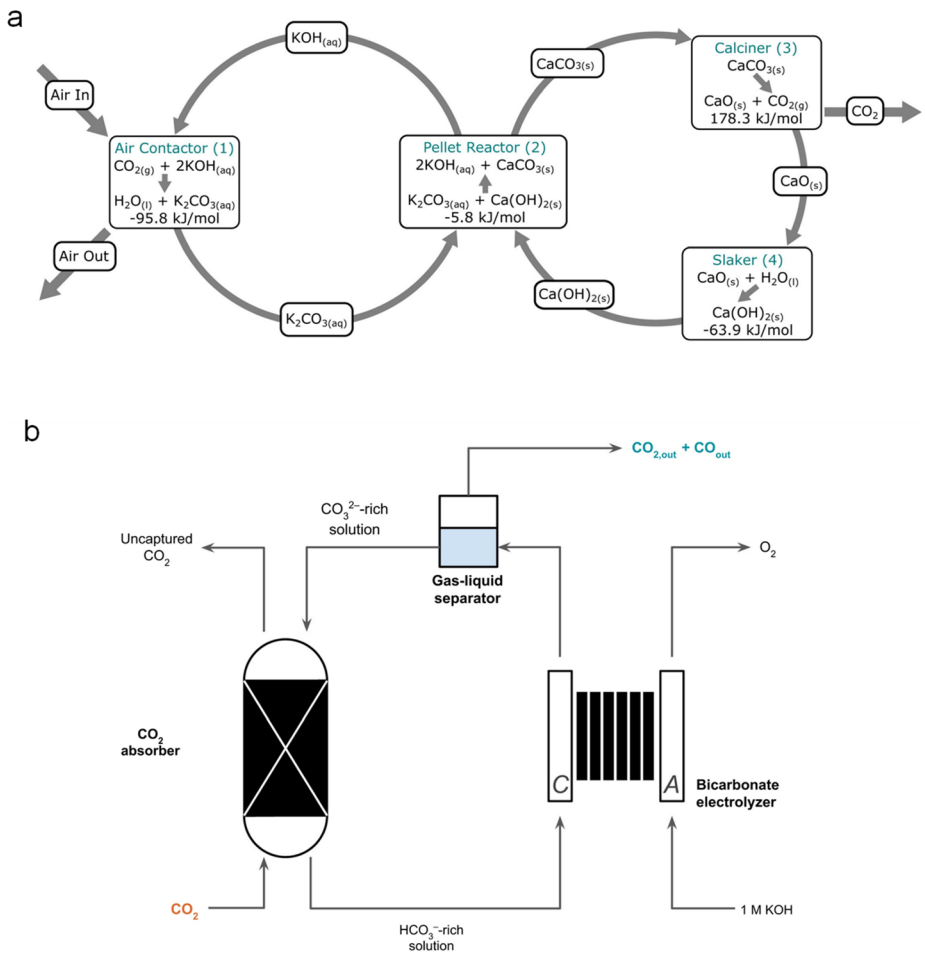


Fig. 12 (a) DAC process using an aqueous KOH absorbent coupled to a calcium looping regeneration cycle. Reproduced from ref. 33 with permission from Elsevier, copyright 2018. (b) Integrated $CO_2$ capture and conversion scheme in which $CO_2$ is absorbed into an alkaline solution to form a bicarbonate-rich reactive carbon stream, which is subsequently fed to a reactive carbon electrolyzer for conversion. Reproduced from ref. 205 with permission from Elsevier, copyright 2024.

promising candidate due to its ability to disrupt the typical linear free energy relationship between redox potential and $CO_2$ binding affinity. The authors note that the amine functionality in the indigo backbone facilitates hydrogen bonding with the carbonate increasing the stability of the intermediate and maintaining a favorable redox potential of approximately −0.9 V *vs.* ferrocene. Futhermore, compound **19** displayed a removal efficiency of >90% with a synthetic feed gas composition of 10 vol% $CO_2$ and an energy consumption of 3.24 GJ $CO_2^{-1}$ during a 16 charge/discharge cycle test. In an electrochemical strategy for DOC, the iron complex $K_3/K_4[Fe(CN)_6]$ (**20**) is used as an electron reservoir to carry out the water splitting reaction in sea water to capture $CO_2$ using a bipolar membrane electrodialysis (BPM) cell.[177] The system displays a capture efficiency of 71% of dissolved $CO_2$ and an electrochemical energy consumption of 3.53 GJ $CO_2^{-1}$. In this system configuration the seawater is recirculated through the BPM stack and directed to membrane contactors with a cold trap for $CO_2$ extraction and gas-phase collection.

Combination of experimental and DFT theoretical work has further laid down the foundations for electrolyte design using nitrogen heterocycles, especially mechanistic insight.[175] The results suggest that dibasic Lewis bases such as 4,4′-bipyridine, quinoxaline, phenazine, 2,1,3-benzothiadiazole, azobenzene and azopyridine follow a ECEC mechanism per nitrogen atom, together with redox potentials suggesting that in EMCC the $CO_2$ is indeed stabilized in the form of carbamate. Additionally, azopyridine and phenazine showed the longest N–C bond, therefore requiring a lower overpotential to release $CO_2$. The role of H-bonding and electron withdrawing groups in the stabilization of $CO_2$ has been elucidated on isoindigos using DFT, suggesting that intramolecular hydrogen bonding between N–H groups and $CO_2$ stabilized as carbonate plays a crucial role in breaking the linear relationship between the $CO_2$ binding constant and electrochemical energy required to release $CO_2$.[183] Advanced *in situ* methods were recently reported for aqueous anthraquinone systems (**11–13**),[184] where an *in situ* reference-electrode is used to determine voltage signatures to deconvolute quinone *vs.* quinone-$CO_2$ adduct contributions. Furthermore, the electrode is coupled to the fluorescence-microscopy method that exploits the adduct's emission at wavelengths characteristic of the reduced form, enabling sub-second and micrometer-scale speciation during redox cycling and flow operation. These tools clarify speciation, kinetics, and the interplay between nucleophilicity-swing and pH-swing mechanisms.

Unlike conventional thermal-swing solvents, redox-active $CO_2$ capture remains a comparatively early-stage technology and therefore faces pronounced challenges upon scale-up.[173,185] Although the approach is modular and compatible with renewable electricity, the electrochemical stack (including membranes, electrodes, and hardware) can dominate capital costs.[185,186] In addition, membranes and separators can undergo swelling, crossover, and fouling during extended operation, increasing resistance and maintenance requirements and sometimes necessitating cell disassembly and cleaning. Importantly, performance does not necessarily scale linearly with geometric area: as systems are enlarged, ohmic losses, mass-transfer limitations, and non-uniform current distribution can increase the work required per unit $CO_2$ captured, reducing economic and energetic viability. For example, for an anthraquinone derivative (compound **9**), scaling from a 4 $cm^2$ cell to a 1008 $cm^2$ cell was reported to increase the regeneration energy by approximately two-fold, from 1.12 GJ $tCO_2^{-1}$ $CO_2$ at the lab scale to 2.11 GJ $tCO_2^{-1}$ in the upscaled device.[173]

Many high-performing redox-active organic mediators exhibit limited solubility in aqueous electrolytes, motivating the introduction of solubilizing substituents which often represents a significant synthetic burden that can also shift redox potentials and stability. Alternatively, dissolution in organic media can alleviate solubility constraints but introduces additional requirements for solvent safety, environmental acceptability, and lifecycle impacts. Finally, despite rapid progress toward oxygen-tolerant mediators, aerobic oxidation and side reactions under oxygen-containing feed gas remain key limitations. While many report oxygen stable molecules at a working temperature of 293–303 K it is not clear if molecules would react in the presence of hot flue gas. Further understanding of molecular stability under hot flue gas may elucidate additional process control parameters such as cooling of the flue gas representing additional cost to the capture plant.

Redox-active molecules thus represent a versatile and rapidly advancing class of carbon capture solvents, offering electrochemically driven operation, tunable redox properties, and potential for integration with renewable electricity. Their diversity provides multiple mechanistic pathways for $CO_2$ binding, spanning direct covalent adduct formation to indirect pH-swing capture. Nevertheless, challenges remain, particularly in enhancing oxygen tolerance, improving long-term cycling stability, and balancing redox potential with binding affinity to minimize energy penalties.

### 3.3. Inorganic bases

Inorganic bases have been explored as simple and low-cost materials for $CO_2$ capture, primarily through the formation of carbonate or $HCO_3^-$ species in aqueous or solid-phase systems. Their mechanism typically relies on the alkaline reactivity of cations such as potassium ($K^+$), calcium ($Ca^{2+}$),[187] or magnesium ($Mg^{2+}$)[188,189] in the presence of hydroxide, oxide or carbonate counterions to react directly with $CO_2$ to form thermodynamically stable carbonate species. Systems such as potassium hydroxide,[190] potassium carbonate,[191] and calcium hydroxide[192] or a combination thereof such as in ref. 33 have been widely studied in both batch and continuous processes, including applications in DAC and PCC. Other inorganic species, such as boronic acid, potassium phosphate, arsenic oxide and vanadium oxide have also been proposed as $CO_2$ capture promoters in potassium carbonate solutions; however, their complex pH-dependent speciation ($VO_2$, $B(OH)_3$, and $As(OH)_3$) in solution and their intrinsic toxicity ($AsO_3$ and $VO_2$) limit their application in the industrial sector.[193] The main advantage of inorganic bases lies in their abundance, low cost, and strong basicity, which allows for fast reaction kinetics under appropriate

 

Table 5 KPIs for selected porous materials

| Material | Rich loading (mmol $CO_2$ $g^{-1}$) | Regeneration energy (GJ $tCO_2^{-1}$)[a] | Regeneration temperature (K) | Gas composition[b] | Ref. |
|---|---|---|---|---|---|
| CALF-20 | 1.2–3.0 | — | 423 | 17% $CO_2$, 5% $H_2O$, 10% $O_2$ | 206 |
| $NH_2$-MFM-136 | 4.35 | — | 393 | 15% $CO_2$ | 207 |
| MOF-808-Lys | 0.612 | — | 393 | 400 ppm $CO_2$ | 208 |
| PEI@UiO-66-$NH_2$ | 3.2 | 1.55 | 393 | 15 vol% $CO_2$, 85 vol% $N_2$ | 209 |
| COF-999 | 0.96–2.05 | 5.89 | 333 | 0.4 vol% $CO_2$ | 210 |
| COF-609 | 0.393 | — | — | 0.4–15 vol% $CO_2$ | 211 |
| TTPEPOP-S | 2.94 | — | | 100 vol% $CO_2$ | 212 |
| Triptycene-ketone | 3.15 | — | 393 | 100 vol% $CO_2$ | 213 |
| HPC-$NH_2$ | 9.41 | — | 410 | 100 vol% $CO_2$ | 214 |
| pTTPA-4 | 3.31 | — | 373 | 100 vol% $CO_2$ | 215 |
| COF-301-PL | 7.04 | — | — | 100 vol% $CO_2$ | 216 |

[a] Values originally reported in kJ $mol^{-1}$. [b] Balance with $N_2$.

temperature and humidity conditions. For instance, calcium hydroxide reacts with $CO_2$ to form calcium carbonate in a highly exothermic process named calcium looping which requires high thermal energy to turn $CaCO_3$ into CaO.[194,195] While effective, this capture limits regeneration and makes such systems more economically suited for mineralization-based storage rather than cyclic capture. In contrast, salts like potassium carbonate operate reversibly in aqueous media and have been used in conventional absorption flow systems such as scrubbers and RPBs.[191,196]

Regeneration is typically achieved through heating, though the associated energy penalties are significant, and as such chemical swing has proven to be more economically feasible for regeneration of inorganic aqueous solvents. A remarkable example of chemical swing coupled to thermal regeneration (calcination) involves cycling KOH to capture $CO_2$ as $K_2CO_3$ and then regenerate KOH by a chemical reaction between $K_2CO_3$ and $Ca(OH)_2$ leading to the formation of insoluble $CaCO_3$ which is in turn regenerated by calcination at 1073 K (Fig. 12a).[33] Despite their operational simplicity, aqueous carbonate systems suffer from low $CO_2$ loading capacity per unit mass of solvent and reduced performance under low partial pressures. In solid-phase systems, alkali and alkaline earth metal oxides or hydroxides are used in packed beds or sorbent loops, though their deployment is constrained by the high energetic requirements for regeneration in the calcination process.[197] Moisture and temperature play a critical role in modulating both capture efficiency and structural stability of these materials. Notwithstanding this, novel technologies have proposed the use of $HCO_3^-$ and carbonate electrolyzers for the regeneration of hydroxide-based solvents by electrochemical reduction of $HCO_3^-/CO_3^{2-}$ species ($HCO_3^{-1}/CO_3^{2-}$) in the rich solvent, to produce high-purity $CO_2$ gas and regenerate $OH^-$ as the reactive capture lean solvent (Fig. 12b).[35,198,199] One of the advantages already discussed in Section 3.2 is that electrochemical regeneration does not require thermal energy, offers a theoretical 100% energy efficiency and can be plugged directly into renewable sources of electricity. It is worth noting that the authors report that electricity required for solvent regeneration accounts for the majority of the operational expenditure (approximately 39%), a value comparable to that observed in thermal solvent regeneration processes.[64] Other inorganic materials for reactive capture in the solid state have been proposed such as tetraperoxotitanates of Li, Na and K ($A_4Ti(O_2)_2$ with A = , Li, Na, K)[200] for DAC and lithium orthosilicate ($Li_4SiO_4$) for PCC.[201,202] Overall, inorganic base systems such as aqueous KOH, $K_2CO_3$, and $CaO/Ca(OH)_2$ provide high $CO_2$ capacities and chemical stability, with strong performance under DAC and flue gas conditions. However, regeneration typically requires high-grade thermal input (up to 800 °C for calcination) which limits implementation. Despite their simplicity and robustness, these systems demand significant energy integration strategies to be viable at scale. Integration of amines or enzymes into carbonate-based solvents has been proposed to improve $CO_2$ solubility and reduce regeneration temperature; however, in such cases inorganic additives are used in the concentration range of 5–15 wt%.[191,203,204]

### 3.4. Porous materials

Porous materials such as MOFs, POPs, COFs and PLs offer several benefits relative to both traditional liquid solvents: high and tunable $CO_2$ capacity under mild conditions, structural versatility enabling selective gas capture, no volatility or degradation products typical of amine solvents, and compatibility with modular solid-sorbent systems and fixed-bed reactors.[206] Additionally, their ability to be processed into mixed-matrix membranes or composites expands their applicability beyond packed beds, potentially enabling their integration into membrane-based separation units or hybrid systems for DAC applications. We provide a perspective on these materials' performance and their design strategies below. The KPIs of representative examples are presented in Table 5.

**3.4.1. Metal–organic frameworks (MOFs).** MOFs are a class of crystalline porous materials formed by the coordination of metal ions or clusters with organic linkers.[217,218] Their high internal surface areas, tuneable pore structures, and chemical modularity have made MOFs one of the most studied families of solid sorbents for $CO_2$ capture.[51,52,219,220] In contrast to traditional solvents and amorphous sorbents, MOFs offer precise

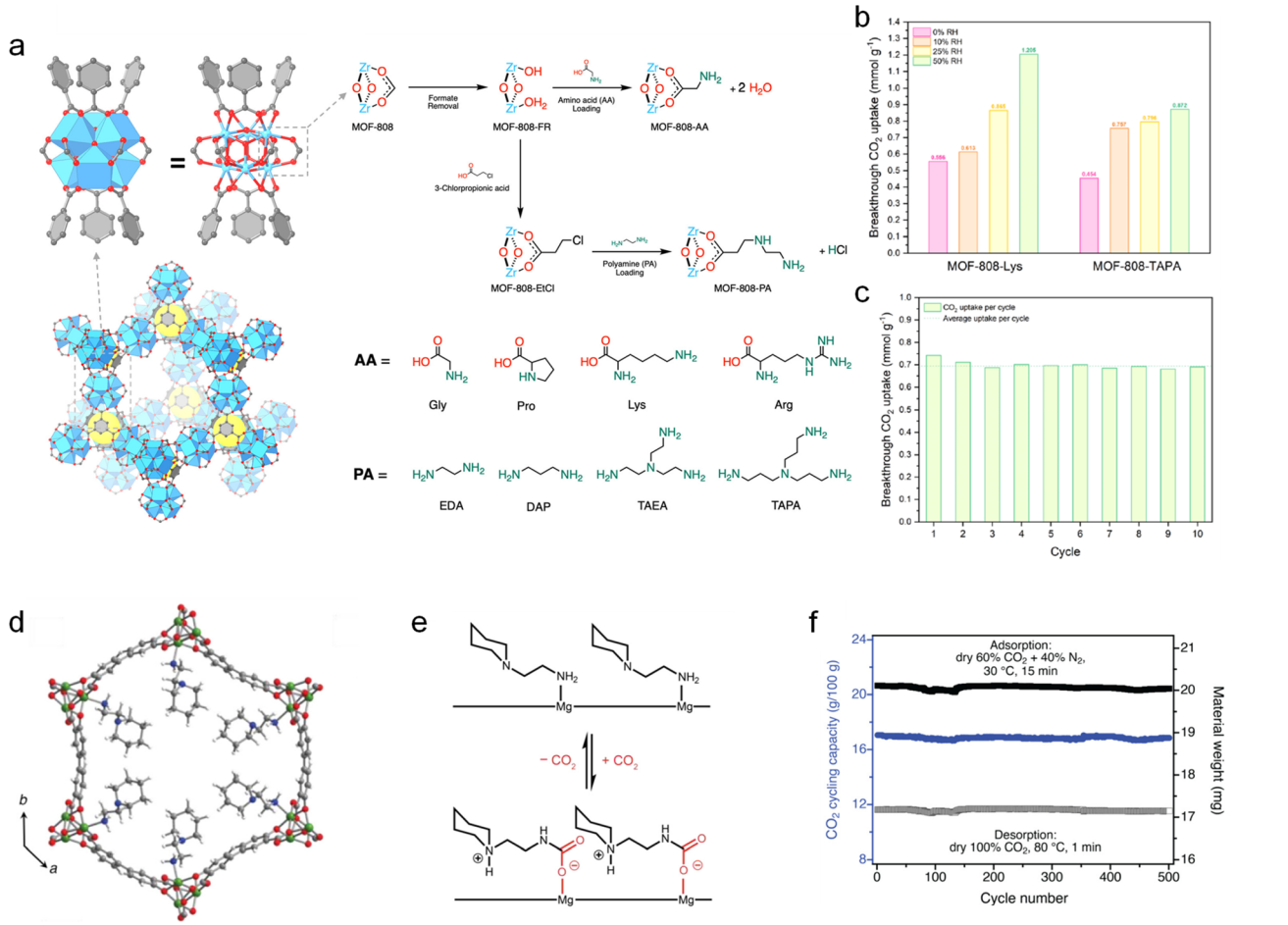


Fig. 13 (a) Chemical structure of MOF-808 and a general post-synthetic functionalization route. (b) Comparison of $CO_2$ loading capacities of MOF-808-Lys and MOF-808-TAPA as a function of relative humidity (RH). (c) $CO_2$ uptake of MOF-808-Lys measured at 400 ppm $CO_2$ and 50% RH. Reproduced from ref. 208 with permission from the American Chemical Society, copyright 2024. (d) Chemical structure of $Mg_2$(dobpdc) functionalized with appended 1-(2-aminoethyl)piperidine units. (e) Proposed $CO_2$ capture mechanism. (f) Repeated absorption/desorption cycling performance of $Mg_2$(dobpdc)-(1-(2-aminoethyl)piperidine). Reproduced from ref. 231 with permission from the American Chemical Society (CC BY), copyright 2024.

control over pore geometry and surface functionality, enabling rational design of materials tailored for specific gas separation and capture applications.[217] MOFs can achieve surface areas exceeding 3000 $m^2\ g^{-1}$ and pore volumes >1 $cm^3\ g^{-1}$, allowing for significant gas uptake under appropriate conditions. Their modular nature permits fine-tuning of adsorption sites *via* the choice of metal nodes (*e.g.*, Cu, Zn, Zr, Al, and Fe) and organic linkers (*e.g.*, carboxylates, azolates, and pyridines) *via* the hard–soft acid–base theory.[221–224] Compared to conventional liquid sorbents, MOFs often require lower regeneration energy, especially those that rely on physisorption or moderate chemisorption.

Temperature-swing and pressure-swing adsorption are the most common regeneration strategies, and several studies report working capacities above 2 mmol $g^{-1}$ under cyclic conditions. However, the actual cycling capacity is highly dependent on material stability over multiple adsorption–desorption cycles. Despite their promising performance, several challenges limit the large-scale deployment of MOFs for carbon capture: moisture sensitivity (many high-performance MOFs, such as copper-based HKUST-1,[225] exhibit structural degradation in humid flue gas environments),[226,227] thermal and oxidative stability (some frameworks degrade at industrial operating temperatures or under oxidizing conditions),[228] cost and scalability (the synthesis of MOFs often involves expensive metal salts or complex linkers), and form factor (most MOFs are synthesized as powders, which are difficult to pack and shape into mechanically stable structures for process-scale adsorption units).

A remarkable example with current application in the industry is Calgary Framework-20 (CALF-20) with a general composition of [$Zn_2$(1,2,4-triazolate)$_2$(oxalate).[206] This MOF is a steam-durable, water-tolerant physisorbent that has been scaled from lab to tonne-scale production and its performance has been demonstrated on real flue gas. In CALF-20 the main interaction with $CO_2$ was attributed to dispersion forces (van der Waals forces ≈86% of the binding energy at 20% relative humidity (RH) and electrostatics ≈14%), and although

 

interactions are weak, the nitrogen atom actually contributes to the stabilization of $CO_2$. These weak interactions are consistent with rapid, reversible physisorption and a low enthalpic regeneration penalty.[229] CALF-20 displays a high loading capacity in the range of 1.2–3.0 mmol $CO_2$ $g^{-1}$ at temperatures ranging from 30 to 373 K. In pilot tests, the flue gas composition was adjusted to resemble a cement-kiln factory (≈17% $CO_2$, 10% $O_2$, 5% $H_2O$, 60 ppm NO and 12 ppm $NO_2$). The CALF-20 beds were tested continuously exceeding 2000 h of operation without appreciable performance loss.[206] The robust material has shown consistent performance in bulk-scale preparation of CALF-20 in 300 kg batches and displays high steam stability with high tolerance tested over 450 000 wet–steam cycles.

The incorporation of amines into the pores of MOFs has proven successful for enhancing low-pressure working capacity and flue-gas discrimination without sacrificing stability. Primary amine incorporation on the linking building blocks is a well-established route to increase low-pressure $CO_2$ adsorption and improve flue-gas performance in MOFs. MFM-136, a Cu-based MOF constructed from 5-(4-(pyrimidin-5-yl) benzoylamino)isophthalic acid, was post-synthetically functionalized with $-NO_2$ or $-NH_2$ groups, with the amine substitution yielding the greatest enhancement.[207] The optimized $NH_2$-MFM-136 exhibited a $CO_2$ uptake of 4.35 mmol $g^{-1}$, approximately 55% higher than that of pristine MFM-136, and delivered a 1.57-fold improvement in $CO_2/N_2$ selectivity. Amination also increased hydrophobicity and resistance to impurity gases after 24 h exposure to simulated flue gas. Furthermore, $NH_2$-MFM-136 retained substantially more capacity, with a 34% lower loss than the non-aminated framework, highlighting its improved stability under realistic operating conditions.

Post-synthetic functionalization of MOF-808 $[Zr_6O_4(OH)_4(BTC)_2(HCOO)_6$, BTC = 1,3,5-benzenetricarboxylate] with amino acids and polyamines produces a moisture stable material that can efficiently operate under DAC conditions with a $CO_2$ capture stoichiometry of *ca.* 1 : 1 $CO_2$/amine (Fig. 13a).[208] Remarkably, MOF-808-Lys and MOF-808-TAPA (TAPA = tris(3-aminopropyl) amine) reach 0.612 and 0.498 mmol $CO_2$ $g^{-1}$ at 400 ppm $CO_2$ (dry), increasing to 1.205 and 0.872 mmol $CO_2$ $g^{-1}$ at 50% RH (Fig. 13b). MOF-808-Lys showed consistent $CO_2$ capture performance under DAC gas composition (400 ppm) over 10 absorption/desorption cycles with an average $CO_2$ release of 0.696 mmol $CO_2$ $mmol^{-1}$ $cycle^{-1}$ (Fig. 13c). Similarly, post-synthetic impregnation of UiO-66-$NH_2$ with polyethyleneimines (PEIs) markedly boosts $CO_2$ uptake and selectivity by introducing primary/secondary amines that chemisorb

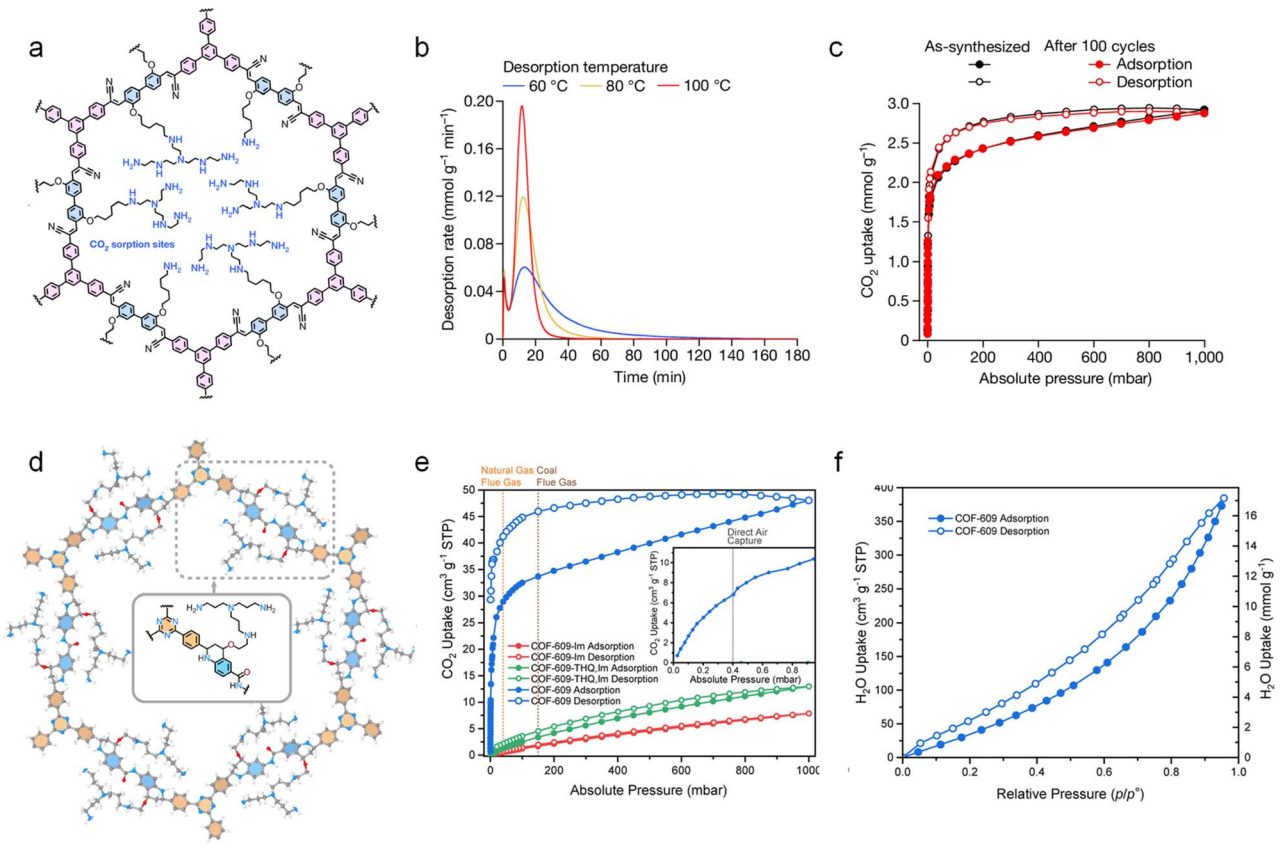


Fig. 14 (a) Chemical structure of COF-999. (b) $CO_2$ desorption profiles of COF-999 at 333 K (blue), 353 K (yellow), and 373 K (red). (c) Single-component $CO_2$ adsorption isotherms of COF-999 measured after 100 DAC cycles, highlighting cycling stability. Reproduced from ref. 210 with permission from Springer Nature, copyright 2024. (d) Chemical structure of COF-609. (e) Single-component $CO_2$ adsorption isotherms for COF-609-Im, COF-609-THQ, and pristine COF-609. (f) Single-component $H_2O$ adsorption isotherm of COF-609 measured at 298 K. Reproduced from ref. 211 with permission from the American Chemical Society, copyright 2024.

$CO_2$ while the UiO pore network preserves diffusion and suppresses amine volatilization.[209,230] The optimized PEI@UiO-66-$NH_2$ sample increased $CO_2$ loading capacity from *ca.* 2.7 to *ca.* 3.2 mmol $CO_2$ $g^{-1}$ and doubled $CO_2/N_2$ selectivity from 25 to 48, while maintaining recyclability and superior moisture endurance relative to the pristine MOF.[209] Other examples of postfunctionaliztion in MOFs involve amine appended $Mg_2$(dobpdc) (dobpdc$^{4-}$ = 4,4′-dioxidobiphenyl-3,3′-dicarboxylate) and $Mg_2$(olz) (olz$^{4-}$ = (*E*)-5,5′-(diazene-1,2-diyl)bis(2-oxidobenzoate)) MOFs to induce a dual $CO_2$ capture effect promoted by direct carbamate formation and $CO_2$ adsorption.[231,232] Remarkably, this type of MOF, unlike MOF-808, has the $CO_2$ active ligands attached to the metal center *via* amine coordination instead of carboxylates (Fig. 13d). This type of M–N bond leads to a $CO_2$ absorption mechanism through the formation of metal stabilized carbamate (Fig. 13e). Furthermore, the MOF $Mg_2$(dobpdc) with appended 1-(2-aminoethyl) piperidine units displays outstanding cycling capacity with a constant loading capacity of 3.83 mmol $CO_2$ $g^{-1}$ over 500 absorption/desorption cycles using simulated flue gas with a composition of 60 vol% $CO_2$ in $N_2$ (Fig. 13f).[231] Together these examples illustrate a robust "amine-in-pore" route for enhancing low-pressure working capacity and flue-gas discrimination without sacrificing stability.

Furthermore, novel synthesis techniques for bottom-up construction of MOFs such as heteroepitaxial $Zn_2L_2$DABCO films (L = functionalized benzene-1,4-dicarboxylic acid; DABCO = 1,4-diazabicyclo[2.2.2]octane) show that adding amine functionality on the linker (–$NH_2$–BDC) and introducing molecular guests within the pores can modulate $CO_2$ uptake at near-ambient pressure *via* reversible, stimulus-responsive (light/temperature) pore transitions-demonstrating fast, fully reversible physisorption in films relevant to device integration.[233] Post-functionalization of $Mg_2$(dobpdc) and $Mn_2$(dobpdc) with diamines containing alkyl side chains improves the amine loss observed in previous analogues. Although this technique has only recently been applied to the design of MOFs for $CO_2$ capture, the strategy further improves $CO_2$ uptake, reduces regeneration temperature and increases stability over two cycles in Mn-based MOFs compared to its Mg-based analog.[234]

**3.4.2. Covalent-organic-frameworks (COFs).** COFs are porous, crystalline polymers built from light elements (C, B, N, O, and H). Their modular linkages (*e.g.* boronate ester, imine, β-ketoenamine, triazine, and imide) set stability and adsorption behavior. In general, unfunctionalized COFs capture $CO_2$ mainly by physisorption, while post-functionalized amine COFs show chemisorption under atmospheric conditions[235] Design strategies to improve capture performance include pore design, post-synthetic addition of polar groups, for example, incorporation of amines containing building blocks[236,237] and post-functionalization of porous structures with amines.[210,211,235,238,239] Two-dimensional diamine-linked imine COFs containing backbone amine sites preferentially adsorb $CO_2$ over $N_2$, but these functionalities are often too weakly basic or sterically hindered to enable efficient chemical $CO_2$ capture at atmospheric $CO_2$ concentrations.[240,241] Studies on model lattices such as IPB-1H and IPB-2H, constructed from a 1,3,5-tris(chloromethyl)benzene node with *p*-diamine or *p*-dihydrazine benzene linkers, report $CO_2$ capacities of 0.767 mmol $g^{-1}$ (IPB-1H) and 0.902 mmol $g^{-1}$ (IPB-2H) under pure $CO_2$ at 298 K and 100 kPa.[241] IPB-2H outperforms IPB-1H due to the presence of an additional aromatic ring in its linker, which enhances π–π interactions improving $CO_2$ adsorption. While larger pores improve overall gas permeability, they tend to reduce $CO_2/N_2$ selectivity, highlighting that low-pressure $CO_2$ capture is governed primarily by tailored pore chemistry and electrostatic interactions rather than pore size alone. For comparison, a triazine/imine porous polymer made from 1,3,5-tris(4-aminophenyl)triazine (TAPT) and terephthaldehyde shows very low uptake at 298 K and 100 kPa, but it increases sharply at 273 K and 500 kPa with loadings of 13.38 mmol $g^{-1}$ (*ca.* 58.9 wt%) illustrating that backbone functionality without targeted pore-wall sites does not deliver strong capture under atmospheric conditions.[240]

Post-functionalization of COFs with polar groups such as carboxylic acids[242] and alkylamines[210,211] has proven successful to overcome the limitations associated with $CO_2$ absorption under atmospheric conditions. For example, building a 2D porphyrin COF by three-component condensation involving tetra-4-aminoporphyrin (TAP) with a 2,5-dihydroxyterephthalaldehyde (DHTA) and 1,4-phthalaldehyde (PA), followed by then functionalizing the OH with –COOH capped alkyl chains, shrinks the pore sizes from *ca.* 2.2 nm to 1.4 nm, and leads to improved room-temperature $CO_2$ uptake from 31–35 mg $g^{-1}$ (0.70–0.80 mmol $g^{-1}$) to 76 mg $g^{-1}$ (*ca.* 1.73 mmol $g^{-1}$).[242] This illustrates how introduction of polar groups on the channel walls enhances $CO_2$ loading capacity without increasing surface area. Imidazation of tris(4-aminophenyl)amine (TAPA) or 1,3,5-tris(4-aminophenyl) benzene (TAPB) with pyromellitic dianhydride (PMDA) or 1,4,5,8-naphthalenetetracarboxylic dianhydride (NTCDA) affords four robust frameworks with stability up to 793–808 K.[236] At 273 K and 100 kPa, these materials exhibit a $CO_2$ loading in the range of 51–66 $cm^3$ $g^{-1}$, with BET areas spanning the range of 580–1430 $m^2$ $g^{-1}$.

A notable recent advance in COFs for DAC is the olefin-linked framework COF-999 (Fig. 14a), whose pores accommodate branched polyamine chains that can capture $CO_2$ from ambient air (~400 ppm).[210] Under dry conditions, COF-999 achieves a $CO_2$ loading capacity of 0.96 mmol $CO_2$ $g^{-1}$, which increases to 2.05 mmol $CO_2$ $g^{-1}$ at 50% RH, and reaches half capacity within 18.8 min at 298 K in humid air. This material can be regenerated under mild conditions with desorption rates of 0.06, 0.12, and 0.19 mmol $CO_2$ $g^{-1}$ $min^{-1}$ at 333 K, 353 K, and 373 K, respectively, releasing 80% of the captured $CO_2$ in 44.1, 21.8, and 15.9 min (Fig. 14b). Remarkably, COF-999 showed consistent performance over 20 days under DAC conditions with atmospheric $CO_2$ concentrations of 410–517 ppm and a relative humidity of 28–51%. The material underwent 100 adsorption/desorption cycles at 333 K, consistently releasing 1.28 mmol $CO_2$ $g^{-1}$ per cycle without any measurable loss in capacity or structural integrity (Fig. 14c). The material exhibits a regeneration energy of 5.89 GJ $tCO_2^{-1}$ at 333 K, nearly twice that of typical small alkylamine solvents, highlighting the

 

inherent energy challenges of DAC, particularly the trade-offs involved in incorporating highly reactive amine tethers. Nonetheless, these results represent one of the most promising demonstrations to date, underscoring both the resilience and practical viability of COF-based adsorbents under realistic DAC conditions. COF-609 provides another outstanding example of pore post-functionalization, in which the pores of an imine-based COF were modified with tris(3-aminopropyl)amine (Fig. 14d).[211] This modification produced a dramatic enhancement in $CO_2$ uptake compared to the parent frameworks COF-609-Im and COF-609-THQ (Fig. 14e), delivering a 1360-fold increase to 0.304 mmol $g^{-1}$ at 298 K and 400 ppm $CO_2$ whereas at 50% RH, the capacity further improves by ~29% to 0.393 mmol $CO_2$ $g^{-1}$. At higher $CO_2$ partial pressures, the uptake reached 1.29 mmol $CO_2$ $g^{-1}$ at 4 kPa and 1.50 mmol $CO_2$ $g^{-1}$ at 15 kPa. Notably, COF-609 exhibited low water uptake, which not only reduces the regeneration energy associated with desorbing co-adsorbed moisture but also enhances $CO_2$ capacity under humid conditions relative to dry operation (Fig. 14f). Substituting benzidine with 3,3′-diaminobenzidine in the imine-linked COF constructed from 2,4,6-trimethylbenzene-1,3,5-tricarbaldehyde ($Me_3TFB$) yields $Me_3TFB$-$(NH_2)_2BD$, while preserving crystallinity and permanent porosity.[238] This structural modification significantly enhances $CO_2$ capture performance: at 295 K and 100 kPa, the $CO_2$ uptake increases from 0.41 ± 0.01 to 0.72 ± 0.07 mmol $g^{-1}$. Moreover, the $CO_2/N_2$ selectivity reaches 83 ± 11 at 273 K and remains as high as 47 ± 11 at 295 K for a 0.15/0.85 $CO_2/N_2$ mixture, demonstrating that introducing additional amine functionalities effectively strengthens $CO_2$ affinity while maintaining framework stability.

The main advantages of COFs lie in their structural precision, chemical versatility, and relatively straightforward synthesis compared to MOFs. They can also offer superior hydrolytic stability, depending on the linkage chemistry and incorporated functional groups. Despite these advantages, many COFs display limited crystallinity, low bulk density, and poor processability, hindering their practical deployment. Moreover, their predominantly physisorptive $CO_2$ binding results in low uptake at sub-atmospheric pressures, constraining their effectiveness for DAC. These drawbacks, however, can be mitigated through targeted incorporation of reactive functional groups, which enhances binding affinity and expands the application scope of COFs in CCUS.

**3.4.3. Porous organic polymers (POPs).** Unlike crystalline frameworks such as MOFs or COFs, POPs lack long-range order but offer high surface areas, thermal stability, and chemical tunability.[243,244] Their synthetic flexibility and modular design allow for the incorporation of various functional groups into the framework backbone or side chains, making them attractive candidates for $CO_2$ capture and gas separation.[29,245,246] POPs are typically synthesized *via* polymerization of rigid aromatic monomers through coupling reactions (*e.g.*, Suzuki, Sonogashira, and Friedel–Crafts alkylation) or dynamic covalent chemistry (*e.g.*, Schiff-base formation and triazine condensation).[247–249] These methods yield highly cross-linked networks with microporous to mesoporous structures, often

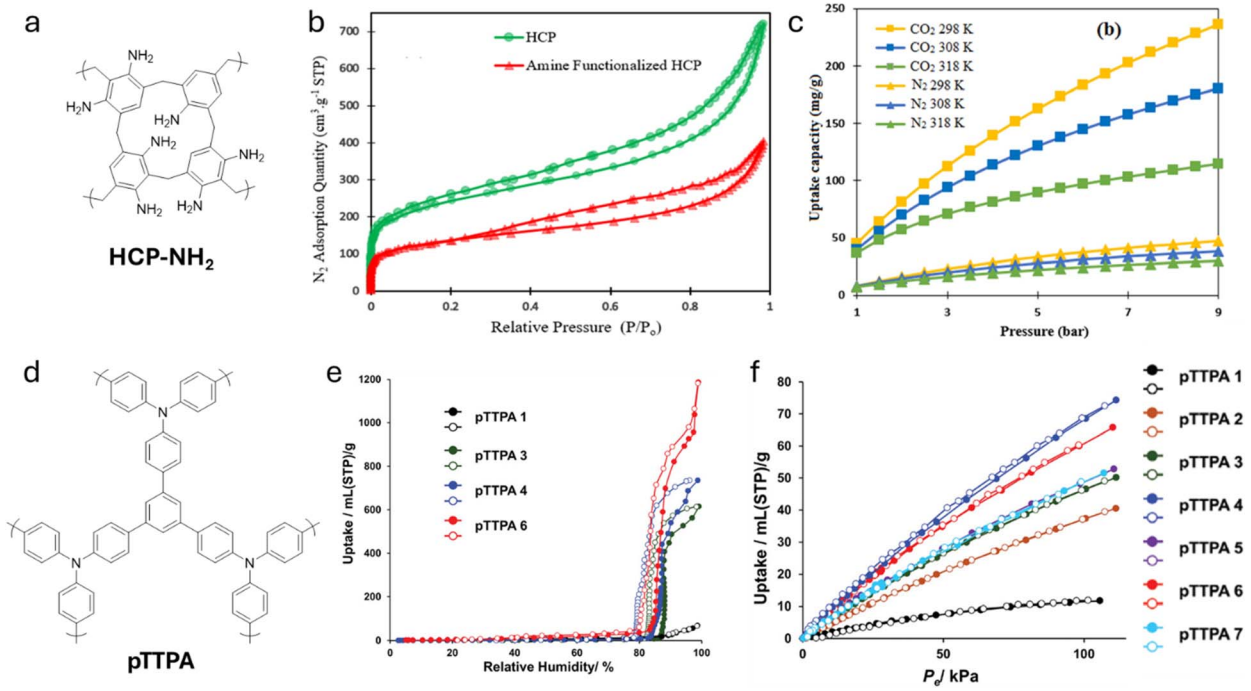


Fig. 15 (a) Chemical structure of HCP-$NH_2$. (b) $N_2$ adsorption–desorption isotherms of pristine HCP and amine-functionalized HCP adsorbents. (c) Selective adsorption performance of HCP-$NH_2$ for a $CO_2/N_2$ mixture (15 : 85). Reproduced from ref. 214 with permission from Springer Nature, copyright 2023. (d) Chemical structure of pTTPA. (e) Water-vapor adsorption–desorption isotherms of selected pTTPA POPs measured at 298 K (filled symbols: adsorption; open symbols: desorption). (f) $CO_2$ adsorption–desorption isotherms of pTTPA POPs measured at 298 K (filled symbols: adsorption; open symbols: desorption). Reproduced from ref. 215 with permission from Wiley-VCH, copyright 2025.

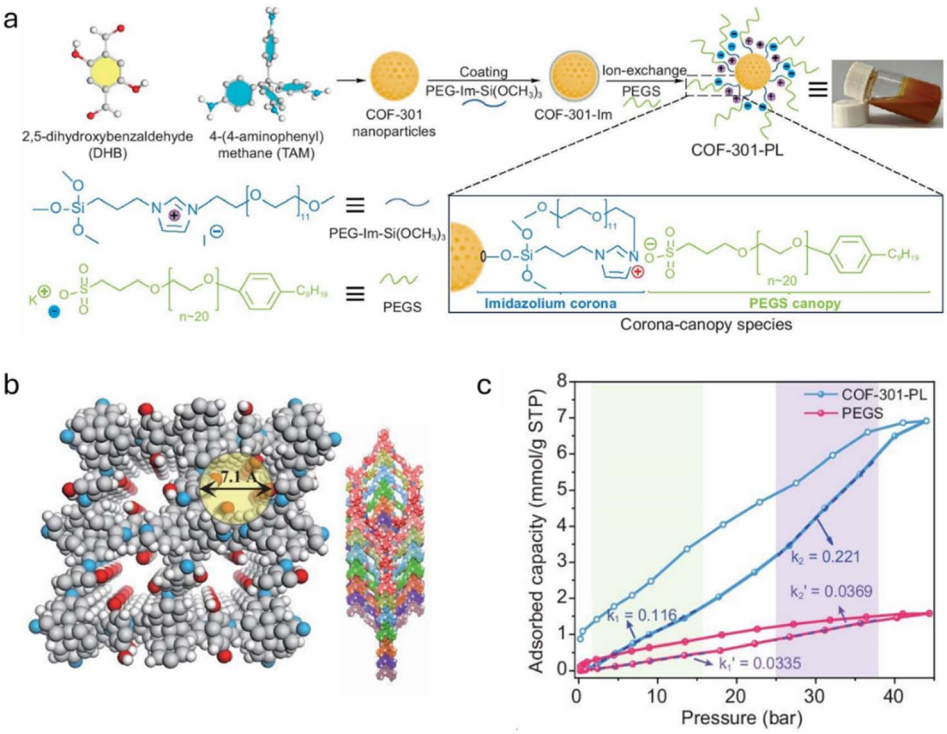


Fig. 16 (a) Synthesis route of COF-301 nanoparticles decorated with surfactants for PLs. (b) Molecular diagram depicting the pore size of the PL. (c) $CO_2$ absorption isotherms of free surfactants (PEGs) and COF-301 PL. Adapted with permission from ref. 216 (CC BY), copyright 2025.

displaying BET surface areas exceeding 1000 $m^2\ g^{-1}$ and tunable pore volumes. The $CO_2$ adsorption performance of POPs depends on surface chemistry, pore structure, and the presence of polar or basic functionalities. Incorporation of amine,[186–188] triazine,[212] amide,[250] or imide[191–193,251,252] groups enhances $CO_2$ affinity through hydrogen bonding or acid–base interactions; furthermore, the introduction of polar groups in the structure can also contribute to high $CO_2$ uptake due to van der Waals interaction between polar functional groups and $CO_2$.[213,253,254] Reported $CO_2$ uptake values typically range from 1 to 5 mmol $g^{-1}$ at 100 kPa and 298 K. Compared to MOFs, POPs generally exhibit higher thermal and oxidative stability, and many are tolerant to humid conditions. For example, two tetraphenylethylene-functionalized nitrogen-rich porous polymers, TTPEPOP-O and TTPEPOP-S, were prepared by reacting 4,4′,4″,4‴-tetra(2,4-diamino-1,3,5-triazin-6-yl)-tetraphenylethene (TTPE) with 2-carboxaldehydefuran or 2-carboxaldehydethiophene leading to highly porous materials with a total pore volume of 741 and 999 $cm^3\ g^{-1}$, respectively.[212] The adsorbents showed high $CO_2$ loading capacity with the 102.9 g $CO_2\ g^{-1}$ material for TTPEPOP-O and 129.4 g $CO_2\ g^{-1}$ material for TTPEPOP-S featuring high selectivity for $CO_2$ over $N_2$ with a ratio of 27 : 1 for TTPEPOP-O and 24 : 1 for TTPEPOP-S at 298 K. Triptycene-based POPs with a ketone linker showed a BET surface area of 889.19 $m^2\ g^{-1}$ and a total pore volume of 0.415 $cm^3\ g^{-1}$.

The material displayed superior performance with a $CO_2$ loading capacity of 138.8 mg $CO_2\ g^{-1}$ material and a selectivity of $CO_2$ over $N_2$ of 56.8 at 298 K and 100 kPa.[213] The high $CO_2$ uptake was attributed to a physisorption process assigned to van der Waals interactions of the ketone groups with $CO_2$. Silane-containing POPs based on the building block tetrakis(4-formylphenyl) with linking units of 1,3,5-benzenetriol, 1,5-naphthalenediol or [1,1′-biphenyl]-2,3′,4,5′,6-pentol presented $CO_2$ loading capacities of 2.3 mmol $CO_2\ g^{-1}$, 3.3 mmol $CO_2\ g^{-1}$ and 4.3 mmol $CO_2\ g^{-1}$, respectively.[254] While weak interactions may favor the desorption of $CO_2$ it is also important to consider that Lewis acid/base groups such as amines will always exhibit larger $CO_2$ uptake compared to their non-aminated counterparts. Fundamental studies comparing the performance of POPs with a central 1,3,5-triazine core or with a benzene core showed that, as expected, the POP with a triazine core displayed a higher $CO_2$ uptake than the POP with a benzene core with 72.1 $cm^3$ $CO_2\ g^{-1}$ and 53.2 $cm^3$ $CO_2\ g^{-1}$ at 298 K, respectively.[255] Therefore, this highlights the importance of amine functionalities in the $CO_2$ process under atmospheric conditions. Polymerization of benzene with formaldehyde dimethyl acetayl leads to the formation of a hypercrosslinked polymeric adsorbent (HPC) which after amination (HPC-$NH_2$, Fig. 15a) affords a material with a $CO_2$ loading capacity of 9.41 mmol $CO_2\ g^{-1}$ compared to the parent material with 6.85 mmol $CO_2\ g^{-1}$, representing a 30% improvement.[214] Similar to previously discussed porous materials, the incorporation of amine in the porous structures leads to a decrease in the specific surface area from 806 $m^2\ g^{-1}$ for HPC to 453 $m^2\ g^{-1}$ for HPC-$NH_2$, leading to 30–50% reduction in the absorption of $N_2$ due to the presence of polar groups (Fig. 15b). Furthermore, ideal adsorbed solution theory (IAST) curves show increasing $CO_2$ loading capacity and

 

Table 6 KPIs for amine-functionalized nanoparticles

| Material | Rich loading (mmol $CO_2$ $g^{-1}$) | Regeneration energy (GJ $tCO_2^{-1}$)[a] | Regeneration temperature (K) | Gas composition[a] | Ref. |
|---|---|---|---|---|---|
| HS-TEPA-70 | 3.34 | 2.36 | 383 | 0.4 vol% $CO_2$ | 270 |
| γ-$Al_2O_3$ + 30 wt% PEI + 20 wt% TEPA | 2.65 | — | 373 | 15 vol% $CO_2$ | 271 |
| Halloysite nanotubes + 30 wt% TEPA | 9.3 | — | 383 | 100 vol% $CO_2$ | 272 |
| $Fe_3O_4$ (propylamine-coated) + 5 wt% MDEA | 1.5 | — | — | 15 vol% $CO_2$ | 267 |
| $Fe_3O_4$ (Lys-coated) + 5 wt% MDEA | 1.4 | — | — | 15 vol% $CO_2$ | 267 |
| $Fe_3O_4$ (Pro-coated) + 5 wt% MDEA | 1.3 | — | — | 15vol% $CO_2$ | 267 |

[a] Balance with $N_2$.

selectivity towards $CO_2$ over $N_2$ when the pressure is varied in the range of 100–900 kPa and temperature is varied in the range of 298–318 K (Fig. 15c). Regeneration of the material was performed at 410 K under vacuum over 8 h, exhibiting a decrease in absorption performance of 3% after ten absorption/desorption cycles. A COF based on 1,3,5-tris[4-(diphenylamino)phenyl] benzene (TTPA) was prepared by using different amounts of iodine as the initiator and temperatures resulting in 7 different derivatives (pTTPA1-7) with the basic structure presented in Fig. 15d. The resultant materials displayed large surface areas in the range of 315–2134 $m^2$ $g^{-1}$ with the highest value observed for pTTPA7.[215] All pTTPAs exhibited water uptake only at high relative humidity (≥80%) (Fig. 15e), consistent with their hydrophobic pore surfaces that hinder cluster formation as the first step in adsorption. Among the series, pTTPA-4 achieved the highest $CO_2$ uptake with 3.31 mmol $g^{-1}$ at 298 K and 100 kPa and the best $CO_2/N_2$ selectivity of 18.6, despite not having the largest BET surface area (Fig. 15f). This performance is attributed to its relatively high micropore volume, which dominates $CO_2$ adsorption and enhances molecular sieving given the smaller kinetic diameter of $CO_2$ (3.30 Å) compared to $N_2$ (3.64 Å). Notably, this capacity is the highest reported for triphenylamine-based amorphous POPs lacking basic amine functionalities, highlighting the central role of microporosity in driving both $CO_2$ capacity and selectivity.

POPs combine synthetic scalability, low density, and robustness, allowing integration into shaped bodies, monoliths, or membranes, and their structures can be tailored through post-synthetic modification.[256] However, they suffer from low selectivity in mixed gases, polymerization variability, and limited structure–property predictability due to their amorphous nature.

**3.4.4. Porous liquids (PLs).** Porous liquids (PLs) merge the permanent cavities of porous solids with the fluidity of liquids. They are typically formed by combining a porous host material (*e.g.* MOFs,[257] COFs,[216] porous organic cage molecules[258] or surface-functionalized nanoparticles[259,260]) with a bulky solvent (*e.g.* poly(ethylene glycol), or an IL). The solid pore generator is often modified with large substituents (fillers) to prevent its intrinsic cavities from collapsing or being filled by the solvent.[261,262] Achieving a stable, high-density colloidal dispersion is crucial as the porous host must remain suspended and not aggregate, even at elevated temperatures, to avoid solvent loss or degradation upon cycling.[49,50] PLs are classified into three main types: type I consists of neat liquids whose molecules contain permanent internal cavities; type II comprises solutions of discrete porous hosts (*e.g.* cage molecules) in a solvent that is size-excluded from entering the pores; and type III are dispersions of porous solids (*e.g.* MOF or COF nanoparticles) in a bulky solvent that cannot penetrate the pores.

In all cases, the effective porosity and gas transport depend on how well the host is stabilized and accessible in the liquid phase. A well-designed PL maintains an ordered arrangement of hosts so that empty cavities are available for gas adsorption. For example, a scrambled imine cage PL dissolved in a size-excluded solvent dramatically increased gas solubility: $CH_4$ uptake increased from 6.7 to 51 μmol $CO_2$ $g^{-1}$, and $CO_2/N_2$ solubilities were similarly enhanced over the neat solvent.[258] Likewise, when HKUST-1 MOF particles were dispersed (15–20 wt%) in a bulky imidazolium IL, $CO_2$ uptake increased by roughly an order of magnitude compared to the IL alone from 0.15 up to 1.8 mmol $CO_2$ $g^{-1}$ at 1 MPa and 293 K, respectively.[257] A solvent-free PL was developed by grafting a C18 organosilane canopy onto hollow silica nanorods and electrostatically coupling a polymer surfactant; the resulting flowing composite showed a $CO_2$ uptake of 3.3–4.8 wt% at 273 K with the highest uptake of 4.8 wt% observed for the nanorods with an aspect ratio of 8.[260] In a recent advance, a flexible COF-301-based PL was prepared by grafting an imidazolium-PEG corona onto COF-301 nanoparticles and mixing with a sulfonated PEG canopy (both components sterically exclude each other from the pores (Fig. 16a).[216] Interestingly, simulations show that the material exhibits a pore size of 7.1 nm (Fig. 16b), which enables the material to interact and absorb $CO_2$ gas. This COF-301-PL is thermally stable up to *ca.* 653 K and exhibits a very high $CO_2$ capacity of 7.04 mmol $g^{-1}$ at 4 MPa and 298 K, which is about 4.5 times that of the pure IL-based solvent (Fig. 16c). These studies highlight how type III PLs can combine the high uptake of solid adsorbents with liquid processability, by carefully matching pore-filled hosts with nonpenetrating liquids. Overall, porous liquids offer a practical route to combine the high $CO_2$ affinity of porous solids with the processability of liquids, but their impact will ultimately depend on achieving long-term

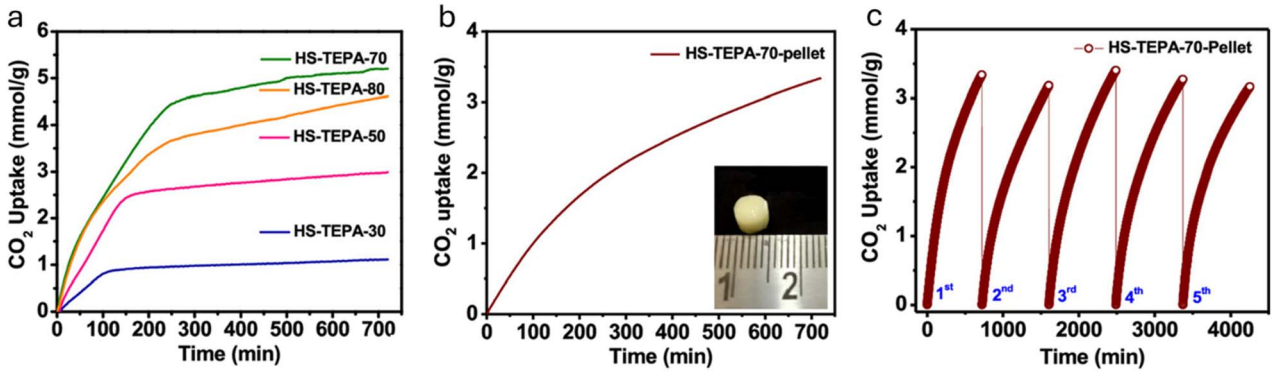


Fig. 17 (a) $CO_2$ uptake profiles of HS-TEPA-30, HS-TEPA-50, HS-TEPA-70, and HS-TEPA-80. (b) $CO_2$ uptake profile of pelletized HS-TEPA-70. (c) Repeated $CO_2$ adsorption/desorption cycling performance of pelletized HS-TEPA-70. Reproduced from ref. 270 with permission from the American Chemical Society, copyright 2023.

colloidal stability and low-energy regeneration under real operating conditions.

### 3.5. Amine-functionalized nanoparticles

Amine-functionalized nanoparticles (ANPs) have emerged as solid-phase $CO_2$ sorbents with tunable surface properties and high surface-to-volume ratios. These materials include silica,[263] metal oxides (*e.g.*, $TiO_2$ and $Al_2O_3$),[264] carbon-based particles (*e.g.* graphene),[265,266] and magnetic nanoparticles,[267,268] which are typically modified with surface-bound amine groups or ILs to enhance $CO_2$ affinity. Their performance depends on particle morphology, pore structure, and surface/pore functionalization. Surface amination either by grafting primary/secondary amines, through co-condensation with organosilanes or by self-assembly of polymers on the surface is the most common strategy to enable chemisorption of $CO_2$ *via* carbamate/$HCO_3^-$

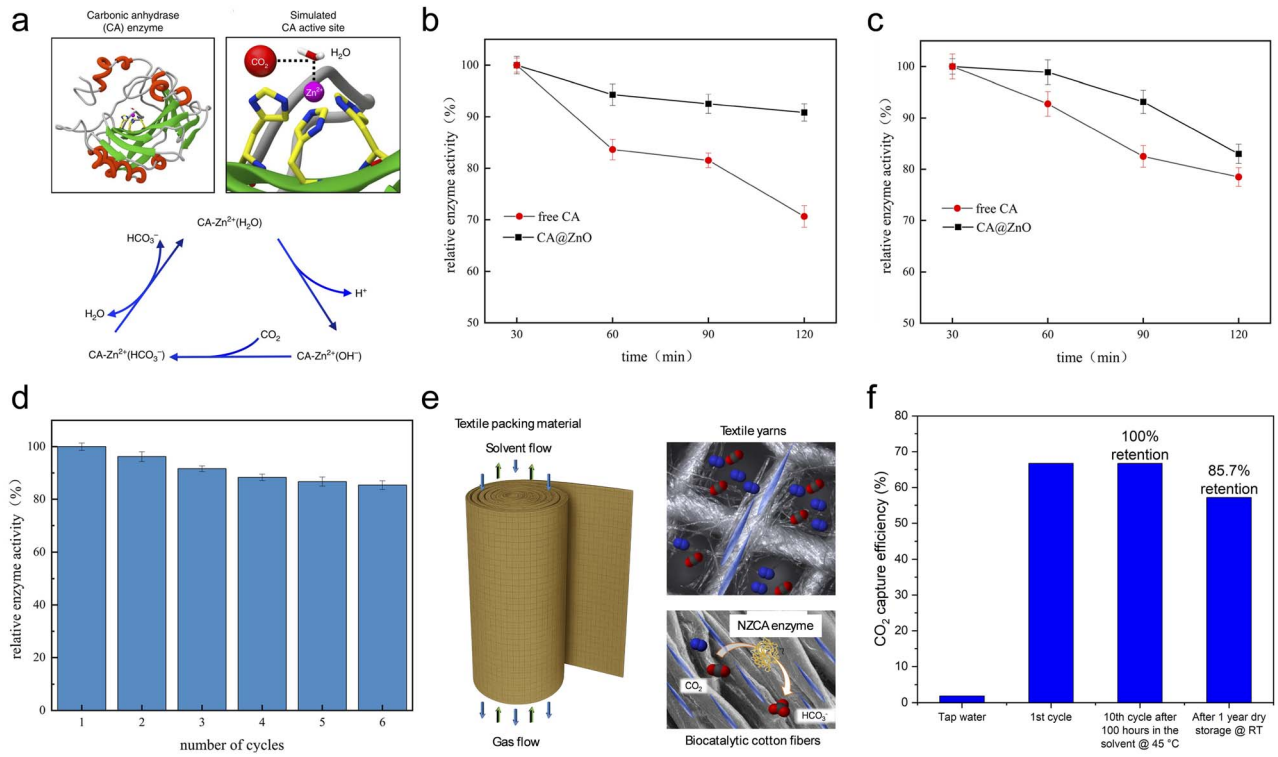


Fig. 18 (a) Structure of carbonic anhydrase and its catalytic $CO_2$ hydration mechanism. Reproduced from ref. 280 with permission from Springer Nature, copyright 2018. (b) Thermal stability at 313 K, and (c) pH stability at pH = 8.00 of free CA and CA bound to ZnO. (d) Bar chart showing the change in enzymatic activity of ZnO-bound CA over multiple $CO_2$ capture cycles. Reproduced from ref. 295 (CC BY), copyright 2025. (e) CA-based structured packing: schematic of a wire-frame support bearing CA-functionalized textiles, with a microscopic depiction of $CO_2$ conversion on the fiber surface. Reproduced from ref. 296 with permission from Wiley-VCH, copyright 2022. (f) Cycling capacity and $CO_2$ capture efficiency of CA-supported textile packing compared with tap water as a control. Reproduced from ref. 288 (CC BY), copyright 2022.

formation. Oligoamines such as TETA and TEPA, and PEI-based polymers have been used to functionalize mesoporous silica particles. $CO_2$ loading capacities typically range from 1 to 3 mmol $CO_2$ $g^{-1}$ depending on the functional group density, support type, and operating conditions.[269] The KPIs of representative examples discussed in this section are presented in Table 6. $SiO_2$ nanoparticles functionalized with branched PEI display a loading capacity of 0.48 mol $CO_2$ $mol^{-1}$ N (where-mol N refers to the total number of nitrogen atoms in the system) compared to 0.45 mol $CO_2$ mol $N^{-1}$ for the pure PEI polymer.[263] Remarkably, the authors determined using $^{13}C$ NMR spectroscopy that the functionalized nanoparticles can stabilize $CO_2$ in the form of carbamate and $HCO_3^-$ in a ratio of 2 : 1 (amine/$CO_2$). Furthermore, it was found that speciation of $CO_2$ in the material is highly dependent on the temperature and the presence of $KHCO_3$. For example, at temperatures above 338 K the dominant species is the primary carbamate, with high formation selectivity in the supported polymer. On the other hand, the presence of 1.0 mol $dm^{-3}$ $KHCO_3$ leads to the formation of primary and secondary carbamates. Although desorption studies were not performed, this highlights the importance of experimental conditions for the speciation which in turn can potentially improve the regeneration energy of the material.

Pore clogging as a result of high amine loading leads to decreased $CO_2$ uptake; therefore hierarchical structures of mesoporous silica have been introduced to maximize amine loading and thus the increase the $CO_2$ loading.[270] Hierarchical silica nanoparticles (HS) functionalized with TEPA loadings of 30, 50, 70 and 80 wt% showed a high $CO_2$ uptake of 1.11, 2.98, 5.20 and 4.61 mmol $CO_2$ $g^{-1}$, respectively (Fig. 17a), compared to pure HS with 0.64 mmol $CO_2$ $g^{-1}$. The pore hierarchy enables high amine loading without sacrificing absorption performance; however, a TEPA loading of 80 wt% leads to a pore filling of 99% whereas optimal $CO_2$ absorption was 88% for a TEPA loading of 70 wt%. For practical applications HS-TEPA-70 was pelletized displaying a maximum $CO_2$ absorption capacity of 3.34 mmol $CO_2$ $g^{-1}$ at 303 K in simulated air (400 ppm $CO_2$ in He) (Fig. 17b), and the lower loading capacity compared to the non-pelletized material is assigned to the pore collapsing/obstruction intrinsic to the fabrication process. The material was tested over 5 absorption/desorption cycles with *ca.* 5% performance loss, and absorption was investigated at 303 K whereas regeneration of the material was performed at 383 K (Fig. 17c). HS-TEPA-70 exhibits a promising regeneration energy of 2.36 GJ $tCO_2^{-1}$ which is approximately 2.5 times lower than that of COF-999 and is competitive with that of small alkylamine solvents. This reduced energy demand may be attributed to the presence of peripheral amine groups on the nanoparticle support, in contrast to porous materials where $CO_2$ is internalized within the framework, requiring higher energy input for desorption. Blended amines comprising 30 wt% PEI and 20 wt% TEPA on $\gamma$-$Al_2O_3$ achieved a $CO_2$ uptake of 2.65 mmol $g^{-1}$ at 333 K under simulated flue gas (15 vol% $CO_2$).[271] The material retained most of its capacity after regeneration at 373 K, with only *ca.* 10% loss observed over seven cycles, indicating moderate stability under repeated operation. Mesoporous nanotubes (MN) of halloysite (hollow tubular structure with a layered structure internally composed of $Al_2O_3$ and an outer structure of $SiO_2$) exhibit improved porosity and therefore allow for improved amine loading.[272] Impregnation of MN with TEPA at concentrations of 10, 20, 30, 40 wt% leads to an outstanding $CO_2$ loading capacity of 9.3 mmol $CO_2$ $g^{-1}$ at 100 vol% $CO_2$, 293 K and 900 kPa for MN with 30 wt% TEPA. Absorption/desorption cycles on MN-TEPA were done under high pressure conditions (600 kPa, 303 K) for adsorption and at high temperature for desorption (1 Pa, 383 K) over 12 cycles without significant loss in performance. Magnetic nanoparticles composed of an $Fe_3O_4$ surface functionalized with Lys, Pro, and propylamine were tested in $CO_2$ absorption experiments at pressures of 2000, 3000 and 4000 kPa.[267] The optimum experimental conditions were found at 3000 kPa with $Fe_3O_4$ coated with Lys, Pro and propylamine displaying a 25.07%, 31.04 and 34.23% increase in $CO_2$ loading compared to water. More importantly, the samples were combined with an MDEA 5 wt% solution displaying a maximum $CO_2$ capture performance of *ca.* 1.5, 1.4 and 1.3 mol $CO_2$ $kg^{-1}$ for surface coatings of propylamine, Lys and Pro, respectively, compared to 1.2 mol $CO_2$ $kg^{-1}$ for MDEA 5 wt%. Magnetic nanoparticles have been proposed as a cheap alternative to solvents although there is no clear application for them in the industry. Furthermore, as mentioned in Section 3.1.2 the combination of amino acids with Fe has been associated with improved solvent degradation.[142] Due to its high surface area, graphene oxide (GO) has been proposed as an amine-grafting support with amines such as TEPA,[273,274] TETA,[275] PEI-polymers,[276] ethylenediamine (EDA),[277] 3-aminopropylsilane (APTES), pentaethylenehexamine (PEHA)[275] and 1,3-diaminobenzene (DAB) to improve the $CO_2$ capture performance. Remarkable examples that exhibit high $CO_2$ loading at 100 kPa involve GO-EDA with 1.18 mmol $CO_2$ $g^{-1}$,[277] GO-TEPA with 1.22 mmol $CO_2$ $g^{-1}$,[274] and GO-APTES with 1.5 mmol $CO_2$ $g^{-1}$.[275] Examples containing GO-DAB, GO-TETA and GO-PEHA showed high performances of 0.91 mmol $CO_2$ $g^{-1}$, 0.74 mmol $CO_2$ $g^{-1}$ and 0.61 mmol $CO_2$ $g^{-1}$, respectively, without losing loading capacity over 4 cycles.[275] It is worth noting that complete regeneration of these samples required a temperature of 383 K over 12 h suggesting sub-optimal conditions for real life applications.

Nanoparticles tend to agglomerate, reducing accessible surface area and complicating processability. In addition, the cost and scalability of nanoparticle synthesis, functionalization, and shaping into usable forms (*e.g.*, pellets or composites) remain challenges. Notwithstanding this, similar to porous materials, integration into structured reactors, membranes, or fixed beds provides versatility to this class of materials.

### 3.6. Enzymes

Enzyme-based systems utilize carbonic anhydrases (CAs), a class of metalloenzymes that catalyze the rapid interconversion between $CO_2$ and $HCO_3^-$ which is stabilized by the zinc ($Zn^{2+}$) metal center of the enzyme (Fig. 18a).[278–280] These systems have attracted attention due to their exceptional catalytic efficiency, with turnover frequencies exceeding $10^6$ $s^{-1}$ under

physiological conditions. The main role of carbonic anhydrase in $CO_2$ capture is to accelerate the hydration of $CO_2$ to $HCO_3^-$, improving overall mass transfer and reaction kinetics in absorption processes.[279,281–283] CAs are typically integrated into aqueous solvent systems such as amine[198,199,205,284] or carbonate solutions,[285] where their presence can reduce absorber size and improve solvent utilization. Hybrid capture systems using immobilized CAs within membrane contactors or solid supports have also been proposed to minimize enzyme leaching and enhance recyclability.[281,286,287] Immobilization strategies, such as surface grafting, entrapment in porous matrices, or covalent attachment to carriers, are often required to preserve enzyme activity and allow operation under non-physiological conditions. CAs behave as a $CO_2$ promoter similar to PZ and they can be used in conjunction with other amines such as MDEA[288,289] or $K_2CO_3$ (ref. 203, 204, 285 and 290) to improve the capture rate. CAs can be immobilized on a variety of solid supports, including textiles, mesoporous silica and silica-derived materials, magnetic nanoparticles, and polymers.[204,281,291] Immobilization prevents enzyme leaching during operation and enables the enzyme to be retained within or recovered from the capture medium.[291–293] The operational stability of immobilized CA depends strongly on the mode of immobilization and the nature of the support material.[292,293] For example, longer activity retention times are typically observed when CA is covalently bonded, cross-linked, or encapsulated within porous materials, compared to electrostatically adsorbed or ionically bound forms.[292,294] Furthermore, supported carbonic anhydrase (CA) has been shown to retain its catalytic activity over longer periods compared to its free (unbound) form. For instance, CA immobilized on ZnO retained 90.85% and 83.12% of its initial activity after 2 hours of incubation at 40 °C (Fig. 18b) and pH 8.0 (Fig. 18c), respectively. Under the same conditions, free CA retained only 70.65% and 78.48% of its activity.[295]

Robust CA-functionalized materials can be prepared by covalently attaching CA to surface-functionalized supports *via* *N*-hydroxysuccinimide (NHS) esters,[297] epoxy-activated polymers,[298,299] or glutaraldehyde linkers.[288,299–301] These functionalities result in covalent C–N bond formation between lysine residues on the CA molecule and amino-functionalized surfaces, producing durable immobilized biocatalysts. In contrast, when CA is weakly immobilized (*e.g.*, *via* electrostatic adsorption, van der Waals interactions, or non-crosslinked encapsulation) enzyme leaching can occur, which compromises the $CO_2$ capture performance during repeated operation. For example, in one system, electrostatically supported CA on ZnO nanoparticles retained 85% of its original activity after 30 days and maintained 85% $CO_2$ hydration activity after five capture/release cycles (Fig. 18d), indicating good but not optimal durability.[295] Recent studies have also demonstrated high-performance CA immobilization using novel materials and methods. For instance, CA encapsulated in biomimetic silica *via* peptide-mediated sol–gel processes retained >90% of initial activity after 35 days and 86% after 10 $CO_2$ absorption cycles.[302] CA covalently bound to glutaraldehyde-crosslinked polyvinylidene fluoride (PVDF) membranes maintained 85% activity after 10 cycles, with minimal leaching.[299] CA immobilized on aminated SBA-15 mesoporous silica *via* physical adsorption showed no detectable enzyme desorption over two

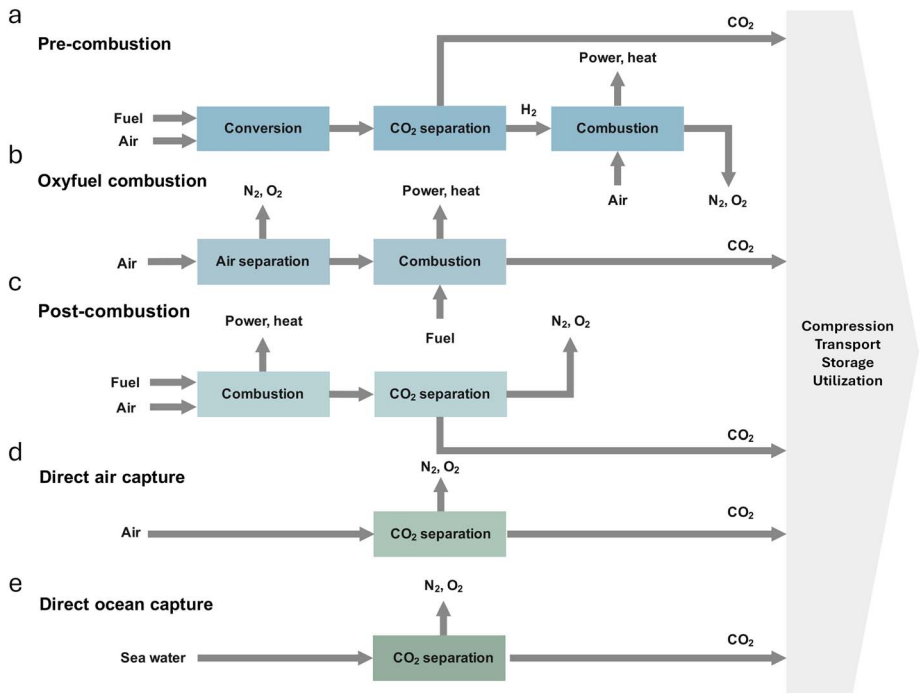


Fig. 19 General flow diagram of reactive $CO_2$ capture approaches: (a) pre-combustion, (b) oxy-fuel combustion, (c) post-combustion, (d) DAC, and (e) DOC. Adapted from ref. 309 with permission from Elsevier, copyright 2015.

 

weeks of testing under simulated flue gas conditions, with significantly improved thermal stability.[303] Overall, covalent immobilization strategies offer the highest retention and reusability, while weaker methods such as physical adsorption may suffer from reduced enzyme lifetime unless supported by surface engineering or stabilizing matrices.[292,293,304] Pioneering studies focus on supporting CAs on textiles which then are rolled into a metal wire mesh and used as a packing material and absorbent in the scrubber columns (Fig. 18e).[204,288,296]The surface-immobilized 3D enzyme packing module was evaluated over 10 reuse cycles across 71 days (Fig. 18f). Between tests, the packing was rinsed, air-dried, and stored under ambient conditions; the final 100 h were conducted under continuous exposure to 10 wt% $K_2CO_3$ solution (pH $\approx$ 10.5) at 318 K, representative of absorber operating conditions.

Remarkably, the enzyme-functionalized packing retained full $CO_2$ capture performance after cycling and solvent incubation. Flow experiments further highlighted the role of the packing structure: static seawater showed negligible $CO_2$ removal, whereas flowing seawater through the textile achieved 19.6% capture efficiency, comparable to enzyme-free textile packing in 10 wt% $K_2CO_3$ solvent (Fig. 18d). With enzyme immobilization, capture efficiency increased to 66.9%, lowering the outlet $CO_2$ concentration to 246 ppm, which is well below both the global atmospheric average and the local indoor baseline, highlighting the synergistic effect of enzyme activity and enhanced gas–liquid contact. The implementation of this novel technology has shown that the hybrid functionalization of CAs with cotton-supported chitosan leads to a 19.1-fold increase in $CO_2$ capture efficiency compared to control experiments and a removal efficiency of *ca.* 67% for both PCC and DAC flue gas composition when combined with 10 wt% $K_2CO_3$.[288] Despite their catalytic advantages, enzyme stability remains a key limitation. Denaturation under thermal, chemical, or mechanical stress restricts long-term performance in industrial environments.[204,278,305,306] Efforts to improve enzyme robustness include the use of thermostable variants and protein engineering.[286,307,308] With the advent of advanced computing, enzymes can be designed to display improved performance and can be engineered *via* high throughput screening.[285,307] While not a standalone capture technology, enzyme-assisted systems have demonstrated the ability to reduce the energy penalty in PCC setups by improving kinetics without requiring stronger chemical driving forces. Nonetheless, enzyme production costs and durability issues continue to limit widespread deployment at scale.

## 4. Capture technologies

Having reviewed the solvent materials, we now consider the engineering contexts in which they operate. Solvent performance can be strongly influenced by the capture scenario and whether capturing $CO_2$ from a fuel gas stream, diluted flue gas, ambient air, or ocean water. Each scenario imposes different requirements. In this section the carbon capture technologies where reactive capture is implemented are discussed, and therefore cryogenic absorption is not discussed. The processes of pre-combustion, oxyfuel combustion, PCC and industrial processes, DAC and DOC are briefly discussed below, to provide

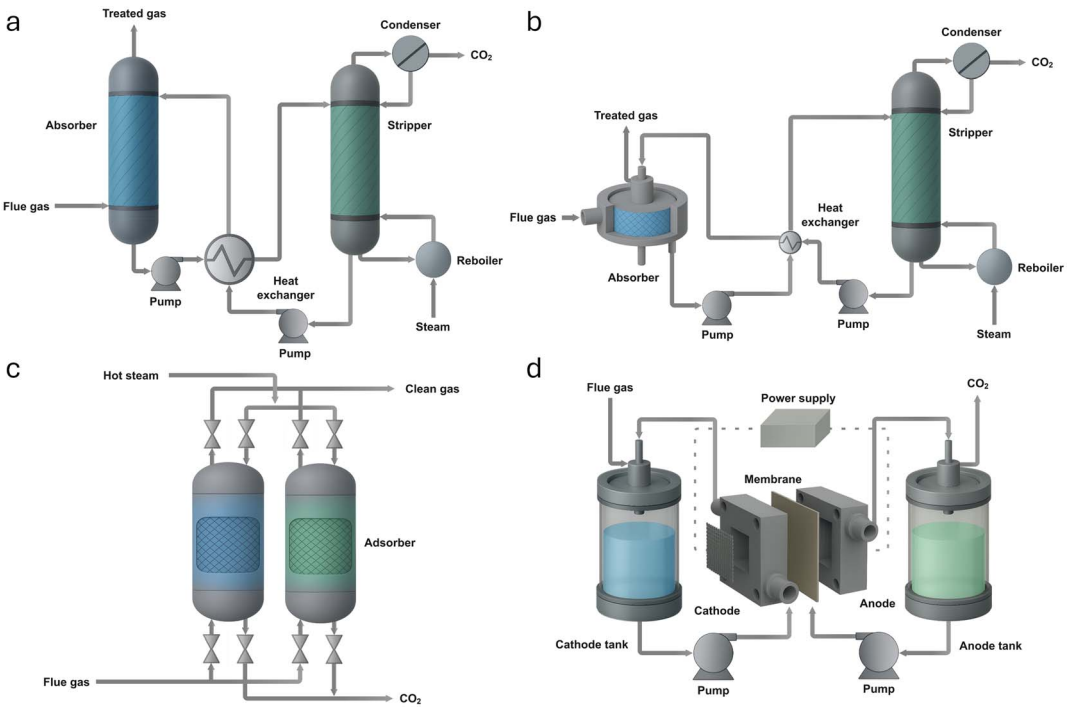


Fig. 20 General process schematics of representative $CO_2$ capture contactors and reactor configurations: a (a) packed-bed scrubber (absorption column), (b) RPB absorber, (c) fixed-bed adsorber, and (d) electrochemical flow cell for $CO_2$ capture/conversion.

a general overview of these $CO_2$ capture pathways and their typical process configurations (Fig. 19).

### 4.1. Source point carbon capture

Carbon capture is a key solution to address climate change caused by anthropogenic $CO_2$ emissions from large point sources such as fossil-fuelled power plants, cement factories, and steel manufacturing facilities. This technology is categorized into post-combustion, pre-combustion, and oxy-fuel combustion capture (Fig. 19a–c). In terms of process configuration, point source carbon capture can involve different configurations depending on the nature of the absorbent (Fig. 20). For liquid solvents in temperature swing systems the process is continuous and typically involves a scrubber (Fig. 20a) or RPBs (Fig. 20b). In scrubbed type systems the liquid interacts with the flue gas in a counter-current packed column. RPBs enable counter-current contact between flue gas and solvent within a rotating packed bed, allowing for a theoretical tenfold reduction in size compared to conventional scrubbers. In both systems, the rich solvent is then transferred to a stripper where $CO_2$ is desorbed by heating the solvent to temperatures above 373 K and the solvent is recirculated back to the absorber. As for solid adsorbents, the process works in batch mode, where the absorbent is packed and supported on a frame and the flue gas is passed through it (Fig. 20c). After the solid solvent has been loaded with $CO_2$, the flue gas is redirected to another reactor containing fresh absorbent, while the previously saturated material is regenerated at high temperatures. Electrochemical capture or "electro-swing" $CO_2$ separation replaces thermal regeneration with electricity with two main strategies widely reported in the literature (a general system diagram of redox flow cells is shown in Fig. 20d). The first is redox-mediated capture, where molecules such as quinones, phenazines, or bipyridinium salts reversibly bind $CO_2$ upon electrochemical reduction and release it upon oxidation (in Fig. 10, Section 3.2 specific examples linked to different solvent classes are discussed). In a typical flow-cell architecture, the capture medium circulates between electrode compartments separated by ion-exchange membranes. Applying a potential drives $CO_2$ uptake at the cathode and release at the anode, analogous to a redox-flow battery. The second is the electrochemical pH-swing approach. Here, electrolysis generates local acidity or alkalinity in the solvent. In the alkaline state, $CO_2$ is absorbed as $HCO_3^-$ or carbonate, reversing the current shifts in the solution to acidic conditions, releasing pure $CO_2$. Bipolar membrane electrodialysis (BPMED) is one implementation, in which ion-exchange membranes split water into $H^+$ and $OH^-$ ions to tune pH between absorption and desorption stages. These strategies share key advantages: regeneration does not require high-temperature heat, and the processes can be directly powered by renewable electricity in modular stacks. Current limitations include parasitic reactions (*e.g.*, hydrogen evolution),

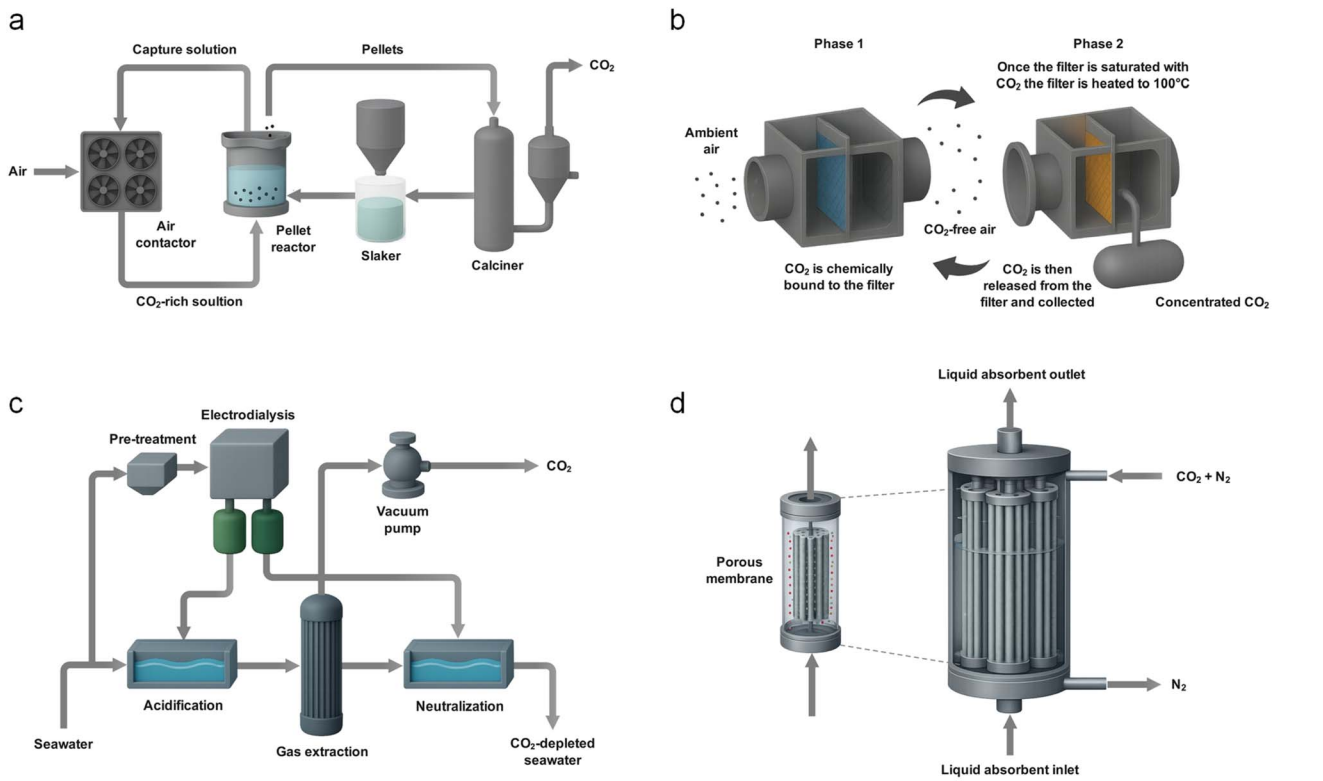


Fig. 21 (a) Wet DAC process (cCarbon eEngineering). (b) Dry DAC process (Climeworks). Adapted from ref. 321 with permission from Frontiers (CC BY), copyright 2019. (c) General process diagram of a DOC concept employing a redox-active solvent. Adapted from ref. 177 with permission from Springer Nature, copyright 2020. (d) General diagram of the $CO_2$ capture process using an HFMC. Adapted from ref. 322 (CC-BY), copyright 2022.

 

modest current densities, and the long-term stability of redox carriers or membranes. Continued progress in molecular carrier design, membrane stability, and electrode engineering will be needed before electrochemical $CO_2$ capture can complement or replace conventional solvent-based systems.

In all the aforementioned cases, after the solvent was regenerated the released $CO_2$ gas is then compressed for utilization or storage. Given thermodynamics and kinetics of carbon capture, the absorption–desorption cycle plays a key role in determining the overall efficiency and feasibility of the process. The trade-off between absorption capacity, regeneration energy demand, and operational cost remains a central topic in the development and optimization of absorbent materials. Nevertheless, high energy requirements for solvent regeneration result in environmental penalties, and also solvent degradation by repeated thermal regeneration and equipment corrosion is a challenging problem in the system.[310,311] Because each absorbent's performance is closely tied to its chemical and physical properties, process configurations must be tailored to accommodate these characteristics.[312,313]

**4.1.1. Pre-combustion capture.** Pre-combustion capture involves the removal of $CO_2$ before the actual combustion process (Fig. 19a). In this method, fossil fuels such as coal, natural gas, or biomass are first converted into a mixture of hydrogen ($H_2$) and carbon monoxide (CO), called syngas, through gasification or reforming processes.[314] The CO is then reacted with steam in a water-gas shift reaction to produce additional hydrogen and $CO_2$. $CO_2$ is separated from $H_2$ using physical or chemical absorption methods, and the $H_2$-rich gas is subsequently combusted for power generation or other industrial uses. It is compatible with integrated gasification combined cycle (IGCC) systems and offers the advantage of relatively high $CO_2$ concentration and pressure, making separation more efficient.[315] However, it typically requires significant process modification and is more applicable to new installations than retrofitting existing plants.

**4.1.2. Oxy-fuel combustion capture.** Oxy-fuel combustion capture refers to a process where fuel is burned in nearly pure oxygen instead of air (Fig. 19b).[316] This results in flue gas composed primarily of $CO_2$ and water vapor, simplifying $CO_2$ separation after condensation of the water. The key advantage of this method is the high purity of $CO_2$ in the flue gas, which reduces the energy required for separation. However, producing pure oxygen *via* air separation units is energy-intensive and costly, and remains a major barrier to large-scale implementation.[317] Furthermore, the process often requires modifications to reboilers or furnaces to accommodate the high flame temperatures associated with oxygen combustion.

**4.1.3. Post-combustion capture (PCC).** PCC refers to the separation of $CO_2$ from flue gases after combustion in point sources such as power plants or industrial furnaces (Fig. 19c). Flue gas at this stage usually contains 3–15 vol% $CO_2$ at near-atmospheric pressure, so large absorber units are required to achieve meaningful removal.[318] The solvent is regenerated in a stripper or reboiler, and the released $CO_2$ is then compressed for transport or storage.[266] PCC is the most developed capture route because it can be retrofitted to existing facilities without major changes to the combustion system. At the same time, the low $CO_2$ partial pressure, the presence of $O_2$, $SO_x$ and $NO_x$, and the high thermal duty of solvent regeneration remain the main limitations. These challenges directly link back to the solvent classes discussed in Section 3, which aim to reduce energy use, improve stability, and maintain efficiency under real flue gas conditions.

### 4.2. Direct air capture (DAC)

DAC provides a promising pathway to remove $CO_2$ from the atmosphere, unlike point-source technologies that operate only at emission sites (Fig. 19d). DAC systems rely on either absorption or adsorption cycles to selectively capture $CO_2$.[319,320] The company Carbon Engineering has developed an absorption-based DAC process using alkaline hydroxides (Fig. 21a).[16] Air is drawn into a large contactor, modelled after cooling towers, where potassium hydroxide solution binds $CO_2$ to form carbonate. The solution then passes into a pellet reactor that produces calcium carbonate pellets while regenerating the capture chemical. The pellets are calcined at high temperature to release pure $CO_2$ gas, leaving behind CaO which is rehydrated in a slaker and recycled into the process. This closed chemical loop operates continuously and delivers a high-purity $CO_2$ stream suitable for compression, storage, or conversion. The design uses established industrial equipment, supports standardized deployment at the megatonne scale, and can be powered by renewable electricity and natural gas. Climeworks, by contrast, employs an adsorption-based DAC system using alkaline-functionalized solid sorbents (Fig. 21b).[319] $CO_2$ collectors carry out both adsorption and desorption cycles, with six units fitting into a 40-ft container, each rated at $\sim$50 $tCO_2\ yr^{-1}$. Capacity is scaled by adding modules, and the design supports automated mass production with standard metal fabrication. The process relies on low-temperature heat (80–120 °C) for $\sim$80% of the energy demand, sourced from renewables or industrial waste heat with a total energy requirement of *ca.* 2000 kWh $tCO_2{}^{-1}$.

Hollow fiber membrane contactors (HFMCs) are increasingly being explored for direct air capture (DAC) applications, where their high surface area-to-volume ratio and modular design offer advantages over conventional packed absorbers (Fig. 21 d).[322,323] In DAC systems, where $CO_2$ concentrations are ultra-dilute (400 ppm, or 40 Pa), HFMCs facilitate efficient gas–liquid contact while avoiding phase dispersion, enabling the use of low-volatility solvents.[323–326] Their compact footprint and compatibility with low-pressure operation make them attractive for distributed or point-of-demand DAC modules.[326,327] Hydrophobic polymer membranes, typically made from polypropylene (PP) or polyvinylidene fluoride (PVDF), are employed to maintain gas–liquid separation, though performance can degrade over time due to membrane wetting, plasticization, or fouling from airborne particulates.[326,328] To improve operational stability, recent work has focused on surface-functionalized or composite membranes, incorporating materials such as silica nanoparticles, fluoropolymer additives, ionic liquid coatings, or polyethyleneimine-based blends to enhance wetting resistance

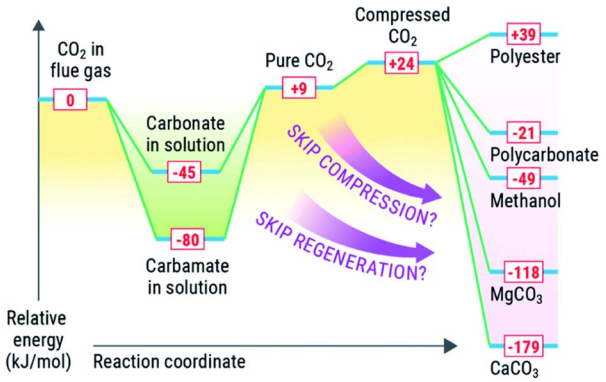


Fig. 22 Conceptual energy comparison for $CO_2$ capture and $CO_2$ conversion pathways. Reproduced from ref. 38 with permission from the Royal Society of Chemistry, copyright 2022.

and $CO_2$ permeability under ambient air conditions.[326,328] However, mass transfer limitations at low $CO_2$ pressure, combined with the need for energy-efficient regeneration of the liquid sorbent, remain significant limitations for HFMC integration into scalable DAC systems.[323,325]

### 4.3. Direct ocean capture (DOC)

DOC has recently emerged as a promising technology for negative carbon emissions, leveraging the fact that the ocean contains significantly more $CO_2$ than the atmosphere, primarily in the form of dissolved inorganic carbon (DIC) species such as bicarbonate, carbonate, and dissolved $CO_2$.[22] DOC systems operate by shifting the carbonate equilibrium of seawater to release dissolved $CO_2$ gas (Fig. 19e), typically using electrochemical methods such as bipolar-membrane electrodialysis. These systems rely exclusively on electricity and avoid thermal regeneration, with energy demands in the range of 100–200 kJ $mol^{-1}$ $CO_2$. Extracting $CO_2$ directly from seawater poses engineering challenges, particularly because the treated water must ideally be returned to the ocean without disrupting marine chemistry. For this reason, DOC systems require precise chemical control to minimize environmental impact. Several pilot-scale demonstrations, including captura, Sea$O_2$, equatic, and Ebb carbon, are advancing electrochemical DOC technologies with annual capacities in the 100–1000 t$CO_2$ range.[329] A proof-of-concept electrochemical system was demonstrated using a bipolar membrane electrodialysis (BPMED) cell coupled with a vapor-fed $CO_2$ reduction ($CO_2$R) cell for integrated capture and conversion of $CO_2$ from ocean water (Fig. 21c).[177] The BPMED configuration replaced the conventional water-splitting reaction with one-electron, reversible redox reactions at the electrodes. This cell design enables operation in both single-stack and multi-stack configurations without introducing side reactions or unintended chemical species, making it suitable for scalable deployment.

HFMCs have been proposed in DOC as a viable technology to extract $CO_2$ from seawater due to the high-surface area gas–liquid contactors that extract molecular $CO_2$ from seawater without direct mixing of solvent streams.[330,331] Because ocean dissolved inorganic carbon exists predominantly as bicarbonate at normal ocean pH, HFMC-based DOC typically couples the contactor with a pH-swing step (electrochemical or chemical acidification) to shift bicarbonate/carbonate to dissolved $CO_2$, which can then be removed by using vacuum or sweep-gas stripping across a hydrophobic microporous membrane.[332] Similar to DAC, in DOC hydrophobic polymers such as PP and PVDF are widely used due to their porosity and resistance to wetting, while recent work emphasizes surface-engineered fibers (*e.g.*, superhydrophobic/antifouling modifications) to mitigate wetting and performance decay during saline operation.[333,334] For example, composite membranes integrating PVDF-grafted polymers, ionic liquid coatings, or nanoparticle fillers have been shown to enhance $CO_2$ permeability and wetting resistance when used with amine or IL solvents.[335–338]

In DOC systems, HFMCs are employed to facilitate $CO_2$ extraction from acidified seawater using inorganic bases or amine solvents as capture media, with the membrane enabling selective $CO_2$ diffusion while preventing solvent-seawater mixing.[329,330] Electrochemically assisted systems that couple pH-swing acidification with $CO_2$ stripping in membrane contactors have also been proposed for scalable, closed-loop DOC.[22] However, challenges remain in membrane material stability under alkaline and saline conditions, long-term resistance to fouling, and scaling under real-world operation. Depending on the process configuration, the extracted $CO_2$ may be collected as a concentrated gas stream (for compression/storage) or absorbed into an alkaline solution for downstream utilization, and the decarbonized seawater is subsequently re-alkalinized prior to discharge to maintain environmental compatibility.[330,331]

## 5. Integrated carbon capture and utilization (ICCU)

ICCU is a significant advancement toward cost-effective and energy-efficient carbon management. The ICCU technology allows direct conversion of captured carbon into value-added products without the need for intermediate desorption, purification, and transport (Fig. 22).[38] Rather than following a sequential approach of capture, purification, and separate conversion, ICCU systems are favored to directly convert captured $CO_2$ often in the chemically bound form, into value-added products within a unified process framework. This concept has attracted considerable interest in recent years to reduce parasitic energy demands and enable modular, distributed carbon utilization. One of the most studied approaches to ICCU involves amine-based chemical absorption paired with the electrochemical $CO_2$ reduction reaction ($CO_2$RR).[339] In conventional capture systems, $CO_2$ is absorbed into an aqueous amine solution, typically 30 wt% MEA solvent, and then thermally desorbed for further processing. However, recent studies have demonstrated that it is possible to electrochemically reduce captured $CO_2$ directly within the amine media. Lee *et al.* demonstrated that direct electrolysis of the chemically absorbed $CO_2$ species in MEA can be achieved by adapting the electrochemical double layer (EDL) through the addition of

 

Table 7 Summary of economic performances of carbon capture based on different capture solvents

| Entry | Solvent/sorbent | Application | Flue gas $CO_2$ concentration | Scale ($tCO_2\ h^{-1}$) | Capture condition | Capture efficiency (%) | SRD ($GJ\ tCO_2^{-1}$) | Capture cost ($USD\ tCO_2^{-1}$) | Ref. |
|---|---|---|---|---|---|---|---|---|---|
| 1 | MEA | Steel plant | 35 wt% | 703 | $T = 313$ K<br>$P = 110$ kPa | — | — | 50.23 | 124 |
| 2 | MEA | Cement plant | 33.9 wt% | 430 | $T = 313$ K<br>$P = 120$ kPa | 90 | 5.5–7.3 $GJ\ tCO_2^{-1}$ | 66.5[a] | 345 |
| 3 | MEA | DAC | 400 ppm | 943 | — | 50 | 10.7 $GJ\ tCO_2^{-1}$ | 1691 | 346 |
| 4 | PZ/MDEA | Steel plant | 35 wt% | 703 | $T = 313$ K<br>$P = 110$ kPa | 94 | 2.8 $GJ\ tCO_2^{-1}$ | 31.43 | 124 |
| 5 | PZ/MEA | Steel plant | 35 wt% | 703 | $T = 313$ K<br>$P = 110$ kPa | — | — | 36.64 | 124 |
| 6 | MEA/MDEA | Steel plant | 35 wt% | 703 | $T = 313$ K<br>$P = 110$ kPa | — | — | 44.8 | 124 |
| 7 | PZ | Natural gas combined cycle power plant | 12 wt% | 1282 | $T = 313$ K<br>$P = 101$ kPa | 90 | 3.56 $GJ\ tCO_2^{-1}$ | 34.65 | 347 |
| 8 | EEMPA | Natural gas combined cycle power plant | 4% | 5234 | — | 90 | 2.7–3.2 $GJ\ tCO_2^{-1}$ | 53.7–57.3 | 348 |
| 9 | AMP | Natural gas combined cycle power plant | — | — | | 90 | 2.94 $GJ\ tCO_2^{-1}$ | — | 349 |
| 10 | IL | — | 13 mol% | — | — | 90 | — | 104.05 | 350 |
| 11 | MOF | Power plant | 15 mol% | 514 | $T = 298$–$313$ K | >90 | — | 91–146.9 | 351 |
| 12 | MOF | Natural gas combined cycle power plant | — | — | — | >90 | — | 205.5–234.6 | 351 |

[a] Value converted from EUR to USD.

alkali cations such as $K^+$, $Rb^+$, and $Cs^+$.[340] These ions effectively alter the interfacial structure, facilitating electron transfer to the carbamate and enabling conversion to CO with up to 72% faradaic efficiency at 50 mA $cm^{-2}$ current density. Furthermore, the authors showed that elevated temperatures (~333 K) improved reaction kinetics and enabled stable operation over multiple capture/conversion cycles, highlighting the potential for solvent recyclability and process intensification. ICCU using sterically hindered amines such as AMP dissolved in propylene carbonate as both the capture medium and electrolyte was explored.[341] This system demonstrated *in situ* $CO_2$ conversion to formate and CO without the need for desorption. The electrochemical performance improved at elevated temperatures (348 K), reaching partial current densities of up to 10 mA $cm^{-2}$ with faradaic efficiencies of 40–50%. The study also provided mechanistic insights into how $CO_2$ speciation (*e.g.*, as $HCO_3^-$ or carbamate) affects electrochemical reactivity, reinforcing the importance of matching solvent chemistry to the catalyst and operating conditions. In addition to electrochemical carbon conversion, thermocatalytic conversion of $CO_2$ to methane is designed within a single process stream using water-lean EEMPA solvent and a Ru-based catalyst.[121] This non-electrochemical system effectively coupled the exothermic methanation reaction with $CO_2$ capture, achieving high methane selectivity at moderate pressures and temperatures. The integration of capture and conversion in this case reduced energy penalties associated with solvent regeneration and gas compression. Notably, the system demonstrated good cycling stability and underscored the versatility of amine solvents beyond purely electrochemical schemes. From a broader perspective, a comprehensive review of ICCU strategies focus on categorizing approaches based on the capture medium (*e.g.*, amine-based and solid sorbents) and conversion pathways (*e.g.*, electrochemical, thermocatalytic, and photocatalytic).[342] The authors highlighted the emergence of dual-functional materials capable of simultaneously adsorbing and activating $CO_2$, as well as the importance of reactor design, especially in continuous flow configurations. Moreover, TEA and life cycle analysis (LCA) were discussed as essential tools to benchmark ICCU technologies against conventional decarbonization pathways.

Economic performances between conventional CCU and an ICCU process that integrates CaO-based calcium looping with the reverse water-gas shift (RWGS) reaction indicates that the ICCU system achieved higher energy efficiency (37.1%) and greater CO production (1.20 Mt per year) compared to the two-step CCU process.[343] Importantly, ICCU showed significantly lower costs for both CO production (720.25 USD $t^{-1}$) and $CO_2$ avoided (317.11 USD $t^{-1}$), highlighting the economic advantages of integration. These improvements are largely attributed to the elimination of intermediate regeneration and transport steps, and the isothermal operation that enhances sorbent stability and reduces purge rates. In addition, the techno-economic and environmental feasibility of electrochemical $CO_2$ reduction directly from amine-based capture media ($eCO_2RR$) was also analyzed, eliminating the need for thermal regeneration and gas purification.[344] Using MEA as a model solvent, they demonstrated that while current $CO_2RR$ systems suffer from lower faradaic efficiency and current density compared to the conventional $CO_2RR$, future system improvements (*e.g.*, >200 mA $cm^{-2}$, >90% FE) could make the $eCO_2RR$ more cost-effective, reducing the levelized cost of CO by up to 6.1%. The study highlights that electrolyzer performance, particularly catalyst activity and stability in chemically rich media, is the key determinant of process viability, emphasizing the need for tailored electrocatalysts and membrane electrode assemblies optimized for direct conversion environments.

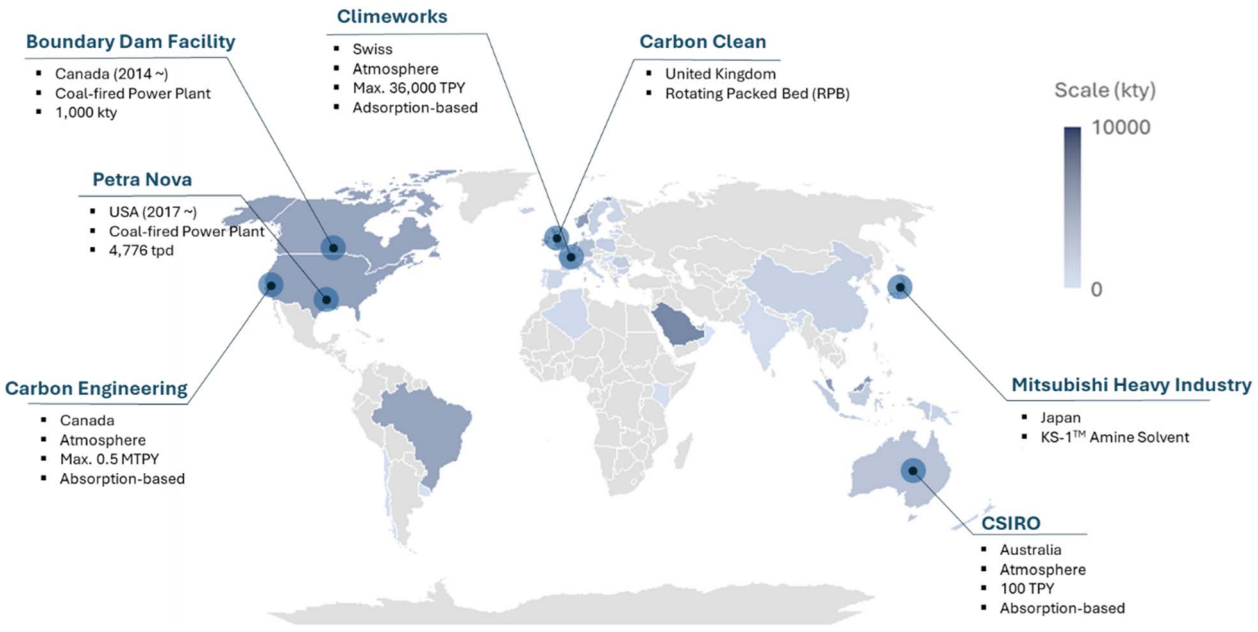


Fig. 23 Global status of carbon capture and utilization projects.

 

These include the need for improved understanding of $CO_2$ speciation and reaction kinetics in complex media, enhanced electrode and catalyst designs that tolerate long-term exposure to reactive solvents, and rigorous system-level analyses that integrate capture and conversion energetics. As ICCU continues to evolve, its potential to enable decentralized carbon utilization and reduce the overall carbon footprint of chemical manufacturing will depend on continued innovation in materials, interface engineering, and process integration.

## 6. Comparison of techno-economic analysis (TEA) of different solvents

The choice of solvent in $CO_2$ capture systems plays a pivotal role in determining the overall energy consumption, capture efficiency, and cost-effectiveness of the process. A comparative analysis of various solvents across industrial and atmospheric capture settings reveals notable differences in performance metrics such as reboiler duty, capture efficiency, and capture cost per metric tonne of $CO_2$ (USD $tCO_2^{-1}$) (Table 7). MEA remains the industrial benchmark due to its chemical simplicity, availability, and relatively well-understood absorption-regeneration behavior. For PCC applications such as steel and cement plants ($CO_2$ concentrations ~34–35 wt%), MEA achieves capture efficiencies of around 90%, with reboiler duties in the range of 5.5–7.3 GJ $tCO_2^{-1}$, and capture costs of 50–57 USD $tCO_2^{-1}$. However, under ultra-dilute conditions like DAC ($CO_2$ ~400 ppm), its performance deteriorates significantly, requiring ~10.7 GJ $tCO_2^{-1}$ and resulting in prohibitively high costs of ~1691 USD $tCO_2^{-1}$, underscoring the need for alternative solvents in low-$CO_2$ scenarios. To improve performance, amine blends such as PZ/MEA and MEA/MDEA have been proposed. These combinations leverage the high absorption capacity of PZ and the favorable thermodynamic properties of secondary or tertiary amines. In the case of steel plant applications, PZ/MEA has demonstrated capture efficiencies exceeding 94%, with reboiler duties as low as 2.8 GJ $tCO_2^{-1}$ and capture costs reduced to 31–37 USD $tCO_2^{-1}$, significantly outperforming MEA alone. Similarly, MEA/MDEA blends offer balanced absorption and regeneration properties, achieving competitive costs of 44.8 USD $tCO_2^{-1}$. For natural gas combined cycle (NGCC) power plants where $CO_2$ concentrations are lower (4–12 wt%), specialized solvents such as EEMPA and AMP have shown promising performance. These solvents achieve ~90% capture efficiency, with relatively low reboiler duties ranging from 2.7–3.2 GJ $tCO_2^{-1}$, and estimated capture costs between 53.7-57.3 USD $tCO_2^{-1}$, suggesting feasibility for large-scale deployment in NGCC applications. PZ alone, when used in NGCC contexts, shows comparable efficiency with a reboiler duty of 3.56 GJ $tCO_2^{-1}$ and a capture cost of 34.65 USD $tCO_2^{-1}$, indicating strong economic viability for high-throughput systems. Emerging solvent classes such as DESs also offer advantages in terms of tunability and low volatility. However, despite achieving high capture efficiency (90%), DES-based systems currently exhibit high capture costs, reported at ~104 USD $tCO_2^{-1}$, with limited available data on regeneration energy. This suggests that while DESs are attractive from a materials standpoint, substantial optimization is required for their competitive integration into large-scale capture systems. In summary, the TEA across solvent systems clearly demonstrates a trade-off between capture efficiency, energy requirement, and cost. While MEA remains a viable baseline, blended amines such as PZ/MEA currently offer the most balanced performance, achieving high efficiency with reduced energy and cost burdens. For low-concentration or high-throughput applications, tailored solvents like AMP- or morpholine-based compounds show potential, though system complexity and solvent stability remain concerns. Further advancements in the solvent formulation, especially targeting lower regeneration energy and higher $CO_2$ loading capacity, will be essential to meet the scalability and sustainability demands of next-generation carbon capture systems.

## 7. Current status of CCUS in the world

CCUS technologies are rapidly expanding across the globe as part of national and industrial strategies to meet climate targets and decarbonize hard-to-abate sectors. In the most recent assessments, over 40 countries are actively developing or operating CCUS projects at various scales, with significant disparities in deployment volume and infrastructure maturity. Fig. 23 presents a global distribution map of CCUS project capacity (in kilotonnes per year, kt per year), based on public data from the International Energy Agency.[26]

The major country, the United States, maintains a substantial footprint (3806 kt per year), driven by a combination of federal tax incentives (*e.g.*, 45Q) and strong private sector participation.[352] As a representative project regarding CCUS, the Boundary Dam Carbon Capture and Storage facility in Canada is one of the pioneering projects that began operation in 2014 and became the first commercial-scale carbon capture project for a coal-fired power station.[353,354] They utilize an amine-based absorption system to capture approximately 1000 kt per year of $CO_2$, with a portion of the captured $CO_2$ utilized for enhanced oil recovery (EOR) and the remainder stored in a deep saline formation. Further in the United States, the Petra Nova project (Texas) was installed in 2017 as a large-scale carbon plant retrofitted to a coal-fired power plant.[355] The system applies KS-1™ amine solvent that was developed by Mitsubishi Heavy Industry (Japan). The capture plant is capable of capturing up to 4776 t per day[51] Although the project was suspended in 2021 due to economic conditions, Petra Nova served as a critical benchmark for evaluating amine-based capture performance under real operating conditions at the commercial scale. In parallel with these projects, several technology providers have advanced the development of solvent-based capture systems with improved energy efficiency and solvent stability. Mitsubishi Heavy Industries has been a global leader in deploying its KM-CDR Process™, utilizing proprietary amine solvents such as KS-1. The company has delivered $CO_2$ capture systems to multiple facilities worldwide, including chemical plants and natural gas

processing sites in the Middle East and Asia.[355] Shell Cansolv, another key technology provider, offers the CANSOLV $CO_2$ Capture System, which employs a regenerable amine solvent optimized for flue gas applications.[356] This technology has been deployed at several industrial sites, including the Boundary Dam CCS facility, offering high capture efficiency and solvent recovery performance. Carbon Clean, a UK-based company, has developed a modular and compact $CO_2$ capture technology known as CycloneCC™ based on a RPB system, targeting small- to mid-scale industrial emitters.[357] The system reduces the physical footprint and capital costs associated with traditional amine absorption systems and has been piloted in India and Europe, including the cement and steel sectors. In summary, global CCUS deployment remains highly region-specific, but the increasing number of participating countries and expanding capacity reflect the growing international consensus on the importance of technology. As more countries shift from pilot to the commercial scale and new capture-utilization hubs emerge, the global CCUS landscape is expected to diversify further, both geographically and technologically. Despite this progress, achieving global scale-up will require overcoming significant technical and economic challenges, as discussed in the following section.

# 8. Challenges and future directions

Despite significant progress in solvent development, several challenges persist across chemical, process, and deployment dimensions. These limitations span mature systems such as aqueous amines to more recent concepts including ILs, DESs, enzymes, amino acids, electrochemical solvents, porous materials and nanoparticle-based hybrid systems.

## 8.1. Trade-offs in solvent performance

No solvent class offers a complete solution; each involves trade-offs between absorption capacity, kinetics, regeneration energy, stability, and viscosity. Aqueous amines remain the benchmark due to their rapid $CO_2$ uptake but suffer from high energy demand for regeneration ($\approx$3–4 GJ $tCO_2^{-1}$), degradation under oxygen and $SO_x$/$NO_x$ exposure, and corrosion.[90,91,358] Amino acid salts were introduced to improve biodegradability and oxidative resistance, but their lower reactivity and precipitation issues limit large-scale deployment.[131,359] Enzyme-enhanced systems (*e.g.*, CA with amino acid or amine solutions) offer fast kinetics, yet enzyme stability, cost, and susceptibility to denaturation under process conditions remain unsolved barriers.[281] Emerging solvents such as DESs and ILs offer structural tunability, negligible volatility, and enhanced thermal stability, but these properties often come at the expense of high viscosity and slow mass transfer. Nanoparticle-enhanced solvents can improve absorption rates by increasing interfacial area or catalytic activity, but they introduce challenges in nanoparticle aggregation, recovery, and long-term stability.[360] Furthermore, a recurring gap is the lack of general data on viscosity, diffusivity, and heat capacity as a function of $CO_2$ loading and the general KPIs presented in this review, which prevents rationalization of molecular and material design coupled to mass-transfer coefficients and SRD under real operation conditions. Without systematic reporting of these properties, comparison of different solvent classes remains a complex task. Furthermore, the challenge ahead is to design solvents and materials that mitigate these trade-offs, for instance, combining fast kinetics with low regeneration energy and high stability, something no current solvent class fully achieves.

## 8.2 Limited techno-economic data

Although hundreds of new solvents have been proposed at the lab scale, systematic TEAs remain rare. Most TEAs extrapolate from amine benchmarks without accounting for differences in solvent chemistry, degradation and regeneration.[55,127] Key process indicators-including reboiler duty, $CO_2$ working capacity, degradation rate, and make-up solvent costs-are inconsistently reported across studies. Electrochemical solvents, which regenerate *via* applied potential rather than thermal swing, are particularly under-characterized: energy efficiency, electrode stability, and solvent-electrolyte compatibility are seldom quantified in a way that permits fair comparison with thermal solvents.[185] The absence of standardized testing and cost reporting impedes objective benchmarking across solvent classes.[124,127] A unified method is needed to establish standardized testing and reporting protocols for new solvents (*e.g.*, common conditions for measuring SRD, degradation rate, *etc.*), to enable "apple-to-apple" comparisons across different materials and solvents.[127] TEAs should be based on experimentally determined, material-specific properties rather than relying on assumptions borrowed from benchmark systems. Key parameters such as heat capacity, thermal conductivity, volatility, foaming tendency, corrosion rate, degradation kinetics, and solvent make-up rates should be treated as essential inputs for accurate cost and performance assessment. For solids, pellet density, binder fraction, attrition resistance, and heat of adsorption in humid mixed-gas streams are required to translate lab uptake into process cost.[55]

## 8.3. Integration with emerging processes

Future carbon capture systems must integrate with utilization and storage pathways, placing new demands on solvent functionality. Integration limitations are often interfacial and material-compatibility problems: catalyst poisoning by capture media (especially when the flue gas contains $NO_x$, $SO_x$ and particulates) and electrode passivation by salts or degradation products thus requiring additional hardware to purify the feed gas or robust electrodes, respectively. Conventional aqueous solvents are generally unsuitable for integrated capture and conversion (ICCU), as they can deactivate catalysts, or lack the conductivity required for electrochemical $CO_2$ reduction.[361] Electrochemical solvents and redox-active liquids offer a route to combine capture and regeneration with conversion, but challenges include limited stability of redox mediators, side reactions under cycling, and compatibility with catalytic surfaces.[362,363] Enzyme-containing systems may enable bio-hybrid ICCU approaches but require stabilization strategies

 

(immobilization and encapsulation) to withstand industrial operating conditions. ICCU-relevant capture media need defined electrochemical windows, ionic conductivity, controlled $CO_2$ speciation at reaction interfaces, and resistance to oxidative side reactions during cycling and $CO_2$ transformations. On the other hand, nanoparticle-enhanced solvents hold potential for catalytic ICCU, yet particle–solvent interactions remain poorly understood, and their application in $CO_2$ transformations remains unexplored.

### 8.4. Environmental and scalability concerns

Scalability and environmental impact of CCUS is a major barrier to adoption. Amines are inexpensive but degrade into toxic byproducts (*e.g.*, nitrosamines)[364] and require large facilities.[74] Amino acids are biodegradable and more environmentally benign, but their precipitation tendencies complicate process design.[365] ILs and DESs, while promising on a molecular level, face issues of synthetic cost, purity control, and uncertain environmental fate, especially those ILs or DES that rely on fluorinated counter ions.[366,367] Nanoparticle-enhanced solvents introduce risks of nanoparticle release into effluents, requiring additional separation or recycling steps; this further complicates the environmental scenario depending on the nature and size of the nanoparticles.[368] Enzyme-based systems are limited by high cost of production and short operational lifetimes necessitating careful operation control over the $CO_2$ capture conditions.[369] Electrochemical solvents often rely on corrosive supporting electrolytes and redox mediators with limited supply chains or toxic precursors, raising sustainability concerns.[370] In the case of porous materials, there are significant challenges associated with the scaling up of such materials especially with reproducible morphology and porosity, and assessment of their environmental impact.[53] LCA for newer solvent classes (*e.g.* PLs and redox-active molecules) are sparse, and long-term ecological effects remain largely unknown. Therefore, regulatory approval and public acceptance also depend on these issues (*e.g.*, nitrosamine emissions from amine plants, or unknown ecotoxicity of DES and ILs), making it imperative to address them for future deployment and environmental protection. Furthermore, in the case of DOC, cross-pollution of sea water (*e.g.* leak of redox active species or excess pH modification *via* acidification or basification) during the DOC process is a major environmental concern and high standards of process control and maintenance should be mandatory.[371,372]

### 8.5. Challenges unique to DAC and DOC

DAC and DOC require harsher operating conditions than flue-gas capture. DAC requires solvents that can bind $CO_2$ efficiently at ~400 ppm, maintain performance despite continuous oxygen exposure, and regenerate at low energy input.

In DAC, the key obstacle is the ultra-low $CO_2$ partial pressure (*ca.* 400 ppm or 40 Pa), which reduces sorption driving force and slows kinetics compared to flue gas capture. As a result, DAC systems require highly reactive sorbents or extensive air-contacting infrastructure, contributing to high energy demands for regeneration, often exceeding 5 GJ $tCO_2^{-1}$.[373] Traditional solvents such as MEA and amino acid salts underperform under these dilute conditions and suffer from oxidative degradation when exposed to atmospheric $O_2$, reducing their long-term effectiveness.[43,311] In contrast, newer media such as ionic liquids (ILs) and enzyme-assisted systems offer potential performance advantages but bring their own limitations: ILs often suffer from high viscosity and slow mass transfer,[374] while enzymes like carbonic anhydrase must be stabilized against heat, UV, and pH fluctuations to remain viable in outdoor DAC systems.[286]

DOC systems, while leveraging seawater's higher inorganic carbon content, introduce another set of chemical and environmental challenges. In seawater, $CO_2$ exists mostly as bicarbonate and carbonate ions, not free $CO_2$, requiring pH-swing approaches (*e.g.*, electrochemical or chemical acidification) to generate molecular $CO_2$ for capture.[22,330] This step demands robust membrane materials and pH-resistant sorbents capable of stable operation in high-salinity, chloride-rich environments. Corrosion, mineral scaling (*e.g.*, $CaCO_3$ and $Mg(OH)_2$), and marine biofouling pose persistent threats to long-term DOC system stability.[375] Moreover, to avoid ecological disruption, DOC must tightly control pH shifts and prevent the release of residual chemicals (*e.g.*, acids, redox agents, or caustics) into marine environments.[371,372] Both DAC and DOC technologies also require material and system designs that tolerate variable ambient conditions (*e.g.*, humidity, temperature, and contaminants), as they are inherently deployed in exposed or remote areas. In summary, while DAC and DOC each offer distinct advantages, their practical implementation demands careful optimization of solvent chemistry, material resilience, and energy integration to overcome these technical and environmental limitations.

## 9. Conclusion

Solvent-based $CO_2$ capture remains a cornerstone of global decarbonization strategies due to its technical maturity, flexibility, and compatibility with both industrial and atmospheric $CO_2$ sources. This review has outlined the landscape of solvent technologies, from conventional aqueous amines to emerging classes such as DESs, ILs, amino acids, redox-active fluids, and electrochemically regenerable solvents. While individual studies have advanced our understanding of each class, there remains a pressing need for integrative assessments that account not only for solvent chemistry but also for process integration and techno-economic performance.

Our comparative analysis of key performance indicators demonstrates that no universal solvent exists. Instead, the optimal choice depends on the application context: MEA and PZ-based blends remain attractive for point-source, and inorganic bases, supported amines or electrochemical solvents may be suitable in DAC and DOC scenarios. However, since most reported performance data are context-specific and in many cases not directly comparable, future work should prioritize reporting standardized solvent parameters to enable consistent benchmarking across different solvent classes.

The coupling of capture with conversion represents a promising shift from a linear to a circular carbon economy. Solvent systems that can not only absorb but also support *in situ* $CO_2$ conversion reactions, especially under electrochemical or catalytic conditions, offer an avenue for energy and cost savings. However, this direction requires new materials with dual functionality and long-term stability, which are still at an early stage of development. Furthermore, it is stressed that progress relies on a synergistic strategy combining chemistry, engineering, and TEA.

In summary, solvent-based $CO_2$ capture technologies continue to evolve rapidly. This review offers a structured framework to navigate current options and to guide the development of new materials and processes. Achieving climate targets will depend not only on developing better solvents, but on deploying them in systems that are integrated, economically viable, and scalable across multiple sectors. This comprehensive comparison of solvent classes and their performance is intended to guide such developments, helping researchers and practitioners identify the most suitable paths forward for the development of next-generation $CO_2$ capture solvents.

## Author contributions

C. Q. wrote the manuscript with the help of the other co-authors. H. Lim and C. Q. supervised, reviewed and edited the manuscript. All the authors discussed and commented on the manuscript.

## Conflicts of interest

There are no conflicts to declare.

## Data availability

No data were generated in this work.

## Acknowledgements

This work was supported by the Carbon Neutrality Demonstration and Research Center of UNIST (Ulsan National Institute of Science and Technology) and the InnoCORE program of the Ministry of Science and ICT(1.260005.01).

## References

1 NOAA, *Carbon Dioxide Now More than 50% High. Than Pre-industrial Levels*.
2 T. M. Lenton, C. Xu, J. F. Abrams, A. Ghadiali, S. Loriani, B. Sakschewski, C. Zimm, K. L. Ebi, R. R. Dunn, J.-C. Svenning and M. Scheffer, *Nat. Sustain.*, 2023, **6**, 1237–1247.
3 International Energy Agency, *$CO_2$ Emissions by Region*, 2023, https://www.iea.org/countries.
4 B. Dziejarski, R. Krzyżyńska and K. Andersson, *Fuel*, 2023, **342**, 127776.
5 F. Nath, M. N. Mahmood and N. Yousuf, *Geoenergy Sci. Eng.*, 2024, **238**, 212726.
6 M. Bui, C. S. Adjiman, A. Bardow, E. J. Anthony, A. Boston, S. Brown, P. S. Fennell, S. Fuss, A. Galindo, L. A. Hackett, J. P. Hallett, H. J. Herzog, G. Jackson, J. Kemper, S. Krevor, G. C. Maitland, M. Matuszewski, I. S. Metcalfe, C. Petit, G. Puxty, J. Reimer, D. M. Reiner, E. S. Rubin, S. A. Scott, N. Shah, B. Smit, J. P. M. Trusler, P. Webley, J. Wilcox and N. Mac Dowell, *Energy Environ. Sci.*, 2018, **11**, 1062–1176.
7 C. Wu, Q. Huang, Z. Xu, A. T. Sipra, N. Gao, L. P. D. E. S. Vandenberghe, S. Vieira, C. R. Soccol, R. Zhao, S. Deng, S. K. S. Boetcher, S. Lu, H. Shi, D. Zhao, Y. Xing, Y. Chen, J. Zhu, D. Feng, Y. Zhang, L. Deng, G. Hu, P. A. Webley, D. Liang, Z. Ba, A. Mlonka-Mędrala, A. Magdziarz, N. Miskolczi, S. Tomasek, S. S. Lam, S. Y. Foong, H. S. Ng, L. Jiang, X. Yan, Y. Liu, Y. Ji, H. Sun, Y. Zhang, H. Yang, X. Zhang, M. Sun, D. C. W. Tsang, J. Shang, C. Muller, M. Rekhtina, M. Krödel, A. H. Bork, F. Donat, L. Liu, X. Jin, W. Liu, S. Saqline, X. Wu, Y. Xu, A. L. Khan, Z. Ali, H. Lin, L. Hu, J. Huang, R. Singh, K. Wang, X. He, Z. Dai, S. Yi, A. Konist, M. H. S. Baqain, Y. Zhao, S. Sun, G. Chen, X. Tu, A. Weidenkaff, S. Kawi, K. H. Lim, C. Song, Q. Yang, Z. Zhao, X. Gao, X. Jiang, H. Ji, T. E. Akinola, A. Lawal, O. S. Otitoju, M. Wang, G. Zhang, L. Ma, B. C. Sempuga, X. Liu, E. Oko, M. Daramola, Z. Yu, S. Chen, G. Kang, Q. Li, L. Gao, L. Liu and H. Zhou, *Carbon Capture Sci. Technol.*, 2024, **11**, 100178.
8 M. Jakob, J. C. Steckel, F. Jotzo, B. K. Sovacool, L. Cornelsen, R. Chandra, O. Edenhofer, C. Holden, A. Löschel, T. Nace, N. Robins, J. Suedekum and J. Urpelainen, *Nat. Clim. Chang.*, 2020, **10**, 704–707.
9 R. Wang, W. Cai, R. Y. Cui, L. Huang, W. Ma, B. Qi, J. Zhang, J. Bian, H. Li, S. Zhang, J. Shen, X. Zhang, J. Zhang, W. Li, L. Yu, N. Zhang and C. Wang, *Nat. Commun.*, 2025, **16**, 241.
10 M. Millinger, F. Hedenus, E. Zeyen, F. Neumann, L. Reichenberg and G. Berndes, *Nat. Energy*, 2025, **10**, 226–242.
11 T. Luo, B. Shen, Z. Mei, A. Hove and K. Ju, *Nat. Commun.*, 2024, **15**, 5900.
12 O. Cavalett, M. D. B. Watanabe, M. Voldsund, S. Roussanaly and F. Cherubini, *Nat. Sustain.*, 2024, **7**, 568–580.
13 S. S. Volaity, B. K. Aylas-Paredes, T. Han, J. Huang, S. Sridhar, G. Sant, A. Kumar and N. Neithalath, *npj Mater. Sustain.*, 2025, **3**, 23.
14 E. Koohestanian and F. Shahraki, *J. Environ. Chem. Eng.*, 2021, **9**, 105777.
15 F. Raganati and P. Ammendola, *Energy Fuels*, 2024, **38**, 13858–13905.
16 K. An, A. Farooqui and S. T. McCoy, *Appl. Energy*, 2022, **325**, 119895.
17 M. Fasihi, O. Efimova and C. Breyer, *J. Clean. Prod.*, 2019, **224**, 957–980.
18 F. Sabatino, A. Grimm, F. Gallucci, M. van Sint Annaland, G. J. Kramer and M. Gazzani, *Joule*, 2021, **5**, 2047–2076.

 

19 K. Sievert, T. S. Schmidt and B. Steffen, *Joule*, 2024, **8**, 979–999.
20 A. Kim, H. Kim, Y. D. Chaniago and H. Lim, *Sustain. Prod. Consum.*, 2023, **41**, 21–35.
21 A. Lieber, M. Hildebrandt, S.-L. Davidson, J. Rivero, H. Usman, T. H. R. Niepa and K. Hornbostel, *Chem.–Eng. J.*, 2023, **470**, 144140.
22 P. Aleta, A. Refaie, M. Afshari, A. Hassan and M. Rahimi, *Energy Environ. Sci.*, 2023, **16**, 4944–4967.
23 A. J. Watson, U. Schuster, J. D. Shutler, T. Holding, I. G. C. Ashton, P. Landschützer, D. K. Woolf and L. Goddijn-Murphy, *Nat. Commun.*, 2020, **11**, 4422.
24 J. J. Cole and Y. T. Prairie, in *Encyclopedia of Inland Waters*, Elsevier, 2009, pp. 30–34.
25 F. Bisotti, K. A. Hoff, A. Mathisen and J. Hovland, *Chem. Eng. Sci.*, 2024, **283**, 119416.
26 International Energy Agency (IAE), *CCUS Proj. database*, https://www.iea.org/data-and-statistics/data-product/ccus-projects-database, accessed August 2025.
27 J. Z. Y. Tan, J. M. Uratani, S. Griffiths, J. M. Andresen and M. M. Maroto-Valer, *Nat. Rev. Chem.*, 2025, **9**, 656–671.
28 S. Babamohammadi, A. Shamiri and M. K. Aroua, *Rev. Chem. Eng.*, 2015, **31**, 383–412.
29 M. G. Darmayanti, K. L. Tuck and S. H. Thang, *Adv. Mater.*, 2024, **36**, 2403324.
30 T. N. Borhani and M. Wang, *Renew. Sustain. Energy Rev.*, 2019, **114**, 109299.
31 G. H. Choi, H. J. Song, S. Lee, J. Y. Kim, M. W. Moon and P. J. Yoo, *Nano Energy*, 2023, **112**, 108512.
32 A. M. Zito, L. E. Clarke, J. M. Barlow, D. Bím, Z. Zhang, K. M. Ripley, C. J. Li, A. Kummeth, M. E. Leonard, A. N. Alexandrova, F. R. Brushett and J. Y. Yang, *Chem. Rev.*, 2023, **123**, 8069–8098.
33 D. W. Keith, G. Holmes, D. St. Angelo and K. Heidel, *Joule*, 2018, **2**, 1573–1594.
34 S. Kumar De, D.-I. Won, J. Kim and D. H. Kim, *Chem. Soc. Rev.*, 2023, **52**, 5744–5802.
35 M. Namdari, Y. Kim, D. J. D. Pimlott, A. M. L. Jewlal and C. P. Berlinguette, *Chem. Soc. Rev.*, 2025, **54**, 590–600.
36 Z. Lv, S. Chen, X. Huang and C. Qin, *Curr. Opin. Green Sustain. Chem.*, 2023, **40**, 100771.
37 C. Choe, S. Cheon, J. Gu and H. Lim, *Renew. Sustain. Energy Rev.*, 2022, **161**, 112398.
38 D. J. Heldebrant, J. Kothandaraman, N. Mac Dowell and L. Brickett, *Chem. Sci.*, 2022, **13**, 6445–6456.
39 S. Sun, H. Sun, P. T. Williams and C. Wu, *Sustain. Energy Fuels*, 2021, **5**, 4546–4559.
40 C. Wang, K. Jiang, H. Yu, S. Li, Y. Zhao, Z. Zheng, H. Liu, X. Xia, P. Zhao, Y. Li, H. Liu, S. Yang, Y. Yang, W. Zhang, H. Zheng, F. Li and K. Li, *Next Mater.*, 2025, **8**, 100660.
41 X. Y. D. Soo, J. J. C. Lee, W.-Y. Wu, L. Tao, C. Wang, Q. Zhu and J. Bu, *J. $CO_2$ Util.*, 2024, **81**, 102727.
42 A. Gautam and M. K. Mondal, *Fuel*, 2023, **334**, 126616.
43 Y. C. Xiao, S. S. Sun, Y. Zhao, R. K. Miao, M. Fan, G. Lee, Y. Chen, C. M. Gabardo, Y. Yu, C. Qiu, Z. Guo, X. Wang, P. Papangelakis, J. E. Huang, F. Li, C. P. O'Brien, J. Kim, K. Han, P. J. Corbett, J. Y. Howe, E. H. Sargent and D. Sinton, *Nat. Commun.*, 2024, **15**, 7849.
44 V. Sang Sefidi and P. Luis, *Ind. Eng. Chem. Res.*, 2019, **58**, 20181–20194.
45 W. Faisal Elmobarak, F. Almomani, M. Tawalbeh, A. Al-Othman, R. Martis and K. Rasool, *Fuel*, 2023, **344**, 128102.
46 M. Ramdin, T. W. de Loos and T. J. H. Vlugt, *Ind. Eng. Chem. Res.*, 2012, **51**, 8149–8177.
47 J. Ruan, L. Chen and Z. Qi, *Green Chem.*, 2023, **25**, 8328–8348.
48 K. S. Song, P. W. Fritz and A. Coskun, *Chem. Soc. Rev.*, 2022, **51**, 9831–9852.
49 N. Mokhtarinori, Z. Yang and S. Dai, *Curr. Opin. Green Sustain. Chem.*, 2022, **38**, 100705.
50 W. Fan, Y. Xin, R. Yang, P. Li, L. Qian, Y. Lu, D. Yao, Y. Zheng and D. Wang, *ACS Appl. Energy Mater.*, 2025, **8**, 9992–10006.
51 W. Li, Q. Shuai and J. Yu, *Small*, 2024, **20**, 2402783.
52 H. Demir, G. O. Aksu, H. C. Gulbalkan and S. Keskin, *Carbon Capture Sci. Technol.*, 2022, **2**, 100026.
53 A. H. Farmahini, S. Krishnamurthy, D. Friedrich, S. Brandani and L. Sarkisov, *Chem. Rev.*, 2021, **121**, 10666–10741.
54 F. Raganati, F. Miccio and P. Ammendola, *Energy Fuels*, 2021, **35**, 12845–12868.
55 P. A. Saenz Cavazos, E. Hunter-Sellars, P. Iacomi, S. R. McIntyre, D. Danaci and D. R. Williams, *Front. Energy Res.*, 2023, **11**, 1167043.
56 G. F. Versteeg and W. P. M. van Swaaij, *Chem. Eng. Sci.*, 1988, **43**, 573–585.
57 R. Neerup, V. E. Rasmussen, S. H. B. Vinjarapu, A. H. Larsen, M. Shi, C. Andersen, K. Fuglsang, L. K. Gram, J. Nedenskov, J. Kappel, P. Blinksbjerg, S. Jensen, J. L. Karlsson, S. Borgquist, J. K. Jørsboe, S. N. B. Villadsen and P. L. Fosbøl, *J. Environ. Chem. Eng.*, 2023, **11**, 111411.
58 Q. Huang, J. Thompson, S. Bhatnagar, P. Chandan, J. E. Remias, J. P. Selegue and K. Liu, *Ind. Eng. Chem. Res.*, 2014, **53**, 553–563.
59 L. Braakhuis and H. K. Knuutila, *Chem. Eng. Sci.*, 2023, **279**, 118940.
60 V. Buvik, S. J. Vevelstad, O. G. Brakstad and H. K. Knuutila, *Ind. Eng. Chem. Res.*, 2021, **60**, 5627–5638.
61 I. M. Bernhardsen and H. K. Knuutila, *Int. J. Greenhouse Gas Control*, 2017, **61**, 27–48.
62 M. K. Aroua, A. Benamor and M. Z. Haji-Sulaiman, *J. Chem. Eng. Data*, 1999, **44**, 887–891.
63 M. K. Aroua, A. Ben Amor and M. Z. Haji-Sulaiman, *J. Chem. Eng. Data*, 1997, **42**, 692–696.
64 J. M. Barlow, L. E. Clarke, Z. Zhang, D. Bím, K. M. Ripley, A. Zito, F. R. Brushett, A. N. Alexandrova and J. Y. Yang, *Chem. Soc. Rev.*, 2022, **51**, 8415–8433.
65 A. T. Bui, N. A. Hartley, A. J. W. Thom and A. C. Forse, *J. Phys. Chem. C*, 2022, **126**, 14163–14172.
66 F. Simeon, M. C. Stern, K. M. Diederichsen, Y. Liu, H. J. Herzog and T. A. Hatton, *J. Phys. Chem. C*, 2022, **126**, 1389–1399.

67 R. A. Shaw and T. A. Hatton, *Int. J. Greenhouse Gas Control*, 2020, **95**, 102878.
68 Y. Liu, H.-Z. Ye, K. M. Diederichsen, T. Van Voorhis and T. A. Hatton, *Nat. Commun.*, 2020, **11**, 2278.
69 H. Seo, M. Rahimi and T. A. Hatton, *J. Am. Chem. Soc.*, 2022, **144**, 2164–2170.
70 J. M. Barlow and J. Y. Yang, *J. Am. Chem. Soc.*, 2022, **144**, 14161–14169.
71 R. Sharifian, R. M. Wagterveld, I. A. Digdaya, C. Xiang and D. A. Vermaas, *Energy Environ. Sci.*, 2021, **14**, 781–814.
72 H. Xie, Y. Wu, T. Liu, F. Wang, B. Chen and B. Liang, *Appl. Energy*, 2020, **259**, 114119.
73 Y. E. Kim, J. A. Lim, S. K. Jeong, Y. Il Yoon, S. T. Bae and S. C. Nam, *Bull. Korean Chem. Soc.*, 2013, **34**, 783–787.
74 G. T. Rochelle, *Science*, 2009, **325**, 1652–1654.
75 S. Choi, J. H. Drese and C. W. Jones, *ChemSusChem*, 2009, **2**, 796–854.
76 K. Sumida, D. L. Rogow, J. A. Mason, T. M. McDonald, E. D. Bloch, Z. R. Herm, T.-H. Bae and J. R. Long, *Chem. Rev.*, 2012, **112**, 724–781.
77 N. Brigman, M. I. Shah, O. Falk-Pedersen, T. Cents, V. Smith, T. De Cazenove, A. K. Morken, O. A. Hvidsten, M. Chhaganlal, J. K. Feste, G. Lombardo, O. M. Bade, J. Knudsen, S. C. Subramoney, B. F. Fostås, G. de Koeijer and E. S. Hamborg, *Energy Procedia*, 2014, **63**, 6012–6022.
78 S. Voskian and T. A. Hatton, *Energy Environ. Sci.*, 2019, **12**, 3530–3547.
79 M. Abdinejad, H. Seo, M. E. Lev Massen-Hane and T. A. Hatton, *Angew. Chem., Int. Ed.*, 2024, **63**, e202412229.
80 J. Kim, K. Kim, H. Lim, J. H. Kang, H. S. Park, J. Park and H. Song, *J. Environ. Chem. Eng.*, 2024, **12**, 112664.
81 T. L. Sønderby, K. B. Carlsen, P. L. Fosbøl, L. G. Kiørboe and N. von Solms, *Int. J. Greenhouse Gas Control*, 2013, **12**, 181–192.
82 H. Zentou, B. Hoque, M. A. Abdalla, A. F. Saber, O. Y. Abdelaziz, M. Aliyu, A. M. Alkhedhair, A. J. Alabduly and M. M. Abdelnaby, *Carbon Capture Sci. Technol.*, 2025, **15**, 100386.
83 N. McQueen, K. V. Gomes, C. McCormick, K. Blumanthal, M. Pisciotta and J. Wilcox, *Prog. Energy*, 2021, **3**, 032001.
84 R. Ben Said, J. M. Kolle, K. Essalah, B. Tangour and A. Sayari, *ACS Omega*, 2020, **5**, 26125–26133.
85 K. A. Mumford, Y. Wu, K. H. Smith and G. W. Stevens, *Front. Chem. Sci. Eng.*, 2015, **9**, 125–141.
86 S. A. Freeman and G. T. Rochelle, *Ind. Eng. Chem. Res.*, 2012, **51**, 7719–7725.
87 S. A. Freeman, R. Dugas, D. H. Van Wagener, T. Nguyen and G. T. Rochelle, *Int. J. Greenhouse Gas Control*, 2010, **4**, 119–124.
88 G. Rochelle, E. Chen, S. Freeman, D. Van Wagener, Q. Xu and A. Voice, *Chem. Eng. J.*, 2011, **171**, 725–733.
89 G. T. Rochelle, K. Akinpelumi, T. Gao, C.-T. Liu, A. Suresh Babu and Y. Wu, *Int. J. Greenhouse Gas Control*, 2022, **113**, 103551.
90 V. Buvik, K. Vernstad, A. Grimstvedt, K. K. Høisæter, S. J. Vevelstad and H. K. Knuutila, *Ind. Eng. Chem. Res.*, 2025, **64**, 11000–11020.
91 V. Buvik, S. J. Vevelstad, P. Moser, G. Wiechers, R. R. Wanderley, J. G. M.-S. Monteiro and H. K. Knuutila, *Carbon Capture Sci. Technol.*, 2023, **7**, 100110.
92 S. B. Fredriksen and K.-J. Jens, *Energy Procedia*, 2013, **37**, 1770–1777.
93 R. H. Weiland, J. C. Dingman and D. B. Cronin, *J. Chem. Eng. Data*, 1997, **42**, 1004–1006.
94 F. Closmann, T. Nguyen and G. T. Rochelle, *Energy Procedia*, 2009, **1**, 1351–1357.
95 B. Zhao, F. Liu, Z. Cui, C. Liu, H. Yue, S. Tang, Y. Liu, H. Lu and B. Liang, *Appl. Energy*, 2017, **185**, 362–375.
96 P. Moser, G. Wiechers, S. Schmidt, J. G. M.-S. Monteiro, E. Goetheer, C. Charalambous, A. Saleh, M. van der Spek and S. Garcia, *Int. J. Greenhouse Gas Control*, 2021, **109**, 103381.
97 A. Hartono, R. Ahmad, H. F. Svendsen and H. K. Knuutila, *Fluid Phase Equilib.*, 2021, **550**, 113235.
98 M. Gilardi, F. Bisotti, H. K. Knuutila and D. Bonalumi, *J. Clean. Prod.*, 2024, **447**, 141394.
99 Z. Qi, F. Liu, H. Ding and M. Fang, *Fuel*, 2023, **350**, 128726.
100 R. F. Zheng, D. Barpaga, P. M. Mathias, D. Malhotra, P. K. Koech, Y. Jiang, M. Bhakta, M. Lail, A. V. Rayer, G. A. Whyatt, C. J. Freeman, A. J. Zwoster, K. K. Weitz and D. J. Heldebrant, *Energy Environ. Sci.*, 2020, **13**, 4106–4113.
101 E. Sanchez Fernandez, K. Heffernan, L. V. van der Ham, M. J. G. Linders, E. Eggink, F. N. H. Schrama, D. W. F. Brilman, E. L. V. Goetheer and T. J. H. Vlugt, *Ind. Eng. Chem. Res.*, 2013, **52**, 12223–12235.
102 X. Liu, Q. Ao, S. Shi and S. Li, *Mater. Res. Express*, 2022, **9**, 015504.
103 Y. Gu, Y. Hou, S. Ren, Y. Sun and W. Wu, *ACS Omega*, 2020, **5**, 6809–6816.
104 T. J. Trivedi, J. H. Lee, H. J. Lee, Y. K. Jeong and J. W. Choi, *Green Chem.*, 2016, **18**, 2834–2842.
105 W. Qian, J. Hao, M. Zhu, P. Sun, K. Zhang, X. Wang and X. Xu, *J. $CO_2$ Util.*, 2022, **59**, 101955.
106 D. Fu and P. Zhang, *Energy*, 2015, **87**, 165–172.
107 C. Wang, H. Luo, D. Jiang, H. Li and S. Dai, *Angew. Chem., Int. Ed.*, 2010, **49**, 5978–5981.
108 L. Qiu, Y. Fu, Z. Yang, A. C. Johnson, C. Do-Thanh, B. P. Thapaliya, S. M. Mahurin, L. He, D. Jiang and S. Dai, *ChemSusChem*, 2024, **17**, e202301329.
109 F. Barzagli, C. Giorgi, F. Mani and M. Peruzzini, *ACS Sustain. Chem. Eng.*, 2020, **8**, 14013–14021.
110 M. B. Danbatta, N. A. Al-Azri, M. A. Qyyum and N. Al-Rawahi, *Carbon Capture Sci. Technol.*, 2025, **15**, 100426.
111 H. Shi, A. Naami, R. Idem and P. Tontiwachwuthikul, *Int. J. Greenhouse Gas Control*, 2014, **26**, 39–50.
112 M. Akram, K. Milkowski, J. Gibbins and M. Pourkashanian, *Int. J. Greenhouse Gas Control*, 2020, **95**, 102946.
113 P. Moser, G. Wiechers, S. Schmidt, K. Stahl, J. Garcia Moretz-Sohn Monteiro, R. Veronezi Figueiredo and E. Skylogianni, *Chem.–Eng. J.*, 2024, **499**, 155928.
114 R. Neerup, K. L. Øbro, I. A. Løge, N. Kottaki, C. F. Frøstrup, I. Gyorbiro, M. Dimitriadi, H. Halilov, S. Jensen, J. L. Karlsson and P. L. Fosbøl, *Chem.–Eng. J.*, 2025, **510**, 161542.

 

115 F. Liu, G. Jing, X. Zhou, B. Lv and Z. Zhou, *ACS Sustain. Chem. Eng.*, 2018, **6**, 1352–1361.
116 A. Gautam and M. Kumar Mondal, *Fuel*, 2023, **331**, 125864.
117 S. Zheng, M. Tao, Q. Liu, L. Ning, Y. He and Y. Shi, *Environ. Sci. Technol.*, 2014, **48**, 8905–8910.
118 X. Zhou, C. Liu, J. Zhang, Y. Fan, Y. Zhu, L. Zhang, S. Tang, S. Mo, H. Zhu and Z. Zhu, *Energy*, 2023, **270**, 126930.
119 D. J. Heldebrant, P. K. Koech, V.-A. Glezakou, R. Rousseau, D. Malhotra and D. C. Cantu, *Chem. Rev.*, 2017, **117**, 9594–9624.
120 R. R. Wanderley, D. D. D. Pinto and H. K. Knuutila, *Sep. Purif. Technol.*, 2021, **260**, 118193.
121 J. Kothandaraman, J. Saavedra Lopez, Y. Jiang, E. D. Walter, S. D. Burton, R. A. Dagle and D. J. Heldebrant, *ChemSusChem*, 2021, **14**, 4812–4819.
122 R. P. Cabral, D. J. Heldebrant and N. Mac Dowell, *Ind. Eng. Chem. Res.*, 2019, **58**, 6604–6612.
123 J. Leclaire, D. J. Heldebrant, K. Grubel, J. Septavaux, M. Hennebelle, E. Walter, Y. Chen, J. L. Bañuelos, D. Zhang, M.-T. Nguyen, D. Ray, S. I. Allec, D. Malhotra, W. Joo and J. King, *Nat. Chem.*, 2024, **16**, 1160–1168.
124 X. Ding, H. Chen, J. Li and T. Zhou, *Carbon Capture Sci. Technol.*, 2023, **9**, 100136.
125 B. Lv, B. Guo, Z. Zhou and G. Jing, *Environ. Sci. Technol.*, 2015, **49**, 10728–10735.
126 F. A. Chowdhury, H. Yamada, T. Higashii, K. Goto and M. Onoda, *Ind. Eng. Chem. Res.*, 2013, **52**, 8323–8331.
127 M. T. Mota-Martinez, J. P. Hallett and N. Mac Dowell, *Sustain. Energy Fuels*, 2017, **1**, 2078–2090.
128 T. G. Amundsen, L. E. Øi and D. A. Eimer, *J. Chem. Eng. Data*, 2009, **54**, 3096–3100.
129 N. B. Kummamuru, Z. Idris and D. A. Eimer, *J. Chem. Eng. Data*, 2019, **64**, 4692–4700.
130 D. Morlando, A. Hartono and H. K. Knuutila, *SSRN Electron. J.*, 2025, **273**, 1.
131 R. Ramezani, S. Mazinani and R. Di Felice, *Rev. Chem. Eng.*, 2022, **38**, 273–299.
132 Y. Li, X. Duan, W. Song, L. Ma and J. Jow, *Chem. Eng. J.*, 2021, **405**, 126938.
133 E. Sanchez-Fernandez, K. Heffernan, L. van der Ham, M. J. G. Linders, E. L. V. Goetheer and T. J. H. Vlugt, *Energy Procedia*, 2014, **63**, 727–738.
134 S. Moioli, L. A. Pellegrini, M. T. Ho and D. E. Wiley, *Chem. Eng. Res. Des.*, 2019, **146**, 509–517.
135 M. T. Ho, E. Garcia-Calvo Conde, S. Moioli and D. E. Wiley, *Int. J. Greenhouse Gas Control*, 2019, **81**, 1–10.
136 M. E. Majchrowicz and W. Brilman, *Energy Fuels*, 2015, **29**, 3268–3275.
137 M. H. Abdellah, A. Kiani, W. Conway, G. Puxty and P. Feron, *Sep. Purif. Technol.*, 2025, **358**, 130390.
138 A. Kiani, W. Conway, M. H. Abdellah, G. Puxty, A. Minor, G. Kluivers, R. Bennett and P. Feron, *Greenh. Gases Sci. Technol.*, 2024, **14**, 859–870.
139 Y. Cao, C. Yang, C. Wang, C. Zhou, L. Song, K. Ma, H. Lu and H. Yue, *Chem. Eng. Sci.*, 2023, **273**, 118627.
140 A. Kasturi, J. Gabitto, C. Tsouris and R. Custelcean, *Sep. Purif. Technol.*, 2021, **271**, 118839.
141 K. A. Garrabrant, N. J. Williams, E. Holguin, F. M. Brethomé, C. Tsouris and R. Custelcean, *Ind. Eng. Chem. Res.*, 2019, **58**, 10510–10515.
142 J. I. Obute and G. T. Rochelle, *Int. J. Greenhouse Gas Control*, 2025, **145**, 104405.
143 E. L. Smith, A. P. Abbott and K. S. Ryder, *Chem. Rev.*, 2014, **114**, 11060–11082.
144 B. B. Hansen, S. Spittle, B. Chen, D. Poe, Y. Zhang, J. M. Klein, A. Horton, L. Adhikari, T. Zelovich, B. W. Doherty, B. Gurkan, E. J. Maginn, A. Ragauskas, M. Dadmun, T. A. Zawodzinski, G. A. Baker, M. E. Tuckerman, R. F. Savinell and J. R. Sangoro, *Chem. Rev.*, 2021, **121**, 1232–1285.
145 X. Li, M. Hou, B. Han, X. Wang and L. Zou, *J. Chem. Eng. Data*, 2008, **53**, 548–550.
146 S. Anwer, I. I. I. Alkhatib, H. A. Salih, L. F. Vega and I. AlNashef, *Sep. Purif. Technol.*, 2024, **330**, 125350.
147 H. Yan, L. Zhao, Y. Bai, F. Li, H. Dong, H. Wang, X. Zhang and S. Zeng, *ACS Sustain. Chem. Eng.*, 2020, **8**, 2523–2530.
148 Z. Li, L. Wang, C. Li, Y. Cui, S. Li, G. Yang and Y. Shen, *ACS Sustain. Chem. Eng.*, 2019, **7**, 10403–10414.
149 H. Ghaedi, J. Fu, P. Kalhor, S. M. Soltani and M. Zhao, *J. Mater. Chem. A*, 2025, **13**, 23655–23670.
150 J. Ju, D. Choi, S. Cho, Y. Yoo and D. Kang, *Chem.–Eng. J.*, 2024, **496**, 153922.
151 S. Foorginezhad, G. Yu and X. Ji, *Front. Chem.*, 2022, **10**, 951951.
152 B. Jiang, J. Ma, N. Yang, Z. Huang, N. Zhang, X. Tantai, Y. Sun and L. Zhang, *Energy Fuels*, 2019, **33**, 7569–7577.
153 Z. Lei, B. Chen, Y.-M. Koo and D. R. MacFarlane, *Chem. Rev.*, 2017, **117**, 6633–6635.
154 T. Numpilai, L. K. H. Pham and T. Witoon, *Ind. Eng. Chem. Res.*, 2024, **63**, 19865–19915.
155 S. Elhenawy, M. Khraisheh, F. AlMomani and M. Hassan, *Molecules*, 2020, **25**, 4274.
156 P. Zhang, P. Yin, L. Yang, X. Cui, H. Xing and X. Suo, *Carbon Capture Sci. Technol.*, 2024, **11**, 100180.
157 Y. Wang, Y. Wang, Y. Zhao, J. Fu and Z. Liu, *Chem. Rev.*, 2025, **125**, 6057–6129.
158 S. Zeng, X. Zhang, L. Bai, X. Zhang, H. Wang, J. Wang, D. Bao, M. Li, X. Liu and S. Zhang, *Chem. Rev.*, 2017, **117**, 9625–9673.
159 N. Noorani and A. Mehrdad, *J. Mol. Liq.*, 2022, **357**, 119078.
160 M. E. Atlaskina, O. V. Kazarina, A. N. Petukhov, A. A. Atlaskin, N. S. Tsivkovsky, P. Tiuleanu, Y. B. Malysheva, H. Lin, G.-J. Zhong, A. N. Lukoyanov, A. V. Vorotyntsev and I. V. Vorotyntsev, *J. Mol. Liq.*, 2024, **395**, 123635.
161 X.-M. Zhang, K. Huang, S. Xia, Y.-L. Chen, Y.-T. Wu and X.-B. Hu, *Chem. Eng. J.*, 2015, **274**, 30–38.
162 A. J. Greer, S. F. R. Taylor, H. Daly, M. G. Quesne, N. H. de Leeuw, C. R. A. Catlow, J. Jacquemin and C. Hardacre, *ACS Sustain. Chem. Eng.*, 2021, **9**, 7578–7586.
163 S. Dongare, M. Zeeshan, A. S. Aydogdu, R. Dikki, S. F. Kurtoğlu-Öztulum, O. K. Coskun, M. Muñoz, A. Banerjee, M. Gautam, R. D. Ross, J. S. Stanley, R. S. Brower, B. Muchharla, R. L. Sacci, J. M. Velázquez,

B. Kumar, J. Y. Yang, C. Hahn, S. Keskin, C. G. Morales-Guio, A. Uzun, J. M. Spurgeon and B. Gurkan, *Chem. Soc. Rev.*, 2024, **53**, 8563–8631.
164 Y. Qu, Y. Zhao, D. Li and J. Sun, *Curr. Opin. Green Sustain. Chem.*, 2022, **34**, 100599.
165 T. Yan, X.-L. Chang and W.-G. Pan, *J. Ind. Eng. Chem.*, 2024, **135**, 43–66.
166 B. Kudłak, K. Owczarek and J. Namieśnik, *Environ. Sci. Pollut. Res.*, 2015, **22**, 11975–11992.
167 J. Flieger and M. Flieger, *Int. J. Mol. Sci.*, 2020, **21**, 6267.
168 S. Jin, M. Wu, Y. Jing, R. G. Gordon and M. J. Aziz, *Nat. Commun.*, 2022, **13**, 2140.
169 S. Pang, S. Jin, F. Yang, M. Alberts, L. Li, D. Xi, R. G. Gordon, P. Wang, M. J. Aziz and Y. Ji, *Nat. Energy*, 2023, **8**, 1126–1136.
170 H. Seo, *MRS Commun.*, 2023, **13**, 994–1008.
171 A. Ozden, *ACS Energy Lett.*, 2025, 1550–1576.
172 E. Sánchez-Díez, E. Ventosa, M. Guarnieri, A. Trovò, C. Flox, R. Marcilla, F. Soavi, P. Mazur, E. Aranzabe and R. Ferret, *J. Power Sources*, 2021, **481**, 228804.
173 T. Liu, Y. Wang, Y. Wu, W. Jiang, Y. Deng, Q. Li, C. Lan, Z. Zhao, L. Zhu, D. Yang, T. Noël and H. Xie, *Nat. Commun.*, 2024, **15**, 10920.
174 A. Tatarczuk, T. Spietz, L. Więcław-Solny, A. Krótki, T. Chwoła, S. Dobras, J. Zdeb and M. Tańczyk, *Energies*, 2025, **18**, 2236.
175 X. Li, X. Zhao, Y. Liu, T. A. Hatton and Y. Liu, *Nat. Energy*, 2022, **7**, 1065–1075.
176 J. H. Rheinhardt, P. Singh, P. Tarakeshwar and D. A. Buttry, *ACS Energy Lett.*, 2017, **2**, 454–461.
177 I. A. Digdaya, I. Sullivan, M. Lin, L. Han, W. H. Cheng, H. A. Atwater and C. Xiang, *Nat. Commun.*, 2020, **11**, 1–10.
178 H. Seo and T. A. Hatton, *Nat. Commun.*, 2023, **14**, 1–11.
179 A. M. Zito, D. Bím, S. Vargas, A. N. Alexandrova and J. Y. Yang, *ACS Sustain. Chem. Eng.*, 2022, **10**, 11387–11395.
180 K. M. Diederichsen, Y. Liu, N. Ozbek, H. Seo and T. A. Hatton, *Joule*, 2022, **6**, 221–239.
181 N. A. Hartley, Z. Xu, T. Kress and A. C. Forse, *Mater. Today Energy*, 2024, **45**, 101689.
182 C. Schimanofsky, D. Wielend, S. Kröll, S. Lerch, D. Werner, J. M. Gallmetzer, F. Mayr, H. Neugebauer, M. Irimia-Vladu, E. Portenkirchner, T. S. Hofer and N. S. Sariciftci, *J. Phys. Chem. C*, 2022, **126**, 14138–14154.
183 X. Li, X. Zhao, L. Zhang, A. Mathur, Y. Xu, Z. Fang, L. Gu, Y. Liu and Y. Liu, *Nat. Commun.*, 2024, **15**, 1175.
184 K. Amini, T. Cochard, Y. Jing, J. D. Sosa, D. Xi, M. Alberts, M. S. Emanuel, E. F. Kerr, R. G. Gordon, M. J. Aziz and J. A. Paulson, *Nat. Chem. Eng.*, 2024, **1**, 774–786.
185 B. Gurkan, X. Su, A. Klemm, Y. Kim, S. Mallikarjun Sharada, A. Rodriguez-Katakura and K. J. Kron, *iScience*, 2021, **24**, 103422.
186 M. Rahimi, A. Khurram, T. A. Hatton and B. Gallant, *Chem. Soc. Rev.*, 2022, **51**, 8676–8695.
187 Y. Geng, Y. Guo, B. Fan, F. Cheng and H. Cheng, *J. Fuel Chem. Technol.*, 2021, **49**, 998–1013.
188 K. Rausis, A. R. Stubbs, I. M. Power and C. Paulo, *Int. J. Greenhouse Gas Control*, 2022, **119**, 103701.
189 R. V. Siriwardane and R. W. Stevens, *Ind. Eng. Chem. Res.*, 2009, **48**, 2135–2141.
190 A. A.-H. Mourad, A. F. Mohammad, A. H. Al-Marzouqi, M. Altarawneh, M. H. Al-Marzouqi and M. H. El-Naas, *Int. J. Greenhouse Gas Control*, 2022, **120**, 103768.
191 T. N. G. Borhani, A. Azarpour, V. Akbari, S. R. Wan Alwi and Z. A. Manan, *Int. J. Greenhouse Gas Control*, 2015, **41**, 142–162.
192 S.-J. Han, M. Yoo, D.-W. Kim and J.-H. Wee, *Energy Fuels*, 2011, **25**, 3825–3834.
193 G. Hu, N. J. Nicholas, K. H. Smith, K. A. Mumford, S. E. Kentish and G. W. Stevens, *Int. J. Greenhouse Gas Control*, 2016, **53**, 28–40.
194 B. Arias, G. S. Grasa, M. Alonso and J. C. Abanades, *Energy Environ. Sci.*, 2012, **5**, 7353.
195 D. P. Hanak, E. J. Anthony and V. Manovic, *Energy Environ. Sci.*, 2015, **8**, 2199–2249.
196 F. Yi, H.-K. Zou, G.-W. Chu, L. Shao and J.-F. Chen, *Chem.–Eng. J.*, 2009, **145**, 377–384.
197 Y. Zhang, Y. Wang, K. Han, J. Zhao, J. J. Wu and Y. Li, *Green Energy Resour*, 2024, **2**, 100078.
198 X. Zhang, Z. Fang, P. Zhu, Y. Xia and H. Wang, *Nat. Energy*, 2024, **10**, 55–65.
199 T. Li, E. W. Lees, M. Goldman, D. A. Salvatore, D. M. Weekes and C. P. Berlinguette, *Joule*, 2019, **3**, 1487–1497.
200 K. Bach, E. Garrido Ribó, J. S. Hirschi, Z. Mao, M. T. Nord, L. N. Zakharov, K. A. Goulas, T. J. Zuehlsdorff and M. Nyman, *Chem. Mater.*, 2025, **37**, 48–61.
201 Y. Tong, C. Qin, L. Zhu, S. Chen, Z. Lv and J. Ran, *Environ. Sci. Technol.*, 2022, **56**, 5734–5742.
202 L. Cai, G. Tan, X. Yang, H. Xue, Y. Lin, X. Hu, Z. Song and Y. Zhang, *Chem.–Eng. J.*, 2024, **483**, 149125.
203 G. Qi, K. Liu, A. House, S. Salmon, B. Ambedkar, R. A. Frimpong, J. E. Remias and K. Liu, *Appl. Energy*, 2018, **209**, 180–189.
204 J. Shen, Y. Yuan and S. Salmon, *ACS Sustain. Chem. Eng.*, 2022, **10**, 7772–7785.
205 Y. Kim, E. W. Lees, C. Donde, A. M. L. Jewlal, C. E. B. Waizenegger, B. M. W. de Hepcée, G. L. Simpson, A. Valji and C. P. Berlinguette, *Joule*, 2024, **8**, 3106–3125.
206 J. Bin Lin, T. T. T. Nguyen, R. Vaidhyanathan, J. Burner, J. M. Taylor, H. Durekova, F. Akhtar, R. K. Mah, O. Ghaffari-Nik, S. Marx, N. Fylstra, S. S. Iremonger, K. W. Dawson, P. Sarkar, P. Hovington, A. Rajendran, T. K. Woo and G. K. H. Shimizu, *Science*, 2021, **374**, 1464–1469.
207 Y. Guo, L. Xu, J. J. Zheng, N. Geng, Y. Wang, M. Yao and T. Zhu, *Environ. Sci. Technol.*, 2024, **58**, 22456–22465.
208 O. I. F. Chen, C. H. Liu, K. Wang, E. Borrego-Marin, H. Li, A. H. Alawadhi, J. A. R. Navarro and O. M. Yaghi, *J. Am. Chem. Soc.*, 2024, **146**, 2835–2844.
209 J. Zhu, L. Wu, Z. Bu, S. Jie and B.-G. Li, *ACS Omega*, 2019, **4**, 3188–3197.
210 Z. Zhou, T. Ma, H. Zhang, S. Chheda, H. Li, K. Wang, S. Ehrling, R. Giovine, C. Li, A. H. Alawadhi,

 

M. M. Abduljawad, M. O. Alawad, L. Gagliardi, J. Sauer and O. M. Yaghi, *Nature*, 2024, **635**, 96–101.
211 H. Lyu, H. Li, N. Hanikel, K. Wang and O. M. Yaghi, *J. Am. Chem. Soc.*, 2022, **144**, 12989–12995.
212 S. Sen, R. Diab, M. H. Al-Sayah, R. Jabbour, A. Equbal and O. M. El-Kadri, *ACS Appl. Polym. Mater.*, 2024, **6**, 1314–1324.
213 S. A. Wahed, A. Hassan, A. Alam, R. Bera and N. Das, *ACS Appl. Polym. Mater.*, 2025, **7**, 5127–5137.
214 M. R. Moradi, A. Torkashvand, H. Ramezanipour Penchah and A. Ghaemi, *Sci. Rep.*, 2023, **13**, 9214.
215 K. Okubo, S. Kitajima, H. Kasai and K. Oka, *Small*, 2025, 2410794.
216 Z.-A. Chen, L. Zou, R. Cao and Y.-B. Huang, *Natl. Sci. Rev.*, 2025, **12**, nwaf032.
217 Q. Qian, P. A. Asinger, M. J. Lee, G. Han, K. Mizrahi Rodriguez, S. Lin, F. M. Benedetti, A. X. Wu, W. S. Chi and Z. P. Smith, *Chem. Rev.*, 2020, **120**, 8161–8266.
218 M. Ding, R. W. Flaig, H.-L. Jiang and O. M. Yaghi, *Chem. Soc. Rev.*, 2019, **48**, 2783–2828.
219 J. Yu, L.-H. Xie, J.-R. Li, Y. Ma, J. M. Seminario and P. B. Balbuena, *Chem. Rev.*, 2017, **117**, 9674–9754.
220 F. Sher, A. Hayward, A. El Guerraf, B. Wang, I. Ziani, H. Hrnjić, E. Boškailo, A. Chupin and M. R. Nemțanu, *J. Mater. Chem. A*, 2024, **12**, 27932–27973.
221 R. G. Pearson, *J. Chem. Educ.*, 1987, **64**, 561–567.
222 R. G. Pearson, *J. Chem. Educ.*, 1968, **45**, 581–587.
223 A. M. Hamisu, A. Ariffin and A. C. Wibowo, *Inorganica Chim. Acta*, 2020, **511**, 119801.
224 Z. Han, Y. Yang, J. Rushlow, J. Huo, Z. Liu, Y.-C. Hsu, R. Yin, M. Wang, R. Liang, K.-Y. Wang and H.-C. Zhou, *Chem. Soc. Rev.*, 2025, **54**, 367–395.
225 J. R. Álvarez, E. Sánchez-González, E. Pérez, E. Schneider-Revueltas, A. Martínez, A. Tejeda-Cruz, A. Islas-Jácome, E. González-Zamora and I. A. Ibarra, *Dalton Trans.*, 2017, **46**, 9192–9200.
226 S. Kumari, M. Gusain, B. Y. Lamba and S. Kumar, *J. Mater. Chem. A*, 2025, **13**, 21352–21388.
227 S. Mahajan and M. Lahtinen, *J. Environ. Chem. Eng.*, 2022, **10**, 108930.
228 A. J. Howarth, Y. Liu, P. Li, Z. Li, T. C. Wang, J. T. Hupp and O. K. Farha, *Nat. Rev. Mater.*, 2016, **1**, 15018.
229 K. Gopalsamy, D. Fan, S. Naskar, Y. Magnin and G. Maurin, *ACS Appl. Eng. Mater.*, 2024, **2**, 96–103.
230 S. Xian, Y. Wu, J. Wu, X. Wang and J. Xiao, *Ind. Eng. Chem. Res.*, 2015, **54**, 11151–11158.
231 Z. Zhu, H. Tsai, S. T. Parker, J.-H. Lee, Y. Yabuuchi, H. Z. H. Jiang, Y. Wang, S. Xiong, A. C. Forse, B. Dinakar, A. Huang, C. Dun, P. J. Milner, A. Smith, P. Guimarães Martins, K. R. Meihaus, J. J. Urban, J. A. Reimer, J. B. Neaton and J. R. Long, *J. Am. Chem. Soc.*, 2024, **146**, 6072–6083.
232 Z. Zhu, S. T. Parker, A. C. Forse, J.-H. Lee, R. L. Siegelman, P. J. Milner, H. Tsai, M. Ye, S. Xiong, M. V. Paley, A. A. Uliana, J. Oktawiec, B. Dinakar, S. A. Didas, K. R. Meihaus, J. A. Reimer, J. B. Neaton and J. R. Long, *J. Am. Chem. Soc.*, 2023, **145**, 17151–17163.
233 S. Klokic, B. Marmiroli, G. Birarda, F. Lackner, P. Holzer, B. Sartori, B. Abbasgholi-NA, S. Dal Zilio, R. Kargl, K. Stana Kleinschek, C. Stani, L. Vaccari and H. Amenitsch, *Nat. Commun.*, 2025, **16**, 7135.
234 M. Kang, J. Youn, J. H. Choe, J.-H. Lee and C. S. Hong, *ChemSusChem*, 2025, **18**, e202401404.
235 M. S. Lohse and T. Bein, *Adv. Funct. Mater.*, 2018, **28**, 1705553.
236 R. van der Jagt, A. Vasileiadis, H. Veldhuizen, P. Shao, X. Feng, S. Ganapathy, N. C. Habisreutinger, M. A. van der Veen, C. Wang, M. Wagemaker, S. van der Zwaag and A. Nagai, *Chem. Mater.*, 2021, **33**, 818–833.
237 H. Fan, M. Peng, I. Strauss, A. Mundstock, H. Meng and J. Caro, *J. Am. Chem. Soc.*, 2020, **142**, 6872–6877.
238 E. Dautzenberg, G. Li and L. C. P. M. de Smet, *ACS Appl. Mater. Interfaces*, 2023, **15**, 5118–5127.
239 J. S. De Vos, S. Borgmans, P. Van Der Voort, S. M. J. Rogge and V. Van Speybroeck, *J. Mater. Chem. A*, 2023, **11**, 7468–7487.
240 R. Gomes, P. Bhanja and A. Bhaumik, *Chem. Commun.*, 2015, **51**, 10050–10053.
241 Y. B. Apriliyanto, N. Darmawan, N. Faginas-Lago and A. Lombardi, *Phys. Chem. Chem. Phys.*, 2020, **22**, 25918–25929.
242 N. Huang, X. Chen, R. Krishna and D. Jiang, *Angew. Chemie*, 2015, **127**, 3029–3033.
243 S. Das, P. Heasman, T. Ben and S. Qiu, *Chem. Rev.*, 2017, **117**, 1515–1563.
244 D. Wu, F. Xu, B. Sun, R. Fu, H. He and K. Matyjaszewski, *Chem. Rev.*, 2012, **112**, 3959–4015.
245 U. Karatayeva, S. A. Al Siyabi, B. Brahma Narzary, B. C. Baker and C. F. J. Faul, *Adv. Sci.*, 2024, **11**, 1–30.
246 Z. Zhong, X. Wang and B. Tan, *Chem.–A Eur. J.*, 2025, **31**, e202404089.
247 Z. Lei, H. Chen, S. Huang, L. J. Wayment, Q. Xu and W. Zhang, *Chem. Rev.*, 2024, **124**, 7829–7906.
248 Y. Liu, S. Li, M. Pudukudy, L. Lin, H. Yang, M. Li, S. Shan, T. Hu and Y. Zhi, *Sep. Purif. Technol.*, 2024, **331**, 125645.
249 J. Yan, Y. Tan, S. Tong, J. L. Zhu and Z. Wang, *Polym. Chem.*, 2024, **15**, 500–507.
250 K. Gokkus, M. Arici, N. Sener, C. Tuncer and S. A. Akalin, *Polymer*, 2025, **324**, 128254.
251 W. A. Elmehalmey, R. A. Azzam, Y. S. Hassan, M. H. Alkordi and T. M. Madkour, *ACS Omega*, 2018, **3**, 2757–2764.
252 G. M. Iyer, C. E. Ku and C. Zhang, *Carbon N. Y.*, 2024, **216**, 118598.
253 G. Scherillo, G. Mensitieri, A. Baldanza, V. Loianno, P. Musto, M. Pannico, A. Correa, A. De Nicola and G. Milano, *Macromolecules*, 2022, **55**, 10773–10787.
254 L. Yang, P. Cai, X. Jin, Z. Wang, H. Zhou and N. Huang, *Chem.–An Asian J.*, 2025, **20**, 1–7.
255 R. Das, R. Kishan, D. Muthukumar, R. S. Pillai and C. M. Nagaraja, *J. Environ. Chem. Eng.*, 2024, **12**, 113777.
256 L. Matesanz-Niño, J. Moranchel-Pérez, C. Álvarez, Á. E. Lozano and C. Casado-Coterillo, *Polymers*, 2023, **15**, 4135.

257 K. Asadi, K. Movagharnejad, M. Taherimehr, F. Launay, F. Shirini and N. Daneshvar, *Energy Fuels*, 2024, **38**, 17741–17749.
258 N. Giri, M. G. Del Pópolo, G. Melaugh, R. L. Greenaway, K. Rätzke, T. Koschine, L. Pison, M. F. C. Gomes, A. I. Cooper and S. L. James, *Nature*, 2015, **527**, 216–220.
259 A. Kulshrestha, R. Kumar and K. P. Sharma, *ACS Sustain. Chem. Eng.*, 2024, **12**, 5799–5808.
260 R. Kumar, P. Dhasaiyan, P. M. Naveenkumar and K. P. Sharma, *Nanoscale Adv.*, 2019, **1**, 4067–4075.
261 S. He, L. Chen, J. Cui, B. Yuan, H. Wang, F. Wang, Y. Yu, Y. Lee and T. Li, *J. Am. Chem. Soc.*, 2019, **141**, 19708–19714.
262 X. Li, Z. Liu, C. Yao, Q. Chen, W. Yang, S. Ren and Y. Miao, *Fuel*, 2025, **387**, 134353.
263 Y. Wang, T. G. Feric, J. Tang, C. Fang, S. T. Hamilton, D. M. Halat, B. Wu, H. Celik, G. Rim, T. DuBridge, J. Oshiro, R. Wang, A. H. A. Park and J. A. Reimer, *Sci. Adv.*, 2024, **10**, eadk2350.
264 J. Hack, N. Maeda and D. M. Meier, *ACS Omega*, 2022, **7**, 39520–39530.
265 M. Isah, R. Lawal and S. A. Onaizi, *Green Chem. Eng.*, 2025, **6**, 305–334.
266 R. Balasubramanian and S. Chowdhury, *J. Mater. Chem. A*, 2015, **3**, 21968–21989.
267 A. Elhambakhsh and P. Keshavarz, *Energy Fuels*, 2020, **34**, 7198–7208.
268 E. Oddo, R. M. Pesce, M. Derudi and L. Magagnin, *Int. J. Smart Nano Mater.*, 2021, **12**, 472–490.
269 R. Navik, E. Wang, X. Ding, K. Qiu and J. Li, *Environ. Chem. Lett.*, 2024, **22**, 1791–1830.
270 V. Kulkarni, D. Panda and S. K. Singh, *Ind. Eng. Chem. Res.*, 2023, **62**, 3800–3811.
271 S. Zhu, B. Zhao and Y. Su, *Fuel*, 2025, **380**, 133186.
272 F. S. Taheri, A. Ghaemi and A. Maleki, *Energy Fuels*, 2019, **33**, 11465–11476.
273 Y. Zhang, Y. Chi, C. Zhao, Y. Liu, Y. Zhao, L. Jiang and Y. Song, *J. Chem. Eng. Data*, 2018, **63**, 202–207.
274 Y. Liu, B. Sajjadi, W.-Y. Chen and R. Chatterjee, *Fuel*, 2019, **247**, 10–18.
275 Y. Hosseini, M. Najafi, S. Khalili, M. Jahanshahi and M. Peyravi, *Mater. Chem. Phys.*, 2021, **270**, 124788.
276 F. Jiang, W. Zhao, Y. Wu, Y. Wu, G. Liu, J. Dong and K. Zhou, *Appl. Surf. Sci.*, 2019, **479**, 963–973.
277 A. Pruna, A. C. Cárcel, A. Benedito and E. Giménez, *Appl. Surf. Sci.*, 2019, **487**, 228–235.
278 A. Sharma, R. Chiang, M. Manginell, I. Nardi, E. N. Coker, J. M. Vanegas, S. B. Rempe and G. D. Bachand, *ACS Omega*, 2023, **8**, 37830–37841.
279 A. de Oliveira Maciel, P. Christakopoulos, U. Rova and I. Antonopoulou, *Chemosphere*, 2022, **299**, 134419.
280 Y. Fu, Y.-B. Jiang, D. Dunphy, H. Xiong, E. Coker, S. S. Chou, H. Zhang, J. M. Vanegas, J. G. Croissant, J. L. Cecchi, S. B. Rempe and C. J. Brinker, *Nat. Commun.*, 2018, **9**, 990.
281 C. Molina-Fernández and P. Luis, *J. $CO_2$ Util.*, 2021, **47**, 101475.
282 J. Wojtasik-Malinowska, M. Piątkowski, M. Blatkiewicz, M. Jaskulski, P. Wawrzyniak and A. Górak, *Chem. Eng. Process. Process Intensif.*, 2023, **184**, 109266.
283 J. Wojtasik, K. Gładyszewski, M. Skiborowski, A. Górak and M. Piątkowski, *Chem. Pap.*, 2019, **73**, 861–869.
284 O. Alvizo, L. J. Nguyen, C. K. Savile, J. A. Bresson, S. L. Lakhapatri, E. O. P. Solis, R. J. Fox, J. M. Broering, M. R. Benoit, S. A. Zimmerman, S. J. Novick, J. Liang and J. J. Lalonde, *Proc. Natl. Acad. Sci. U. S. A.*, 2014, **111**, 16436–16441.
285 K. Rigkos, G. Filis, I. Antonopoulou, A. de Oliveira Maciel, P. Saridis, D. Zarafeta and G. Skretas, *Environ. Sci. Technol.*, 2024, **58**, 17732–17742.
286 M. Fedai, J. Shen, Z. Bognár, A. L. Kwansa, A. Grunden, S. Helveg, S. Salmon and Y. G. Yingling, *Trends Biotechnol.*, 2025, **43**, 3040.
287 S. Ren, S. Jiang, X. Yan, R. Chen and H. Cui, *J. $CO_2$ Util.*, 2020, **42**, 101305.
288 J. Shen, Y. Yuan and S. Salmon, *Catalysts*, 2022, **12**, 1108.
289 M. Leimbrink, K. G. Nikoleit, R. Spitzer, S. Salmon, T. Bucholz, A. Górak and M. Skiborowski, *Chem.–Eng. J.*, 2018, **334**, 1195–1205.
290 P. Shao, H. Chen, Q. Ying and S. Zhang, *Energy Fuels*, 2020, **34**, 2089–2096.
291 R. A. Sheldon and S. van Pelt, *Chem. Soc. Rev.*, 2013, **42**, 6223–6235.
292 H. Rasouli, K. Nguyen and M. C. Iliuta, *Sep. Purif. Technol.*, 2022, **296**, 121299.
293 Y. Zhang, J. Zhu, J. Hou, S. Yi, B. Van der Bruggen and Y. Zhang, *J. Membr. Sci. Lett.*, 2022, **2**, 100031.
294 D. Sillu and V. Achal, *Environ. Chem. Lett.*, 2024, **22**, 2213–2239.
295 L. Liu, X. Wang, Z. Gao, Y. Zhan, M. Yao and J. Bao, *Water, Air, Soil Pollut.*, 2025, **236**, 235.
296 M. Xiao, J. Thompson, J. Shen, S. Salmon and K. Liu, *AIChE J.*, 2023, **69**, e18191.
297 H. Nagata, M. Yoshimoto and P. Walde, *ACS Omega*, 2023, **8**, 18637–18652.
298 S. S. Hays and J. K. Pokorski, *RSC Appl. Polym.*, 2024, **2**, 296–306.
299 J. Sun, L. Wei, Y. Wang, Z. Zhao and W. Liu, *Biotechnol. Appl. Biochem.*, 2018, **65**, 362–371.
300 S. Chang, Y. He, Y. Li and X. Cui, *J. Clean. Prod.*, 2021, **316**, 128163.
301 S. Peirce, M. E. Russo, R. Isticato, R. F. Lafuente, P. Salatino and A. Marzocchella, *Biochem. Eng. J.*, 2017, **127**, 188–195.
302 S.-C. How, X.-S. Kong, C.-J. Hu and C.-Y. Yu, *Catalysts*, 2025, **15**, 907.
303 M.-S. Svanberg Frisinger, D. Mimiroglu, L. Ullah, S. Verma, M. Martinelle, P. Berglund and N. Hedin, *ACS Appl. Mater. Interfaces*, 2025, **17**, 61919–61928.
304 M. E. Hassan, X. Zhu, E. F. de Souza, M. M. Elnashar and F. Lu, *Green Chem.*, 2025, **27**, 11289–11311.
305 F. Fonck, H. K. Karlsson, I. Antonopoulou and H. Svensson, *Clean. Eng. Technol.*, 2025, **25**, 100918.
306 Y. Xu, Y. Lin, N. G. P. Chew, C. Malde and R. Wang, *J. Memb. Sci.*, 2019, **572**, 532–544.

 

307 I. Antonopoulou, S. Varriale, E. Sapountzaki, A. de Oliveira Maciel, U. Rova and P. Christakopoulos, *Comput. Struct. Biotechnol. J.*, 2025, **27**, 2675–2687.
308 M. S. Mesbahuddin, A. Ganesan and S. Kalyaanamoorthy, *Protein Eng. Des. Sel.*, 2021, **34**, gzab021.
309 Y.-P. Chen, S. Bashir and J. Liu, in *Advanced Nanomaterials and Their Applications in Renewable Energy*, Elsevier, 2015, pp. 329–366.
310 G. Lu, Z. Wang, U. H. Bhatti and X. Fan, *Clean Energy Sci. Technol.*, 2023, **1**, 32.
311 D. Loachamin, J. Casierra, V. Calva, A. Palma-Cando, E. E. Ávila and M. Ricaurte, *ChemEngineering*, 2024, **8**, 129.
312 U. Khan, C. C. Ogbaga, O.-A. O. Abiodun, A. A. Adeleke, P. P. Ikubanni, P. U. Okoye and J. A. Okolie, *Carbon Capture Sci. Technol.*, 2023, **8**, 100125.
313 S. Y. W. Chai, L. H. Ngu and B. S. How, *Greenh. Gases Sci. Technol.*, 2022, **12**, 394–427.
314 A. Abdelshafy and G. Walther, *J. $CO_2$ Util.*, 2022, **57**, 101866.
315 N. M. A. Al Lagtah, S. A. Onaizi, A. B. Albadarin, F. A. Ghaith and M. I. Nour, *J. Environ. Chem. Eng.*, 2019, **7**, 103471.
316 R. Stanger, T. Wall, R. Spörl, M. Paneru, S. Grathwohl, M. Weidmann, G. Scheffknecht, D. McDonald, K. Myöhänen, J. Ritvanen, S. Rahiala, T. Hyppänen, J. Mletzko, A. Kather and S. Santos, *Int. J. Greenhouse Gas Control*, 2015, **40**, 55–125.
317 C. Zhou, K. Shah and B. Moghtaderi, *Energy Fuels*, 2015, **29**, 2074–2088.
318 C.-H. Yu, C.-H. Huang and C.-S. Tan, *Aerosol Air Qual. Res.*, 2012, **12**, 745–769.
319 X. Zhu, W. Xie, J. Wu, Y. Miao, C. Xiang, C. Chen, B. Ge, Z. Gan, F. Yang, M. Zhang, D. O'Hare, J. Li, T. Ge and R. Wang, *Chem. Soc. Rev.*, 2022, **51**, 6574–6651.
320 E. S. Sanz-Pérez, C. R. Murdock, S. A. Didas and C. W. Jones, *Chem. Rev.*, 2016, **116**, 11840–11876.
321 C. Beuttler, L. Charles and J. Wurzbacher, *Front. Clim.*, 2019, **1**, 10.
322 R. Ramezani, L. Di Felice and F. Gallucci, *Processes*, 2022, **10**, 2103.
323 K. M. Diederichsen and T. A. Hatton, *Ind. Eng. Chem. Res.*, 2022, **61**, 11964–11976.
324 R. V. McQuillan, A. Momeni, M. S. Alivand, G. W. Stevens and K. A. Mumford, *Chem.–Eng. J.*, 2024, **481**, 148764.
325 A. Momeni, R. V. McQuillan, M. S. Alivand, A. Zavabeti, G. W. Stevens and K. A. Mumford, *Chem.–Eng. J.*, 2024, **480**, 147934.
326 J. Sun, P. Xu, D. Gong, X. Kong, K. Fu, X. Chen, M. Qiu and Y. Fan, *Sep. Purif. Technol.*, 2023, **309**, 122978.
327 A. Imtiaz, M. H. D. Othman, A. Jilani, I. U. Khan, R. Kamaludin, M. Ayub, O. Samuel, T. A. Kurniawan, N. Hashim and M. H. Puteh, *Chemosphere*, 2023, **325**, 138300.
328 A. Zare, A. K. Boukalfa, A. Nogalska, A. Puga, P. Cerruti, B. Pascual-Jose, A. Ribes-Greus and M. Giamberini, *J. $CO_2$ Util.*, 2023, **78**, 102629.
329 O. Al Yafiee, F. Mumtaz, P. Kumari, G. N. Karanikolos, A. Decarlis and L. F. Dumée, *Chem.–Eng. J.*, 2024, **497**, 154421.
330 J. Rivero, A. Lieber, C. Snodgrass, Z. Neal, M. Hildebrandt, W. Gamble and K. Hornbostel, *Chem.–Eng. J.*, 2023, **470**, 143868.
331 S.-J. Cho, H. G. Jeong, T. H. Choi, S. J. Kwon, S. U. Hong, J. H. Kim and J.-D. Jeon, *Desalination*, 2025, **614**, 119143.
332 S. Kim, M. P. Nitzsche, S. B. Rufer, J. R. Lake, K. K. Varanasi and T. A. Hatton, *Energy Environ. Sci.*, 2023, **16**, 2030–2044.
333 X. Ding, F. Wang, G. Lin, B. Tang, X. Li, G. Zhou, W. Wang, J. Zhang and Y. Shi, *Chem. Eng. Sci.*, 2023, **280**, 119106.
334 A. Shiravi, M. S. Maleh, A. Raisi and M. Sillanpää, *Carbon Capture Sci. Technol.*, 2024, **10**, 100160.
335 M. Rahbari-Sisakht, A. F. Ismail, D. Rana and T. Matsuura, *J. Memb. Sci.*, 2012, **415–416**, 221–228.
336 T. Song, X. Zhang, Y. Li, K. Jiang, S. Zhang, X. Cui and L. Bai, *Ind. Eng. Chem. Res.*, 2019, **58**, 6887–6898.
337 K. Yang, Y. Wang, C. Zhu, W. Wu and X. Fan, *Materials*, 2025, **18**, 2303.
338 R. S. K. Valappil, M. Waseem, N. Ghasem and M. Al-Marzouqi, *J. Taiwan Inst. Chem. Eng.*, 2025, **169**, 105958.
339 W. Zhang, Y. Yang, Y. Li, F. Li and M. Luo, *Mater. Today Catal*, 2023, **2**, 100006.
340 G. Lee, Y. C. Li, J. Y. Kim, T. Peng, D. H. Nam, A. Sedighian Rasouli, F. Li, M. Luo, A. H. Ip, Y. C. Joo and E. H. Sargent, *Nat. Energy*, 2021, **6**, 46–53.
341 E. Pérez-Gallent, C. Vankani, C. Sánchez-Martínez, A. Anastasopol and E. Goetheer, *Ind. Eng. Chem. Res.*, 2021, **60**, 4269–4278.
342 H. Ning, Y. Li and C. Zhang, *Molecules*, 2023, **28**, 4500.
343 Y. Qiao, W. Liu, R. Guo, S. Sun, S. Zhang, J. J. Bailey, M. Fang and C. Wu, *Fuel*, 2023, **332**, 125972.
344 S. Lee, W. Choi, J. H. Kim, S. Park, Y. J. Hwang and J. Na, *Green Chem.*, 2023, **25**, 10398–10414.
345 D. Ferrario, T. Pröll, S. Stendardo and A. Lanzini, *Chem. Eng. J.*, 2024, **494**, 152900.
346 A. Kiani, K. Jiang and P. Feron, *Front. Energy Res.*, 2020, **8**, 92.
347 O. Otitoju, E. Oko and M. Wang, *Appl. Energy*, 2021, **292**, 116893.
348 S. Xu, Y. Jiang, C. J. Freeman and D. J. Heldebrant, *Ind. Eng. Chem. Res.*, 2025, **64**, 15023–15033.
349 E. I. Aburime, O. Omoregbe, N. A. Amenaghawon, D. S. Aziaka and B. C. Tashie-Lewis, *Carbon Capture Sci. Technol.*, 2022, **2**, 100024.
350 D. Hospital-Benito, J. Lemus, C. Moya, R. Santiago, V. R. Ferro and J. Palomar, *Chem.–Eng. J.*, 2021, **407**, 127196.
351 R. Hughes, D. Yancy-Caballero, M. Zamarripa-Perez, B. Omell, M. Matuszewski and D. Bhattacharyya, *Energy Fuels*, 2024, **38**, 2511–2524.
352 Carbon Capture Coalition, *45Q Tax Credit for Carbon Capture Projects*, https://carboncapturecoalition.org/wp-content/uploads/2025/09/45Q-primer-Carbon-Capture-Coalition.pdf, accessed March 2026.
353 United Nations Framework Convention on Climate Change, *Boundary Dam Carbon Capture and Storage Project – Canada*, https://unfccc.int/climate-action/momentum-for-change/activity-database/boundary-dam-carbon-capture-and-storage-project, accessed August 2025.

354 A. Singh and K. Stéphenne, *Energy Procedia*, 2014, **63**, 1678–1685.
355 M. Hanifa, R. Agarwal, U. Sharma, P. C. Thapliyal and L. P. Singh, *J. $CO_2$ Util.*, 2023, **67**, 102292.
356 T. Urych, J. Chećko, M. Magdziarczyk and A. Smoliński, *Front. Energy Res.*, 2022, **10**, 827794.
357 F. de Meyer and S. Jouenne, *Curr. Opin. Chem. Eng.*, 2022, **38**, 100868.
358 W. Peeters, R. Neerup and P. L. Fosbøl, *Int. J. Greenhouse Gas Control*, 2025, **147**, 104500.
359 G. Hu, K. H. Smith, Y. Wu, K. A. Mumford, S. E. Kentish and G. W. Stevens, *Chinese J. Chem. Eng.*, 2018, **26**, 2229–2237.
360 W. Yu, T. Wang, A.-H. A. Park and M. Fang, *Nanoscale*, 2019, **11**, 17137–17156.
361 S. Xie, Z. Li, H. Li and Y. Fang, *Catal. Rev.*, 2024, **66**, 1478–1517.
362 R. G. Grim, Z. Huang, M. T. Guarnieri, J. R. Ferrell, L. Tao and J. A. Schaidle, *Energy Environ. Sci.*, 2020, **13**, 472–494.
363 C. A. R. Pappijn, M. Ruitenbeek, M.-F. Reyniers and K. M. Van Geem, *Front. Energy Res.*, 2020, **8**, 557466.
364 P. Chen, D. Wang, N. Yi, J. Jiang, L. Herraiz, X. Zhou, J. Chen, Y. Ren, S. Xu, S. Garcia and X. Li, *J. Environ. Chem. Eng.*, 2025, **13**, 119605.
365 E. Sanchez-Fernandez, F. D. E. M. Mercader, K. Misiak, L. van der Ham, M. Linders and E. Goetheer, *Energy Procedia*, 2013, **37**, 1160–1171.
366 M. Hayyan, *J. Mol. Liq.*, 2025, **439**, 128928.
367 X. Wang, X. Hu, D. Zhang, Y. Zhang, H. Xu, Y. Sun, X. Gu, J. Luo and B. Gao, *J. Environ. Chem. Eng.*, 2024, **12**, 114638.
368 K. Jumle, S. S. Lakhawat, H. Ajmera, B. Thakuria, V. Sharma, V. Jain, V. Kumar, S. Singh, A. Kumar, N. Malik, S. L. Kothari, S. Kumar and P. K. Sharma, in *One- and Two-Dimensional Nanomaterials*, Elsevier, 2025, pp. 223–235.
369 M. Ding, Y. Ji and D. Yanchen, *J. $CO_2$ Util.*, 2026, **103**, 103284.
370 S. E. Renfrew, D. E. Starr and P. Strasser, *ACS Catal.*, 2020, **10**, 13058–13074.
371 G. Hooper, H. S. Findlay, T. G. Bell, R. W. Wilson and P. R. Halloran, *Front. Clim.*, 2025, **7**, 1528951.
372 P. R. Halloran, T. G. Bell, W. J. Burt, S. N. Chu, S. Gill, C. Henderson, D. T. Ho, V. Kitidis, E. La Plante, M. Larrazabal, S. Loucaides, C. R. Pearce, T. Redding, P. Renforth, F. Taylor, K. Toome, R. Torres and A. Watson, *Front. Clim.*, 2025, **7**, 1487138.
373 J. Kotowicz, K. Niesporek and O. Baszczeńska, *Energies*, 2025, **18**, 496.
374 C. D. L. Taylor, A. Klemm, L. Al-Mahbobi, B. J. Bradford, B. Gurkan and E. B. Pentzer, *ACS Sustain. Chem. Eng.*, 2024, **12**, 7882–7893.
375 P. Vuong, A. McKinley and P. Kaur, *npj Mater. Degrad.*, 2023, **7**, 50.